Effect of Mining on Regional Climate

Von der Fakultät für Umweltwissenschaften und Verfahrenstechnik der Brandenburgischen Technischen Universität Cottbus-Senftenberg zur Erlangung des akademischen Grades eines Doktors der Naturwissenschaften (Dr. rer. nat.) genehmigte Dissertation

Vorgelegt von

Master of Science

Manish Nawdiyal

aus Roorkee, Indien

Gutachter: Prof. Dr. rer. nat. Eberhard Schaller

Gutachter: Apl. Prof. Dr. rer. nat. habil. Uwe Harlander

Tag der mündlichen Prüfung: 10.12.2014

ABSTRACT

Intensive coal mining over the region of Lusatia covers a large area in southern Brandenburg and Saxony. Post mining this region has been filled with water resulting in lake formation. People living in the vicinity of mining area believe that the lake formation will increase convective precipitation in the neighboring area which shall lead to weathering of their structures. This was the prime reason to investigate the Lusatia region. The study about the impact of lake was carried out using data and CCLM simulation analyses.

For data analysis, stations Senftenberg, Cottbus and Elsterheide-Geierswalde were selected. For the analysis, six 10 years running time series, CPDF were analyzed for all the three stations. Last three time series included the period of lake formation at station Elsterheide-Geierswalde. The CPDF time series showed little deviation for station Elsterheide-Geierswalde as compared to that for other two stations during lake formation periods. But in absence of parameters (temperature, wind data) data analysis was inconclusive.

To observe effect of LULC (Land use and land cover) change on precipitation, three different simulations have been carried out,

1. VAT010: This simulation represents the potential vegetation of the whole domain. This describes the pre mining stage of the area when there was no mining.
2. VAT020: This simulation represents the introduction of lake points in the model domain. This describes the situation of area post mining, when lakes are formed.

3. VAT030: This simulation represents the mining time (without vegetation). This describes the phase when mining is in progress.

On comparing simulations VAT020 to VAT010 a slight increase in precipitation over Lake Grid cells is observed during summer and early fall. This difference is because of factors viz. surface roughness, westerly winds, small Bowen ratio and thermal heat capacity of lake. As the aim of this study was to investigate the effect of lake on convective precipitation parameter over the neighboring region, hence it is concluded that no effect over the vicinity of lake area is observed.

TABLE OF CONTENTS

LIST OF FIGURES

LIST OF TABLES

1. INTRODUCTION AND MOTIVATION

According to Baede (2007) ‘’Climate in a narrow sense is usually defined as the average weather, or more rigorously, as the statistical description in terms of the mean and variability of relevant quantities over a period of time ranging from months to thousands or millions of years. The classical period for averaging these variables is 30 years and decadal average is the minimum possible time frame for meaningful assessment of climate change, as defined by the World Meteorological Organization (WMO). The relevant quantities are most often surface variables such as temperature, precipitation and wind. Climate in a wider sense is the state, including a statistical description, of the climate system’’. Climate change is one of the most important concerns of the 21st century, be it global or regional. It is receiving unprecedented attention due to the possibility that human activity on Earth, during the past couple hundred years will lead to significantly large changes in environmental conditions. These changes could well affect our health, comfort levels, and ability to grow and distribute food. Since ancient time, great societies have flourished around rivers and big lakes, when agriculture was at peak. Regional climate makes the social structure of the place. A regional change in climate, such as precipitation and temperature, can disturb this social structure, especially in agricultural driven areas where cultivation depends on precipitation. Hence, a change in temperature and precipitation can be devastating.

Studies have shown effects of different land-use or surface patterns and alteration made to them on local or regional scales (Avissar 1995, Pielke 2001, Roy & Avissar 2002, Clark et al. 2004, Pitman et al. 2004, Pitman & Narisma 2005, Sen et al. 2004, Marshall et al. 2004 & Cooley 2005). These studies point to the triggering and

support of local convection processes by virtue of land/surface characteristics. Results are modeling based and analyses including field measured data are rare. Analyses are based on the effects of water bodies (lakes) and urbanization on surrounding regions but the aspects of land use and land cover (LULC) change are not included. It means that analyses show the effects of different landscape without including the effects of alteration made in landscape.

Studies showing change in precipitation caused by altering the land surface into water surface are also rare. A study has shown that human activities can influence the water vapor abundance in the atmosphere directly through changes in LULC which modify surface properties and evaporation (Pielke Sr. 2002). One such effect of LULC change can be alteration in precipitation (Avissar & Liu 1996, Cotton & Pielke Sr. 2007, Pielke Sr. et al. 2009). Another study of tropical deforestation in Costa Rica showed significant regional effect on the ecological environment of adjacent mountains. The longitudinal distribution of thunderstorms in the tropics is also changed (Lawton et al. 2001). More related studies are mentioned in chapter 2.2.

The German coal mining dates back to the 19th century. The German coal industry has lived through many ups and downs. It has laid the foundations for growth and prosperity and today it still provides the country with energy security. Its future has now become a political issue. Economic conditions on the one side have to be carefully balanced against energy-policy risks on the other. Since mid-nineteenth century over 2 billion tones of lignite coal have been mined from excavations as deep as 60 meters in the region between Senftenberg, Spremberg, and Hoyerswerda. Since the mid-1990s the LMBV has been responsible for reclaiming and rehabilitating contaminated former mining industry sites in the area.

Although during last 20 years brown coal output has declined significantly (statistik der Kohlewirtschaft e.V. 2009 & Bundesanstalt für Geowissenschaften und Rohstoffe, 2009), it is still the leading lignite producer in the world. In 2007, the year for which the most recent data are available, Germany had mined 180 million tons of brown coal, over twice as much as the next highest producer (Krümmelbein et al. 2010 & 2012). Coal mining is distributed over the three main areas of Rhineland, Central Germany and Lusatia. Lusatia is the region surrounding the towns of Cottbus and Senftenberg in eastern Germany. It is one of the largest mining areas in Germany and has been strongly economically dependent on lignite mining and processing industry since the middle of the 19th century (Großer 1998 & Schulz 2000). The Lusatian lignite-mining area belongs to the warm continental areas of the lowlands of northeastern Germany. Total mined area is approximately 850 km^2 (Statistik der Kohlewirtschaft e.V. 2009), with an additional 300 km^2 (Vattenfall Europe AG 2009) approved for mining. In Lusatia the landscape has undergone strong modifications due to mining. The Lusatian lignite-mining area belongs to the warm continental areas of the lowlands of northeastern Germany. Proportion of forestall land use before and after mining is relatively equal; agricultural use decreases, while water area increases which is mainly due to the remaining voids of the opencast mines and will be filled by water and is proposed in future to form the largest are of connected lakes in Germany. Around 25% of mining area will form lake post mining (Zweckverband Elstertal 2006 & Vattenfall Europe AG 2009).

People living in the vicinity of the mining area have concern that, the conversion of surface post-mining into lake might enhance precipitation events thereby damaging the structure (weathering) and effect vegetation. This concern, keeping in mind the previous studies and knowledge obtained has formed the very basis of this thesis

and precipitation is considered as an important parameter (especially convective). The focus of this work is on the coal mining region in Brandenburg and Saxony state especially Lusatia. The research work is mainly divided into three periods as:-

1. Pre Mining (Potential natural vegetation):- Period when no mining was in action.
2. During Mining: - Period when mining was being carried out.
3. Post Mining: - Period when mining was over and after re-cultivation, lake was formed.

In this thesis, research is carried out using data analysis and regional climate simulation using Regional climate model (CCLM). For the data analysis, stations near mining areas are considered, which have intensive data to cover the above three mentioned periods. More information is provided in chapter 4.2. For simulation analysis, period of 10 years is considered. In order to make simulation analysis as close to real situation (keeping future expansion into consideration), in Lusatia only four grids, which together make an area of 400 km^2, are subjected to landscape change in CCLM simulations. In this way, simulation analysis will depict the real life future situation in that region.

The idea behind the analysis is to look for LULC change effect on precipitation. In this thesis LULC change is the conversion of area first into mining and later into lake. Even though, main focus is only on the changes that occur from the transition of area from potential natural vegetation into lake. It is assumed that during the process of this transformation (from no mining to lake) there will be change in the land surface characteristics which can lead to changes in their sensible and latent turbulent heat fluxes. Increase in both heat fluxes might result in increase of precipitation events.

This thesis consists of 5 chapters. Hypotheses for this study along with some information about related previous work which will help in giving direction and understanding the results are in chapter 2. Chapter 3 will start with the background history of mining in Germany. It will be followed by choice of stations relevant for the study and at last their analyses. Brief introduction to CCLM model and experimental setup relevant for the thesis are explained in chapter 4 followed by different simulation analyses. Chapter 5 gives the summary of the thesis and the conclusion of both the studies (data analyses and simulations), followed by suggestions for future research focusing on critical open questions.

2. THESIS BACKGROUND

2.1 Surface Effects

The Sun is the power source to our climate on Earth. It doesn't heat the Earth evenly as it is a sphere. The Sun heats equatorial regions more than Polar Regions. The atmosphere and ocean work non-stop to even out solar heating imbalances through evaporation of surface water, convection, precipitation, winds, and ocean circulation. Any alteration made in the landscape of a certain region will change the surface heat and moisture energies of that region. These changes might result in influencing the key dynamic properties of the air and hence may result in a change in precipitation. As this is a very important part for understanding this thesis, it is discussed in detail below (snow and ice effects are not considered in this discussion).

The surface energy can be written as

$$R_N = G + H + L(E + T_{ran}) \qquad (1)$$

$$P = E + T_{ran} + RO + I \qquad (2)$$

where R_N represents the net radiative flux density; P is the precipitation; E is the evaporation (this term represents the conversion of liquid water vapor by nonbiophysical processes, such as from the soil surface, water surface and from the surfaces of leaves and branches); T_{ran} is transpiration (which represents the phase conversion to water vapor, by biological processes, through stomata on plants); G is the subsurface heat flux; H is the sensible heat flux; $L(E + T_{ran})$ is the latent heat flux (where L is the latent heat of vaporization); RO is precipitation surface runoff; I is the amount of precipitation got infiltrated.

Sensible heat flux (H) is the process in which heat energy is transferred across the surface to the atmosphere and vice versa by conduction and convection. For example when a ground is warmer than the air in the atmosphere, then for the air in contact with the surface, heat will be transferred by conduction and then turbulence and convection will move the heat higher up into the atmosphere.

Latent heat flux moves energy when solid and liquid water is converted into vapor. Movement of air carries heat and moisture away from an object. Evaporation occurs when a moist surface is exposed to drier air. Water evaporates from the surface, increasing the amount of water vapor in the surrounding air. When the air is saturated with water vapor, evaporation ceases. Evaporation is therefore related to the vapor pressure deficit of air i.e. the difference between the actual amount of water in air and the maximum possible when saturated.

Further R_N as net radiative flux density can be described as

$$R_N = R_S(1 – A) + R_{LW\downarrow} - R_{LW\uparrow} \qquad (3)$$

Where R_S is downward solar insolation; A is albedo; $R_{LW\downarrow}$ is the downwelling and $R_{LW\uparrow}$ is the upwelling longwave radiation

Albedo is the fraction of Sun’s radiation reflected from a surface. . It is expressed as a percentage of reflected to incoming solar radiation. A value of zero means solar radiation is totally absorbed by the surface while 1 refers to total reflection of downward solar insolation. The quantity (1- A) represents the fractional component of shortwave radiation that is absorbed. In terms of visible colors, darker colors have a lower albedo, that is, they absorb more incoming solar radiation, and lighter colors have high albedo, or higher rates of reflection. Smooth surfaces have a higher albedo while rough surfaces reduce it. Averaged surface albedo varies from near 0.1 over

forests (Oguntoyinbo 1970, Stewart 1971) to as high as 0.4 over some sandy deserts (Rockwood and Cox 1978, Kondratyev et al. 1982), over 0.9 over fresh snow (Kondratyev et al. 1982) and 0.08 over lake.

$R_{LW\uparrow}$ can be described as

$$R_{LW\uparrow} = (1 - \varepsilon) R_{LW\downarrow} + \varepsilon\sigma T_S^4 \qquad (4)$$

Where ε is the surface emissivity; σ is the Stefan-Boltzmann constant; T_S is the surface temperature.

The emissivity of a surface is defined by its ability to emit energy by radiation. It is the ratio of energy emitted by a particular surface to energy radiated by a black body at the same temperature. A true black body would have an ε = 1 while any real surface would have ε < 1. It is a dimensionless quantity. In general, the duller and blacker surface is, the closer is its emissivity to 1 (0.97 for water).

For detailed discussion of these terms Pielke (1984) can be referred. It is clear from equations (1) to (4) that these equations are not independent of each other. A reduction in evaporation and transpiration in equation (2), for example, increases G and/or H in equation (1) when R_N does not change. This reduction can occur, for example, if runoff is increased (such as by deforestation). The precipitation rate and type, also obviously influence how water is distributed between runoff, infiltration and the interception of water on plant surfaces and this can be explained as:

1. If a precipitation occurs in the form of rainfall it starts immediately as surface runoff depending upon rainfall intensity while precipitation in the form of snow does not result in surface runoff.

2. If the rainfall intensity is greater than infiltration rate of soil then runoff starts immediately after rainfall. While in case of low rainfall intensity runoff starts later. Thus high intensities of rainfall yield higher runoff.
3. And duration of precipitation is directly related to the volume of runoff because infiltration rate of soil decreases with duration of rainfall. Therefore medium intensity rainfall even results in considerable amount of runoff if duration is longer.

We also know that change in LULC might change albedo which will directly affect the surface energy balance. Studies made in semiarid regions have shown that an increase in albedo leads to a loss of radiative energy absorbed at a surface and this might decrease precipitation and evaporation (Sud and Fennessy 1982, Laval and Picon 1986 & Sud and Molod 1988). However, the drying effects are not limited to the subtropics. Similarly reductions in precipitation and evapotranspiration have been found for increased albedo in tropical Africa (Kitoh et al. 1988) and the Amazon basin (Mylne and Rowntree 1992).

The relative amounts of sensible heat flux (H) and latent heat fluxes [$L(E + T_{ran})$] are used to define the Bowen ratio (B).

$$B = H/[L(E + T_{ran})] \qquad (5)$$

Equation (5) shows Bowen ratio, which is the amount of sensible to latent heat lost (or gained) by a surface to the Earth's atmosphere by the processes of heat conduction, convection and atmospheric turbulence. In arid zones, B values are much greater than unity; in humid zones they are much below unity. The relation of R_N to sensible heat flux (H) and Latent heat flux [$L(E + T_{ran})$] can also be written as(Segal et al. 1988).

$$H = (R_N - G)/(B^{-1} + 1) \qquad (6)$$

It is shown that with G << H and E + T_{ran}, as discussed by Segal et al. (1988),

$$H = BR_N/(1 + B) \qquad (7)$$

Segal et al. (1995) studied the effect of surface characteristics for development of deep convection resulting from heat and moisture flux evaluated by conceptual, scaling and numerical modeling approaches. Study shows that deep convection depends significantly on the Bowen ratio. One of the study conclusions is that for smaller Bowen ration, the thermodynamic potential for deep convection increases.

Therefore any land use change that alters one or more variable in equations (1) and (2) will directly affect the potential for thunderstorms, and their resultant intensity, if they occur. For instance, decrease in A (i.e., a darkening of the surface) would increase R_N, thus making more heat energy available for G, H, E and T_{ran}. Pielke (1984) showed that if surface is dry and bare, all of the heat energy would necessarily go into G and H as found out in study of Saudi Arabia. In another study, a reduction of H in southwestern Australia, as a result of the conversion of land to agriculture was found (Lyons et al. 1996). A reduction in H was found due to leafing out of vegetation in the spring (Fitzjarrald et al. 2001 & Schwartz 1994).

A conclusion of these analyses is that a change in the Earth's surface might result in changing the surface energy and moisture energies. These changes will influence the heat and moisture fluxes within the planetary boundary layer (Segal et al. 1989), atmospheric circulation (Dirmeyer & Shukla 1993, 1994), boundary layer depth and other measures of the deep cumulus cloud activity. Horizontal variations in H and boundary layer depth can subsequently result in local wind circulations (Segal & Arritt 1992). In these areas, the potential for deep cumulus convection are increased in

response to convergence associated with the local wind circulations (Pielke et al. 1991). These wind convergence zones can also trigger specific vertical motion to initiate deep cumulus convection. Therefore the landscape can influence and produce focused regions for deep cumulonimbus convection.

2.2 Some Relevant Studies

Some work has been already carried out in the field of LULC change and also it's effect on regional and global climate change. These studies might help in understanding the thesis results.

A study on large dams in North America shows that dam influence local climate most in mediterranean and semi arid climates, while for humid climates the influence was least apparent (Ahmed et al. 2011). In this study, large dams are defined as a dam with an embankment height of more than 15 meters or a storage volume exceeding 3 million m^3 were considered. Such systematic changes to LULC, by construction of a dam, can lead to increased availability of local moisture and have significant impact on mesoscale (10-100km) circulation (Niyogi et al. 2010, Takata & Yasunari 2009).

For the study, 92 large dams located in various climate zones of the United States were selected. To understand the potential effect of LULC changes near the dams, main purposes of the dams were identified and categorized into three broad types (irrigation, hydropower and 'other'). Here, 'other' includes applications such as flood control, domestic water supply and recreation. Study premise is that the existence of a dam was a necessary (if not sufficient) indicator of LULC change near reservoirs and can therefore help explain features of study's observational findings. For example, dams made for the irrigation purpose, results in intensified agriculture near

reservoirs, whereas hydropower dams most likely contribute to only sporadic land cover change through urbanization.

For the atmospheric observational record, variables considered relevant to mesoscale precipitation patterns were obtained from National Center for Environmental Prediction (NCEP) and North American Regional Reanalysis (NARR) data bases. These parameters are viz. Convective Available Potential Energy (CAPE), specific humidity and surface evaporation. Analysis was carried out for a period from 1979 to 2009. Study area was dived into three spatial bands. First band is over the dam. The second band extends from shoreline of reservoir to 100 km around the reservoir. The third band starts from outside boundary of second band to doubling of area under second band.

The results of percentage increase for these parameters (30 year climatologic mean) showed changes in the values around semi-arid region and no significant changes around humid climate region (figure 1.1). One of the interpretations for this result was that humid regions were forested and exhibit comparable moisture fluxes due to transpiration as from evaporation from open water bodies. Thus the clearing of a forest to create an artificial lake is unlikely to create any change. For semi-arid and Mediterranean regions, the open water body of a reservoir however added more moisture than the sparsely vegetated surrounding. Hence clear spatial gradient of water vapor flux for most dams was observed. A series of studies have indicated that land surface irrigation may have important effects on surface temperature and vapor flux to the atmosphere by evapotranspiration (Asokan et al. 2010, Boucher et al. 2004, Gordon et al. 2005, Lobell et al. 2006, Kueppers et al. 2007 & Shibuo et al. 2007).

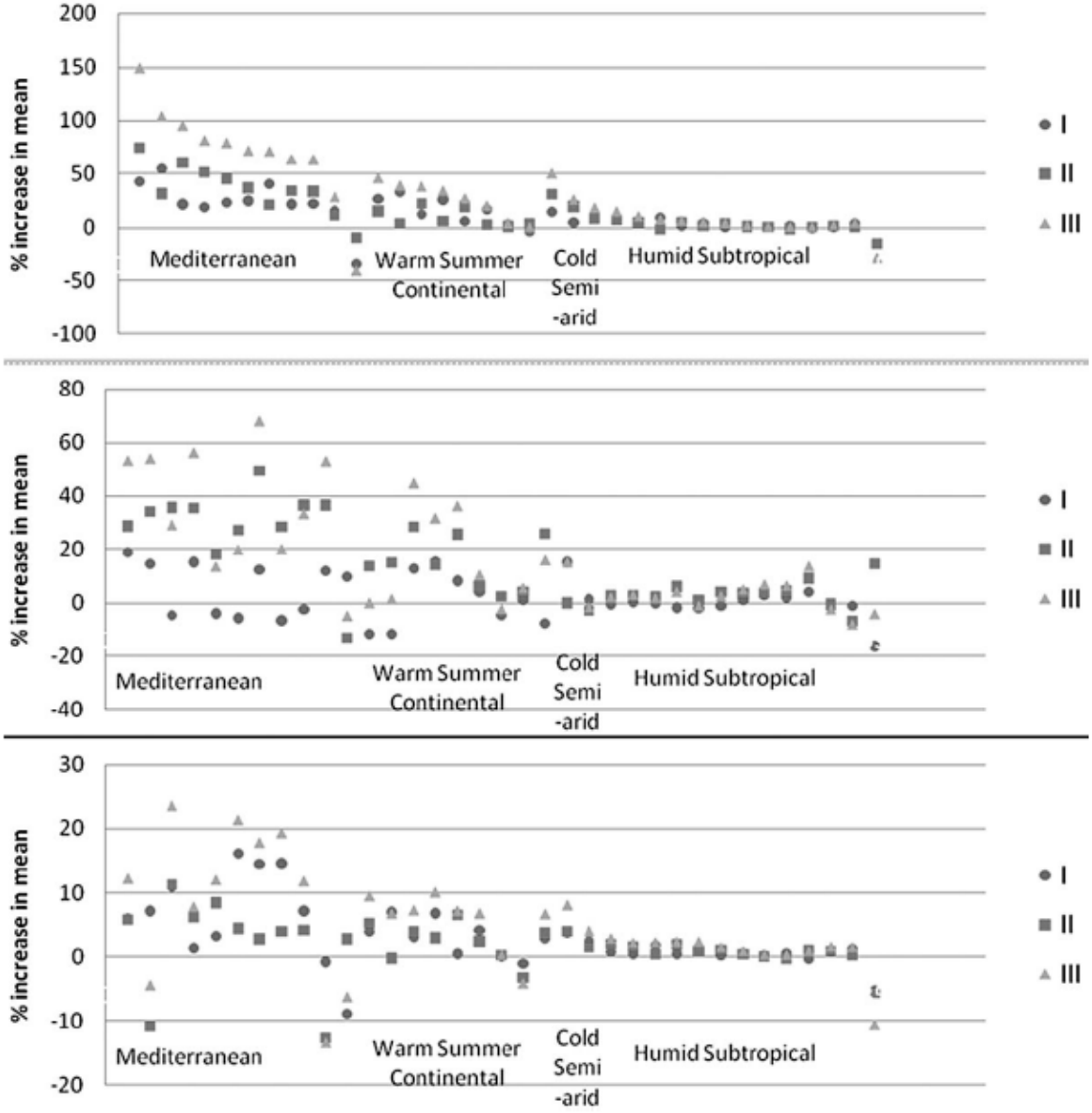

Figure 2.1: Spatial gradients exerted by dams for the whole season (% increase of the 30 year climatologic mean from one band to another). Each dam is represented on the x-Axis far a specific scenario. The last three data points from right represent selected dams in hot summer continental and continental subarctic climate zones. (top) CAPE, (middle) surface evaporation, and (bottom) specific humidity. Scenario I - % increase = (First band - Second band)*100/Second band. Scenario II - % increase = (Second band - Third band)*100/Third band. Scenario III - % increase = (First band – Third band)*100/Third band (Source: Ahmed et al. (2011)).

As a follow up study on the influence of dams on local climate, corresponding influence on precipitation patterns using daily rainfall data from Global Historical Climate Network (GHCN) was done. In warm semi arid and Mediterranean dam region more than 8 % stations showed increase in precipitation but in Warm Summer

Continental regions out of 1000 stations less than 4 % showed increase in precipitation (they were at an average distance of 265 km from nearest dam). But the author states that this list of stations is likely to include stations that have undergone a historical increase due to long-term changes in large scale weather patterns (Cuo et al. 2009). The author concluded that increasing correlation was observed between CAPE and precipitation in Mediterranean and arid region but none was observed in Warm Summer Continental region. More details can be found in Cuo et al. 2009.

Precipitation effects of lakes have been studied extensively at Great Lakes in North America using radar and gage data. Wilson (1977) in order to compare lake and nearby land precipitation amounts averaged the precipitation for four zones over and around Lake Ontario (figure 2.2).

Figure 2.2: Precipitation averaging zones

Figure 2.2 shows the four zones. Zone 1 is over mid-lake more than 15 km of the land; zone 2 is over the lake, within 15 km of the shore; zone 3 is over land, within 15 km of the shore; and zone 4 is over land between 15 and 30 km from the shoreline. Table 2.1 shows the analysis result for one year starting April 1972 through March 1973. Warm season include May-September and cold seasons include November-March.

Table 2.1: Precipitation differences between zones for different time periods

Difference from zone 1 (%)		
Zone	**Warm season**	**Cold season**
2	+1.5	-1.4
3	+4.4	-2.5
4	+16.3	-2

In Table 2.1 it can be seen that during warm season, precipitation for land areas within 30 km of the lake Ontario was 10% more than for the lake. For the cold season, land received 2% less than the lake. The increase of land precipitation over lake precipitation is concentrated at eastern end of lake (winds were generally westerly) and is partially an orographic effect produced by Tug Hill Plateau. Considering just western two-thirds of the lake and corresponding land areas, the land and lake precipitation are essentially equal for the year. The land receives 5.1% precipitation during the warm season and 4.8% less during the cold season. It is concluded that the distribution of precipitation over the Lake Ontario drainage basin is significantly affected by lake and hills.

Rouse et al. (2002) studied the interannual and seasonal variability in the thermal regime and surface energy fluxes in central Great Slave Lake (GSL). GSL is the fifth largest lake in North America in terms of surface area (28,568 km^2) and the mean depth of the lake, exclusive of the eastern arm, is estimated at 32 meters. The research was carried out from the largest of the Inner Whaleback Islands (IWI), a group of small rock islands located in the main body of Great Slave Lake, 80 km southwest of Yellowknife (Figure 2.3).

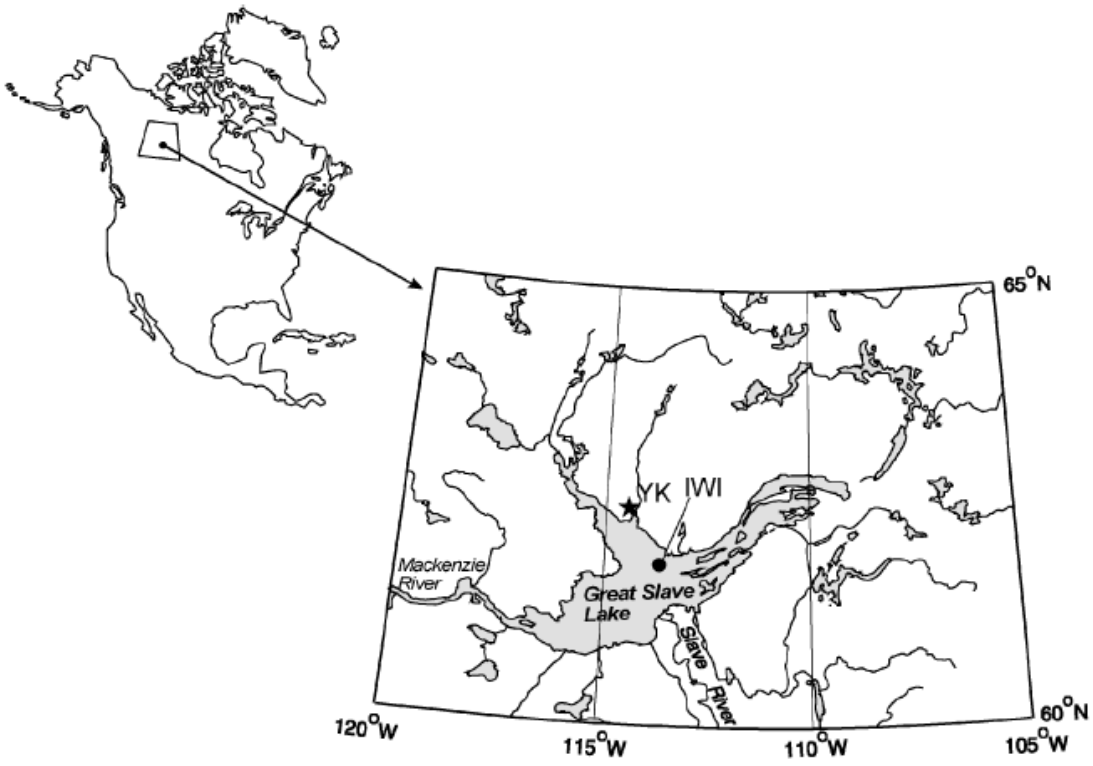

Figure 2.3: Location of the main research site on the largest of Inner Whaleback Islands, Great Slave Lake; YK and IWI are shown.

Instrument setup was according to details mentioned in Balken et al. (2000). It consisted of 14-m-long retractable horizontal boom equipped with instruments to measure net radiation and fluxes. Radiation measurements were considered free of the island's influence.

Study concluded that from the final lake ice melt in mid-June through to mid- to late August, the surface waters strongly absorb solar radiation. The latent heat flux is small and directed upwards, and sensible heat flux is small and directed downwards into the lake. During this period, the net solar radiation is largely used in heating the lake. From mid- to late August to freeze up in December to early January, the absorbed solar radiation is small and latent and sensible heat fluxes becomes positive (Figure 2.4) and lake starts to lose its stored heat.

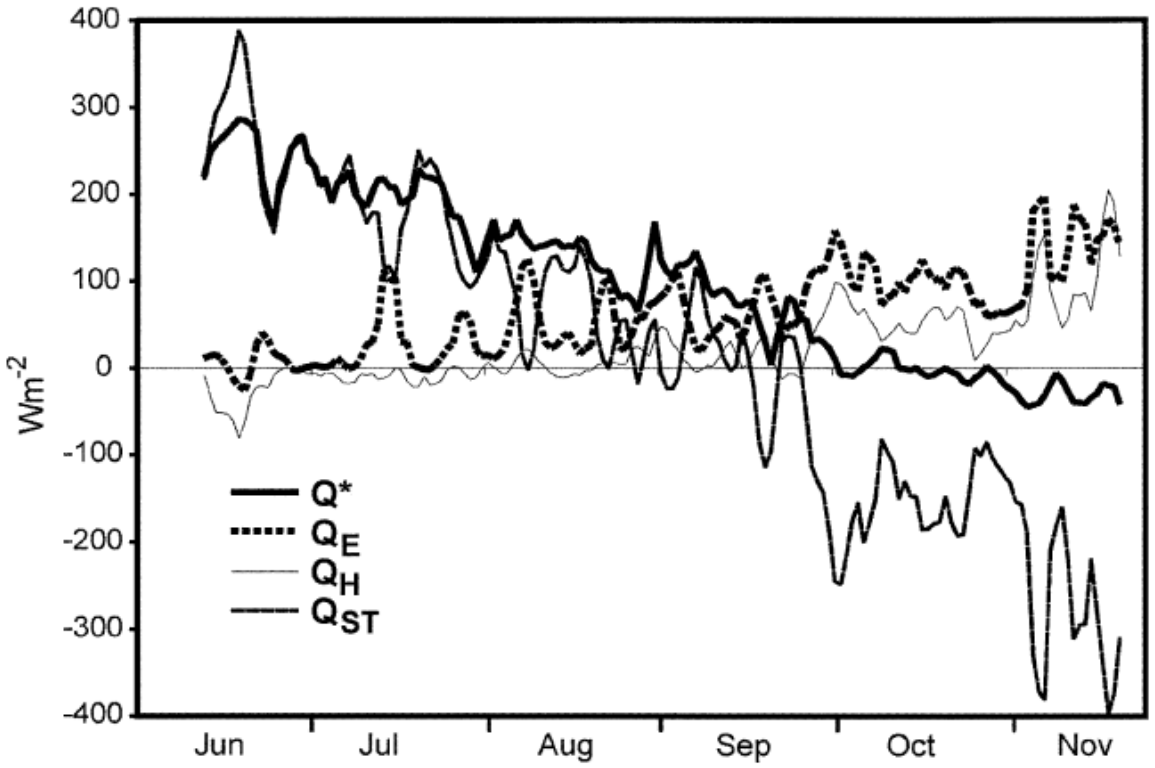

Figure 2.4: The energy balance at IWL in 1999; Q*, Q_E, Q_H and Q_{ST} designate net radiation, latent heat flux, sensible heat flux and calculated change in storage respectively.

Scott and Huff (1996) studied the lake-induced changes on six climate variables (precipitation, mean minimum and maximum temperature, cloud cover, vapor pressure and wind speed) for entire Great Lake basin. Lake effects were most noticeable in precipitation and temperature and vary considerably by season, time of day, and lake size. In the study, analytical techniques were devised to extract lake effects from the full analysis of climate data encompassing the basin. Past research at the Illonois State Water Survey on the Lake Michigan basin provided climatological technique for defining the extent of lake effects on monthly, seasonal, and annual precipitation, temperature, and other weather conditions. Inspection of these results and those of other studies found significant effects within a variety of distances from the lake shores. Greatest lake influences were found near Lake Superior where 100% more precipitation falls downwind of the lake in winter compared to that

expected without its presence. During summer, all lakes cause a downwind decrease in precipitation of 10% to 20%.

Some analytical and numerical studies have shown that heterogeneity in surface sensible and latent heat flux can produce strong mesoscale circulations (Avissar & Liu 1996, Avissar & Schmidt 1998, Wang et al. 1996, Wang et al. 1998). These circulations significantly affect the structure of the Planetary boundary layer, heat flux and moisture flux (Chen & Avissar 1994a, Dalu & Pielke 1993, Dalu et al. 1996, Li & Avissar 1994, Lynn et al. 1995) and can affect cloud organization and precipitation (Chen & Avissar 1994b, Wang et al. 2000, Wetzel et al. 1996).

2.3 Uncertainty Analysis Methodology

Different techniques to investigate uncertainty in a climatological time series are available. Different techniques have been used in CCLM time series sensitive analysis by Roesch et al. (2008) and Bachner et al. (2008). The similarity in their analyses is that they had ensembles of time series and an observational dataset as a reference.

In this thesis, the problem with CCLM time series for precipitation is the unavailability of reference and ensembles of time series. So techniques mentioned in the articles above could not be used. For this purpose Monte Carlo simulation (MCS) method is used for uncertainty analysis. MCS was devised as an experimental probabilistic method to solve difficult deterministic problems; since computers can easily simulate a large number of experimental trials that have random outcomes. When applied to uncertainty estimation, random numbers are used to randomly sample parameter uncertainty space instead of point calculation carried out by conventional methods. Such an analysis is closer with the underlying physics of actual measurements

processes that are probabilistic in nature (Basil, M. et al., 2001). Nicolis (1995), pointed out that in nature the process of measurement, by which the observer communicates with a physical system, is limited by a finite precision. AS a result, the 'state' of a system must in reality be understood not as a point in phase space but rather as a small region whose size reflects the finite precision of the measuring apparatus. On the probabilistic view, we look at our system through a 'window' (phase space cell). So the application of MCS in the uncertainty estimation of different states of a system seems to offer a more realistic approach. More is described in detail with some application examples by Basil (2001).

MCS technique is used to generate new sets of monthly values from available monthly value using equation 8 shown below.

$$NV_K = OV_M + Var_M * RN_K \quad (8)$$

Where, NV_K represents set of new values (K number of values); OV_M is the original value of a grid in a month (M); Var_M is maximum expected variability; RN_K is random number generated and subscript K and M represents number of values and months. In this thesis K = 1000.

The main information required in the simulations is maximum expected variability for each month (Var_M) of the simulated parameter (in this thesis convective precipitation). Var_M is determined for each month, from the decadal monthly difference plots of CCLM simulations (VAT020-VAT010 and VAT030-VAT010), from the undisturbed (not influence by LULC change) region of the model domain for convective precipitation parameter. Domain size is mentioned in chapter 4.

OV_M values are the value of decadal monthly difference of CCLM simulations (VAT020-VAT010 and VAT030-VAT010) for each month (M) of interested grid.

A random number generator is selected based on Box-Muller technique (Gaussian). Random number generator will generate numbers within the range of -1 to +1. Equation 8 is used to generate 1000 (K) new NV_K values for each month. So, in the end there will be 1000 new values (NV_K) generated for each month corresponding to its OV_M counterpart.

Using this generated NV_K and known OV_M values uncertainty is determined using equation 9 as shown below.

$$\Sigma_M = \sqrt{\left(\frac{1}{1000-1}\sum_{K=1}^{1000}(NV_K - OV_M)^2\right)} \qquad (9)$$

Where, σ_M = monthly uncertainty

Monthly uncertainty is shown by the range of $OV_M \pm \sigma_M$.

3. DATA ANALYSIS

3.1 Study Area

For this study, stations close to the mining area, covering mainly Brandenburg and northern Saxony are considered. In total 55 stations close to different mining areas are identified. The very first approach is to look for stations surrounding mining areas with availability of parameters like temperature, precipitation, wind direction and speed. The purpose to consider these parameters is to study the effect of various phases of LULC change (see chapter 1) on precipitation and to help in explaining it. Data are extracted from DWD (Deutscher Wetterdienst) database (https://werdis.dwd.de/werdis/start_js_JSP.do).

Table 3.1 below shows the data availability of different parameters viz. DMT, DminT, DmaxT, DMWS and DSP at some meteorological stations. Here,

DMT is daily mean temperature. It is an average of hourly temperatures over a day.
DMinT is daily minimum temperature. It is the minimum recorded temperature over a day.

DMaxT is daily maximum temperature. It is the maximum recorded temperature over a day.

DMWS is daily mean of wind speed. It is the average speed of wind recorded over a day.

DSP is daily sum of precipitation. It is the total summation of precipitation recorded in a day.

Green color means that data for the corresponding parameter is available and no colour means that data for that parameter are unavailable. It can be seen that DMT,

DMinT and DMaxT are only measured for the four stations viz. Cottbus, Doberlug-kirchhain, Klettwitz and Schwarze Pumpe. DMWS parameter data set is available at Cottbus and Doberlug-Kirchhain stations only.

Table 3.1: Stations showing availability of different climate parameters. Green color indicates that parameter is available

S.No.	Station Name	DMT	DminT	DMaxT	DMWS	DSP
1	Cottbus					
2	Doberlug-Kirchhain					
3	Klettwitz					
4	Schwarze Pumpe					
5	Altdöbern					
6	Bahnsdorf					
7	Burghammer-Burgneudorf					
8	Burg/Spreewald					
9	Drebkau					
10	Elsterheide-Geierswalde					
11	Graustein					
12	Hoyerswerda					
13	Komptendorf					
14	Lohsa					
15	Ogrosen					
16	Peickwitz					
17	Ruhland					
18	Sallgast					
19	Senftenberg					
20	Sollschwitz					
21	Trebendorf					

It is clear from Table 3.1 that most of the stations have precipitation data set. So, further data analysis will be based on precipitation data only. And, as precipitation is one of the most important parameters (see Chapter 1), so stations with precipitation values around mining areas are sought. Initially, it is decided to look for stations around a mining area but located in different geographical directions. This will help in quantifying the effect of a single lake with respect to different directions. Further, parameters like wind speed and direction could have provided more information but

unfortunately no data for these parameters are available. During search for the mining area two assumptions are laid out as:-

1. Location of measuring stations, in different geographical directions, should be more or less at the same distance from the mining area. This will help making sure that effective potential influence of lake (mining area) is same in all directions. If some stations are very close to the mining area (later transformed into lake) then they might show more influence than those who are far.
2. Stations should have data during three phases of LULC i.e. before mining, during mining and post mining (when it is being transformed into lake). This will help in noticing the effect of each phase on precipitation data and will also help to summarize the analysis based on precipitation change after introduction of lake.

First assumption could not be followed as no mining area with equidistant measuring stations could be found. In some cases, like in case of mining area Graebendorf, stations were located in different geographical directions but were very far away from the site. Hence they were not further analyzed. Also, many stations though equidistant to particular mining area were found; they had missing values and thus were discarded from the analysis. First assumption was thus redefined and now, measuring stations were selected which were located close to any mining area instead of looking for equidistant measuring stations around one particular mining area. But the purpose will remain same as to see the effect during- and after mining i.e. after being transformed into lake.

There are many stations fulfilling this redefined assumption criteria but are not considered because either they don’t have long time series or have many missing values. Some stations don’t have data during- and post mining period and especially

when the area is transformed into a lake. Keeping assumptions in mind, stations Senftenberg, Elsterheide-Geierswalde and Cottbus are selected for further analysis. Brief descriptions of selected stations are below in the Figure 3.1 and Table 3.2, 3.3, and 3.4.

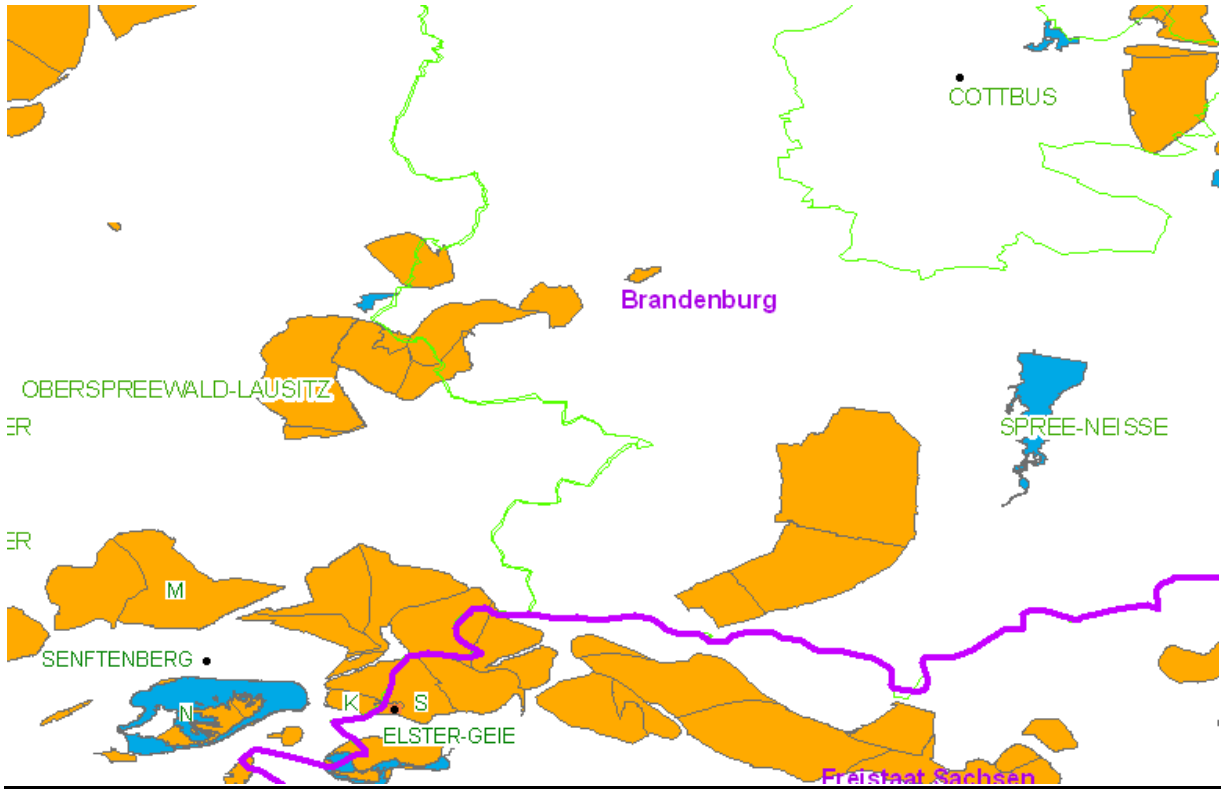

Figure 3.1: Location of stations for data analysis marked as black dot. M, N, K and S Stands for mining area Meuro, Niemtsch, Koschen and Skado. Orange and blue colors represent active mining and lake area respectively for the year 1990 (map not to scale).

Figure 3.1 represents the situation of different mining areas in Lausitz by the end of year 1990. Orange coloured area denotes area where mining was active during 1990's and blue coloured area represents lakes. The figure describes area controlled only by Vattenfall/LMBV Company. So, it is clear from the figure that by the end of 1990, mining area Meuro (M), Koschen (K) and Skado (S) were still active or open pit is formed. Niemtsch (N) mining area, located south of Senftenberg is a lake now. Selected stations are marked with black dots. Thick purple line is the boundary line separating states of Brandenburg and Sachsen. Stations Cottbus and Senftenberg

are in Brandenburg while station Elsterheide-Geierswalde is in Sachsen. The figure is not to scale as the motive here is just to give an idea about the location of different stations. It can be seen that station Elsterheide-Geierswalde lies within the mining area Koschen while other two are separate stations. Further details are given in Table 3.3 and 3.4.

Table 3.2: Geographical details of stations and data availability for precipitation parameter

Station Name	**Latitude (Degree)**	**Longitude (Degree)**	**From**	**Until**
Cottbus	51.78	14.32	1951	Today
Elsterheide-Geierswalde	51.5	14.12	1976	2006
Senftenberg	51.52	14.02	1969	Today

Table 3.2 shows the geographical location and availability of precipitation parameter for different stations. Latitude and longitude values are used in calculating distance between various stations. Stations Elesterheide-Geierswalde and Senftenberg are around 7 km away from each other and Cottbus is around 35 km away from both stations in the North-east direction. From Table 3.2 it can be seen that for Cottbus, precipitation values are available from the year 1951 until today and for Senftenberg from year 1969 until today. So, both these stations are still active and precipitation parameter is being measured. But at Elsterheide-Geierswalde station, precipitation data is available from the year 1976 until year 2006 only. Station Elsterheide-Geierswalde is not active anymore.

Table 3.3: Mining areas detail

Mining -Active	Area (km^2)	Water-filling	Area (km^2)	Volume (mio m^3)	Depth (m)
Elsterheide-Geierswalde					
Koschen (Geierswalde See)					
1955-1972	9.03	2004-2006	6.2	92	34
Skado (Partwitzer See)					
1940-1977	20.18	2004-2010	11.2	130	41
Senftenberg					
Niemtsch (Senftenberg See)					
1941-1966	15.44	1967-1972	12.16	80	26
Meuro (llse See)					
1965-1999	35.83	2006-2018	7.71	153	55

Table 3.3 gives details about various mining areas close to the three selected stations. From the table it can be seen that two mining areas (Koschen and Skado) surround station Elsterheide-Geierswalde. In Koschen, mining was active during year 1955 to 1972. It covered area of around 9.03 km^2. Water filling duration was from 2004 to 2006. After water filling process, this mining area is known as Geierswalde See (Lake) and is of capacity 92 mio m^3, covering area of about 6.2 km^2 with maximum depth of 34 m. In Skado, mining was active during 1940 to 1977. Mining covered area of about 20.18 km^2. Water filling duration was from 2004 to 2010. After water filling process, this mining area is known as Partwitzer See (Lake) and is of capacity 130 mio m^3, covering area of about 11.2 km^2 with maximum depth of 41 m. Station point Senftenberg is surrounded by mining areas Niemtsch and Meuro. Mining area Niemtsch was active from 1941 to 1966. It covered area of around 15.44 km^2. Water filling process started during 1967 to 1972. After water filling process, the mining area is known as Senftenberg See (Lake) and is of capacity 80 mio m^3, covering area about 12.16 km^2 with maximum depth of 26 m. Mining area Meuro was active during 1965 to 1999. It covered area of around 35.83 km^2. Water filling process started from 2006 and will be on until 2018. After water filling process, the

mining area will be known as Ilse See (Lake) and will be of capacity 153 mio m^3, covering area about 7.71 km^2 with maximum depth of 55 m.

Table 3.4: Station distance from nearest mining site

Station Name	**Distance (km)**
Senftenberg	
Niemtsch (Senftenberg See)	1.112
Meuro (Ilse See)	1.668
Elsterheide-Geierswalde	
Koschen (Geierswalde See)	0
Skado (Partwitzer See)	0.4
Cottbus	
Cottbus Nord	10

Table 3.4 gives the information of distance of various station points from neighboring mining areas. For this purpose the coordinates for the outline of various mining areas were obtained and then by using coordinates of stations, closest distance is measured. Station Senftenberg is around 1.112 km away from mining area Niemtsch and corresponding Lake Senftenberg See. It is also at a distance of about 1.668 km away from the mining area Meuro and corresponding Lake Ilse See. Station Elsterheide-Geierswalde is inside the mining area of Koschen and corresponding Lake Geierswalde See. It is also only 0.4 km away from the mining area Skado and corresponding lake Partwitzer See. Station point Cottbus is 10 km away from the neighboring mining area Cottbus-Nord.

From Figure 3.1 and Table 3.4 it is clear that station Elsterheide-Geierswalde is located within the mining area of Koschen. Senftenberg is located between a lake in the south and a mining area in the north, so it might exhibit effect of both lake and mining area. Cottbus is the only station which lies further away from the other two stations and its nearest mining area Cottbus-Nord is 10 km away. Cottbus station can

help in realizing the trend in precipitation and will serve as a reference station for further analysis. No measurement is available for the station Elsterheide-Geierswalde after year 2006. The reason for this is unknown but it is assumed that since this station lies in the mining region of Koschen and by year 2006 it was being filled with water and hence the measuring station was removed.

3.2 Results

Main purpose of the study is to study the change in precipitation parameter when a surface is transformed from mining to lake therefore the focus is on convective precipitation. For this purpose only summer period viz. June, July and August are considered. After closely examining the stations and the neighboring mining areas with the help of Figure 3.1 and Tables 3.1 to 3.4, station Elsterheide-Geierswalde is considered as a main station and further analysis will be carried out keeping this in mind. It is because as this station has a precipitation values during the time when mining area was transformed into the Lake and other stations also have data for this period.

It is clear from Table 3.4 that water filling process started in the Koschen region during 2004 to 2006. As data availability at station Elsterheide-Geierswalde is only until 2006 there are only three years which will include the effect of forming lake. So, in order to see how the formation of lake (from year 2004 to 2006) will affect the station Elsterheide-Geierswalde, 10 years time series for precipitation values are plotted in cummulative probability density function (CPDF). As only three years data are available with water filling, so only three more years previous to water filling years are used to plot 10 years CPDF. Hence three series will include the period before water is being filled and other three will include water filling period (transformation

into lake). First time series includes 10 year data from year 1992 to 2001, second series from years 1993 to 2002 and so on till last series which runs from 1997 to 2006. This will help in deducing the effect of lake during the time it is being formed. Same time series duration is chosen for stations Cottbus and Senftenberg to see the pattern of precipitation.

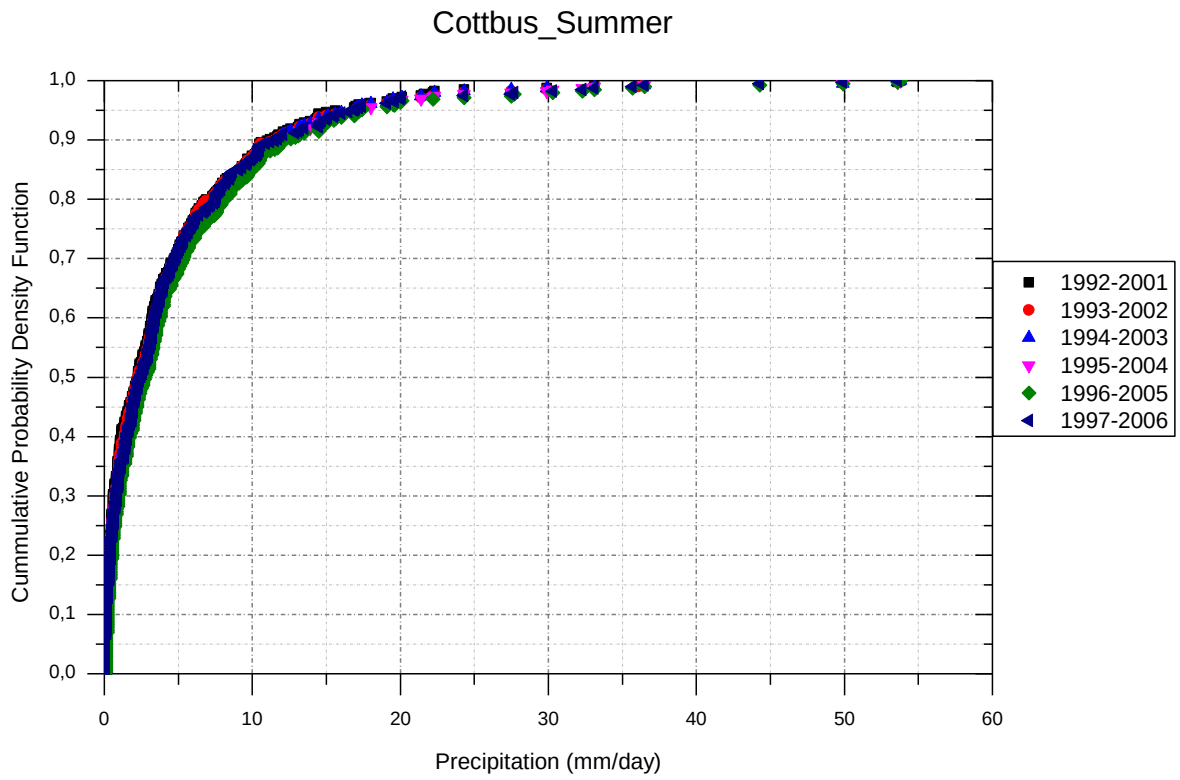

Figure 3.2: CPDF of 10 years running values for station Cottbus.

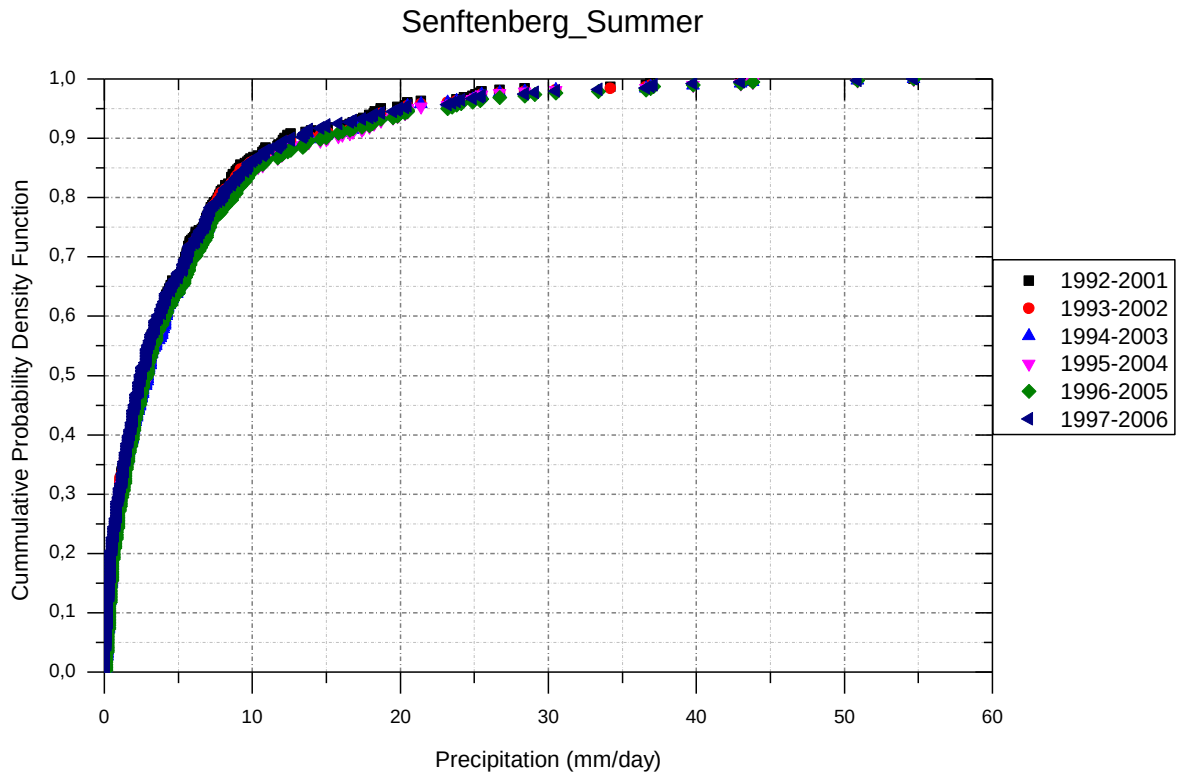

Figure 3.3: CPDF of 10 years running values for station Senftenberg.

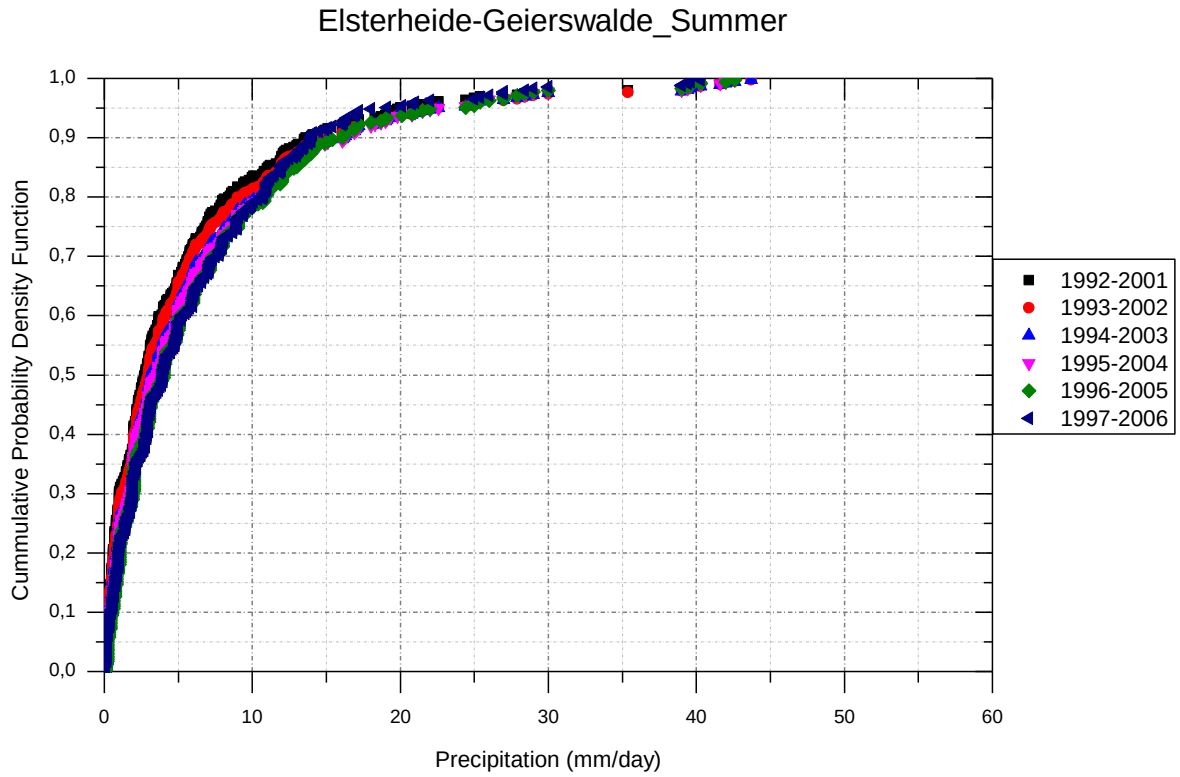

Figure 3.4: CPDF of 10 years running values for station Elsterheide-Geierswalde.

The aim here is to see whether the lake formation shows change in precipitation time series for station Elsterheide-Geierswalde in comparison to other two stations. If all three stations shows the same pattern after introduction of precipitation values from years 2004 to 2006 then it might be possible to say that the lake has no effect. If there is a difference in the pattern then the lake might have an effect. Figure 3.2 shows the 10 years precipitation CPDF plotted for station Cottbus. Cottbus station is 10 km away from the nearest mining area (Table 3.5). 10 years running values, plotted in CPDF, from 2001 to 2006 show almost same precipitation values when compared to other time series. No differences over these years can be seen from the graph. So, it can be said that introduction of successive years didn't bring change in precipitation pattern.

Figure 3.3 shows the 10 years precipitation values during summer season plotted in CPDF for the station Senftenberg. From the Figure, 10 years time series for daily sum of precipitation values show similarity. No clear difference in precipitation over different time series can be observed. So, it can be said that there was not much change in the precipitation values from Year 2001 to 2006. Station Senftenberg is located between an active mining area and a lake while station Cottbus is located far away from nearest mining area (see Table 3.5). Regardless the difference in locations the stations Senftenberg and Cottbus (Figure 3.2) exhibit similar behavior for the different time series. Figure 3.4 shows the 10 years precipitation values during summer season plotted in CPDF for the station Elsterheide-Geierswalde. It is known that during the years 2004 to 2006 mining area was transformed into Lake (Table 3.4) and station point was inside the mining area (Table 3.5). When the time series with years 2005 and 2006 are introduced, a small deviation in CPDF of precipitation can be observed. Ignoring the extreme high- and low values, precipitation amount

difference of about 1 mm/day to 3 mm/day can be observed among time series with and without lake filling processes (years 2004 to 2006). When the Figure 3.4 is compared to stations Cottbus and Senftenberg (Figures 3.2 and 3.3) then, it can be seen that in case of stations Senftenberg and Cottbus; precipitation patterns for different time series are identical even though they are from different geographical locations and have different surroundings (Tables 4.2 and 4.5). This is in contrast in the case of station Elsterheide-Geierswalde. Station Elsterheide-Geierswalde is located within the mining area (later lake) so it can be said that effect was limited over to the mining- and Lake Region. As, no other station is located near station Elsterheide-Geierswalde hence the effect in the vicinity cannot be calculated to see the extent of Lake's effect.

Even though station Elsterheide-Geierswalde shows slight deviation for the year 2006 (Figure 3.4) but owing to unavailability of parameters like temperature, wind profile etc. and absence of data after year 2006, further analysis is hard. Therefore, no further interpretation can be made for station Elsterheide-Geierswalde .

4. CCLM ANALYSIS

4.1 Introduction to Regional Climate Model

Generally with respect to modeled regions, there are two kinds of dynamic climate models. The Global Climate Models (GCMs) look at the climate from a global perspective while Regional Climate Models (RCMs) seek to resolve the climate and possible changes in specific areas in more detail. GCMs have one big shortcoming which is their inability to obtain information on regional and local scales because of their coarser resolution. RCMs in contrast to GCMs work on finer resolutions and therefore are able to resolve climate statistics which are not represented in global models. This indeed makes RCMs a necessary asset in climate science. To show the usefulness of RCMs, the following examples are highlighted by Wang et al. (2004):

- Land-atmosphere interactions: RCMs are better in resolving land surface heterogeneities and in representing associated feedback processes with the atmosphere.
- Topographic effects on regional climate: Regional climate may be orographically forced and regulated, and needs to be resolved accordingly.
- Effects of land use change on regional climate: High resolution RCMs are able to incorporate spatially highly inhomogeneous land use changes.

RCMs are able to improve the information contents that are obtained from GCM simulations alone because of their potential to resolve land-sea contrast, complex terrain and land use in more detail, eg., near coastal regions or mountains (Laprise 2006). Further, data produced by RCMs is used by other modeling groups focusing on various aspects of climate change and its consequences in the field of impact assessment or resource management (Finger et al. 2011).

In this thesis, simulations are analyzed which have been performed with the climate version CLM of the ‘’Local Model’’ (LM). The LM was originally developed by the German Meteorological Service (DWD) (Steppeler et al., 2003) and is now further developed by COSMO, the consortium of national weather services for small scale modelling. The CLM (Böhm et al., 2006) was developed by the CLM Community, an international network of scientists from universities and research centers (http://www.clm-community.eu). In this time, several projects have used the CLM in their studies. CLM has already been validated for different purposes and has shown to perform comparably to other state-of-the-art RCMs (Kotlarski et al., 2005, Frei et al., 2006, Jacob et al., 2007). General tendency to refine horizontal and vertical resolution is in progress. Its evaluation is an essential task in the climate modeling community.

4.2 Experiment Setup

For the simulation, climate version of Cosmo CLM (CCLM) has been used. CCLM model is configured and simulated by Mr. Michael Woldt (contact: woldt@tu-cottbus.de) but post processing has been carried out by the author of the present study. To observe effect of LULC change on precipitation, three different kinds of simulations have been carried out i.e.

4. VAT010: This simulation represents the potential vegetation of the whole domain. This describes the pre mining stage of the area when there was no mining.
5. VAT020: This simulation represents the introduction of Lake Points in the model domain. This describes the situation of area post mining, when Lakes are formed.

6. VAT030: This simulation represents the mining time (without vegetation). This describes the phase when mining is in progress.

Model domain is same in all the three different simulations.

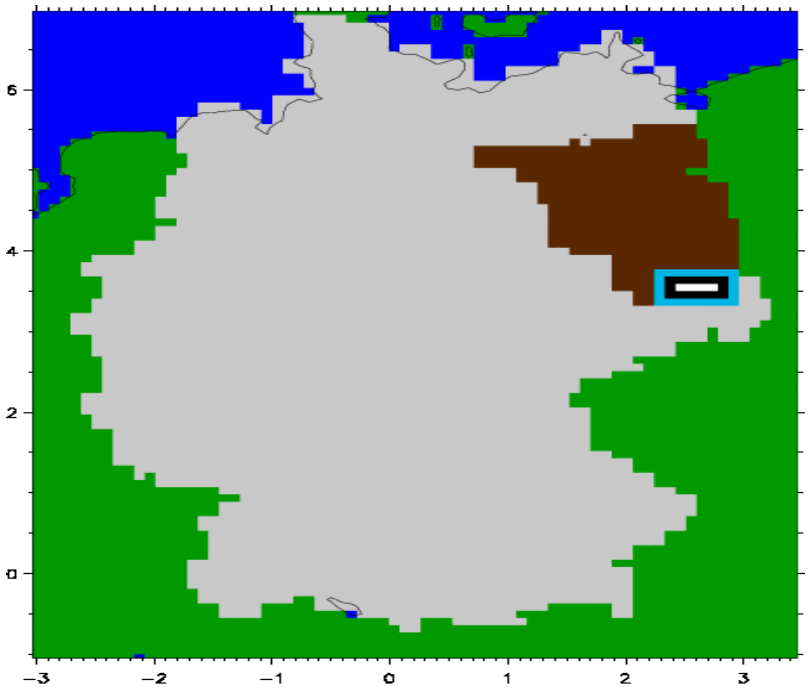

Figure 4.1: Study area of model domain in the CCLM simulations. Green, brown, deep blue and grey colors represents land, Brandenburg state, water bodies and Germany respectively. White rectangle represents 4 grid cells as lake and surrounding black and light blue rectangles represent grid cells surrounding Lake.

Figure 4.1 shows the model domain consisting of area of study in the simulations VAT010, VAT020 and VAT030. The domain shows the outline of Germany in the grey color. Green- and dark blue colors represent land- and water bodies surrounding Germany respectively. Brown color represents federal state of Brandenburg in Germany. The only difference among the three simulations is the white rectangular box within black- and blue rectangular boxes. The white rectangular box consists of four grid cells which represent the changing landscape, lake in VAT020 simulation and mining in VAT030 simulations. These points are in the Brandenburg state of

Germany and representing mining area Welzow and its surrounding. Black- and light blue rectangles surrounding the white rectangle represent grid cells at a distance of 10km and 20 km corresponding to grid cells in white rectangle respectively.

Table 4.1: Model configuration

Parameter	Value
Number of grid cells in X direction	252
Number of grid cellst in Y direction	260
Number of grid cells in Z direction	40
Horizontal resolution	10 km x 10 km

Table 4.1 shows the model configuration used in all the three simulations. Whole model domain (Figure 4.1) is divided into square grid cells, each of size 10 km in either direction. Area under each grid cell is 100 km^2. Network of grid cells are comprised of 252 grid cell boxes in X direction (West to East) and 260 in the Y direction (North to South) and 40 layers in Z direction (vertical).

All the simulations are carried out for 10 years, starting from January 1st 1989 till December 31st 1998. As four grid cells (white rectangle in Figure 4.1) represent different LULC change in three simulations so, difference among these three simulations is the surface characteristics of these four grid cells only.

The coupling between the atmosphere and the underlying surface is modeled by a stability and roughness-length dependent surface flux formulation using SVAT (Soil Vegetation Atmosphere Transfer) model. These surface fluxes constitute the lower boundary conditions for the atmospheric part of the model. Their calculation requires the knowledge of the temperature and the specific humidity at the ground. In this work, the coupling of ground processes and corresponding atmosphere is accomplished using multi layer soil model; TERRA_LM. The task of soil model is to

predict surface temperature and humidity by the simultaneous solution of a separate set of equations which describe various thermal and hydrological processes within the soil. More can be read in CCLM documentation (http://www.cosmo-model.org/content/model/documentation).

Orography, land cover and associated vegetation parameters as well as soil characteristics are the key information in SVAT schemes widely applied in atmospheric models in parameterization of surface exchange processes (Smiatek et al. 2008). Apart from seasonal changes, e.g. in the Leaf Area Index (LAI), the geospatial input is usually kept constant in a simulation and can therefore be considered as time invariant. The PrEProcessor (PEP) is intended to serve as a preprocessor of the time invariant boundary data for the COSMO model in climate mode. It fully integrates the existing DWD preprocessor EXPAR (Doms et al., 2005) providing input data on rotated coordinates (specified by the user) and facilitates access to additional geospatial data and processing routines. PEP is externally prescribed data, characterizing soil and surface conditions of every grid cell for a specific simulation (in this study for simulations VAT010, VAT020 and VAT030). Corresponding to changes in 4 grid cells, equivalent changes have been accounted for in the PEP files of different simulations and are shown in Table 4.2 below.

Table 4.2: List of all time invariant lower boundary variables for the four grid cells

Parameter (unit)	VAT010	VAT020	VAT030
PLCOV_MX	0.74 /0.77 /0.68 /0.63	0 /0 /0 /0	0 /0 /0 /0
PLCOV_MN	0.61 /0.62 /0.51 /0.55	0 /0 /0 /0	0 /0 /0 /0
LAI_MX	2.85 /2.79 /2.35 /2.46	0 /0 /0 /0	0 /0 /0 /0
LAI_MN	0.91 /0.91 /0.69 /0.78	0 /0 /0 /0	0 /0 /0 /0
ROOTDP (m)	0.73 /0.74 /0.70 /0.62	0 /0 /0 /0	0 /0 /0 /0
HSURF (m)	102.467 /113.105 /113.627 /115.578	Same as VAT010.	25 m deeper.
FR_LAND	0.939 /0.895 /0.970 /0.963	0 /0 /0 /0	1 /1 /1 /1
Z0 (m)	0.52 /0.4 /0.27 /0.52	0 /0 /0 /0	0.03 /0.03 /0.03 /0.03
SOILTYP	5 /5 /5 /5	9 /9 /9 /9	3 /3 /3 /3
FOR_D	0.07 /0.07 /0.04 /0.03	0 /0 /0 /0	0 /0 /0 /0
FOR_E	0.40 /0.33 /0.13 /0.35	0 /0 /0 /0	0 /0 /0 /0
FR_LAKE	Not applicable.	1 /1 /1 /1	Not applicable.
DEPTH_LK (m)	Not applicable.	25	Not Applicable.

We know that the only differences in the PEP file among various simulations are the four grid cells shown as white rectangle in Figure 4.1, so the Table 4.2 shows the changes made in values of these four grid cells for simulations VAT010, VAT020 and VAT030 only. These changes are made in the original external parameter file NHCM_extpar.nc (used for VAT010 simulation) for simulations VAT020 and VAT030. Values shown in Table 4.2 are tabulated from West to East direction of four grid cells. PLCOV_MX stands for maximum plant cover and represents area during the time of vegetation. Likewise PLCOV_MN stands for minimum plant cover and represents the area during the time of rest. Its value shows the percentage of area covered with vegetation in a grid cell, where value of 1 stands for 100% and 0 for 0%. Value for simulation VAT020 and VAT030 is set to 0 as in either case no vegetation is present. LAI_MX and LAI_MN stand for Maximum and Minimum Leaf Area Index respectively. It represents the ratio of area of upper surface of leaf to the area under the vegetation for the period of vegetation time and time of rest respectively. For simulation VAT020 and VAT030 value is again set to 0 as no vegetation is present.

ROOTDP stands for root depth and it shows how deep roots are present in this area. Values are in meter (m). As for simulation VAT020 and VAT030 no vegetation is present so root depth is 0 meters. HSURF stands for height of surface topography. It is a measure of altitude of grid cells. Simulation VAT020 has same values as VAT010 as these four grid cells are transformed into a Lake so instead of soil now water has filled its space. But simulation VAT030 has a pit of 25 meter so its height in the four grid cells is 25 meters less than in VAT010 simulation. Parameter FR_LAND represents the fraction of land in the grid cell. A value of 1 means that grid cell has 100% covered with soil. As there is only a pit present in simulation VAT030, so its contribution is 1 for all four grid cells while in VAT020 water is present so it has a value of zero. A value greater than 0.5, is treated as grid cell fully covered by land fraction. Z0 stand for surface roughness. It affects the intensity of mechanical turbulence and the fluxes of varies quantities above the surface. VAT020 has zero value because of the smooth surface of water. Parameter SOILTYP stand for the soil type present in the grid cell. For VAT010 SOILTYP is 5 for all four grid cells which means soil is Loam. For simulation VAT020 SOILTYP 9 stands for water and for VAT030 simulation SOILTYP 3 represents sand in all the four grid cells. Parameters FOR_D and FOR_E stand for, fraction of ground covered by deciduous and evergreen forest respectively. Simulation VAT020 and VAT030 has no trees hence value is zero. Parameter FR_LAKE represents the fraction of lake in a grid cell. A value of 1 means, grid cell is 100% lake and 0 means no lake. Lake is only present in VAT020 simulation. DEPTH_LK stands for depth of lake and which is 25 m in all the four grids of VAT020 simulation.

Lake Model is switched on only for VAT020 simulation. It’s the first mode version where this lake sub-model was available and could be applied for the first time. Rest

of the configuration and forcing data is same for all the three simulations. The lake model termed Flake (Mironov 2008) is capable of predicting the vertical temperature structure and mixing conditions in lake of various depths on the time scales from few hours to many years.

4.3 CCLM Results

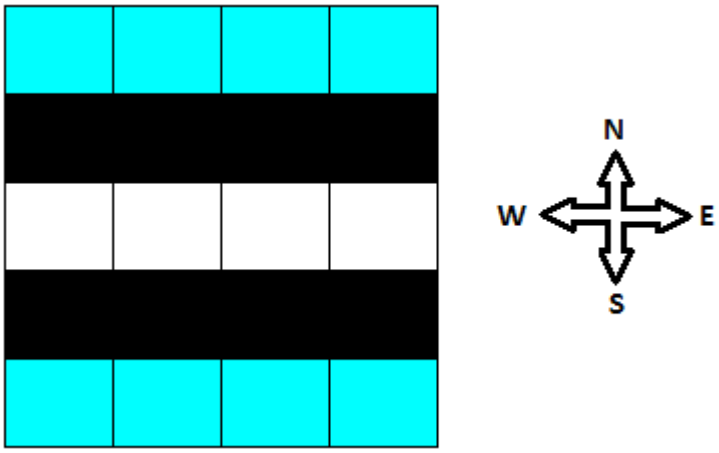

Figure 4.2: Magnification of investigated area (white rectangle) and area around it as shown in Figure 4.1. Grid cells from CCLM simulation in and around mining area Welzow.

Figure 4.2 is the magnified view of grid cells shown in white, black and blue rectangles in Figure 4.1. It shows mining area Welzow along with its surrounding area in North- and South directions. In Figure 4.2, square boxes represent CCLM grid cells, each of dimension 10 km X 10 km. Grid cells in white color are those which will be changed into lake and sandy pit in CCLM simulations VAT020 and VAT030 respectively. Black- and light blue colored grid cells represent areas which are not altered (PNV) and are 10km and 20 km away from corresponding central grid cells in North- and South directions respectively.

It is clear from the Figure 4.2 that in the model simulation, lake is oriented from West to East. As wider portion of Lake (40 km) is spread on the North- and South directions, it is thought to start investigating the lake effect on nearby areas in these

directions. In order to investigate the impact of LULC change and extent in the regional area, keeping knowledge gathered from previous chapters 1 and 2; it is decided to include grid cells as far as 20 km each in the north- and south directions from the central grid cells. So, apart from the four main grid cells (white colored in Figure 4.2) eight more grid cells each in north- and south directions are selected for further analysis.

For further analysis average of 4 grid cells (each row in Figure 4.2) are considered. Four grid cells in white color (Figure 4.2) are averaged and are called as Central in below mentioned analysis. Likewise average of four grid cells shown in black- and light blue colors in Figure 4.2 are made and accordingly termed as North20, North10, South10 and South20 based on their distances from the Central grid cell for further analysis.

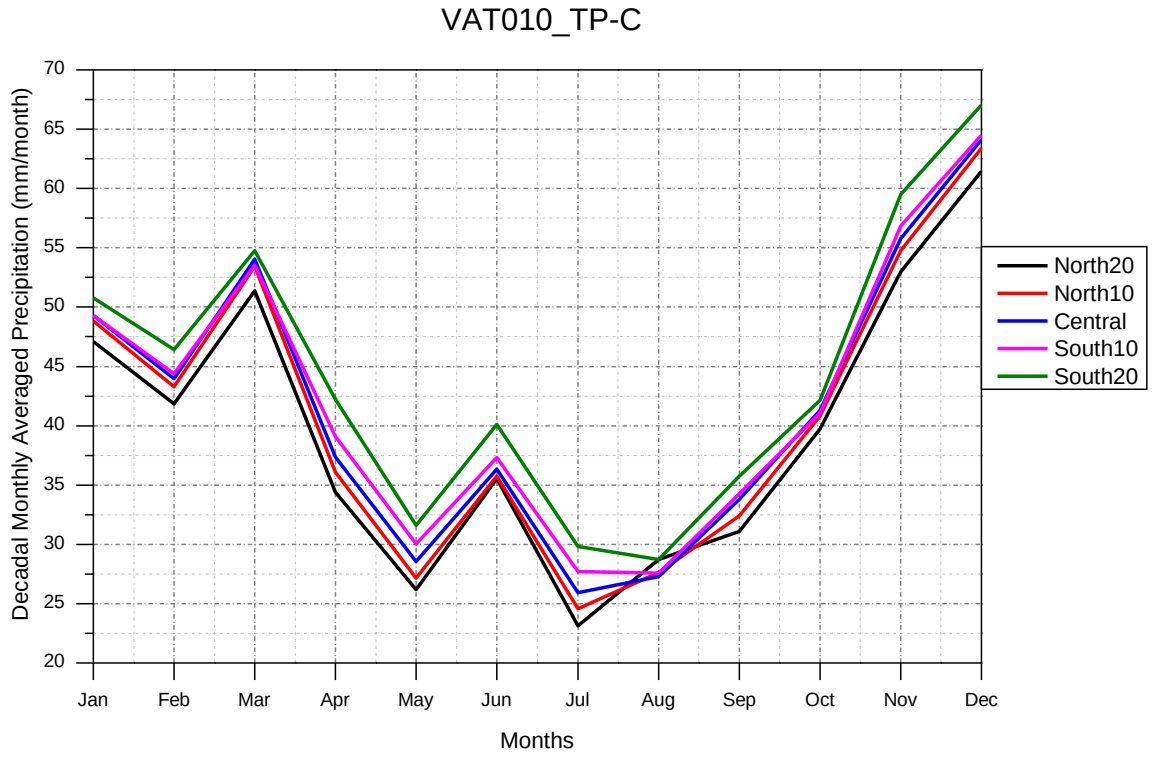

Figure 4.3: Decadal averaged large scale precipitation (mm/month) for VAT010 simulation.

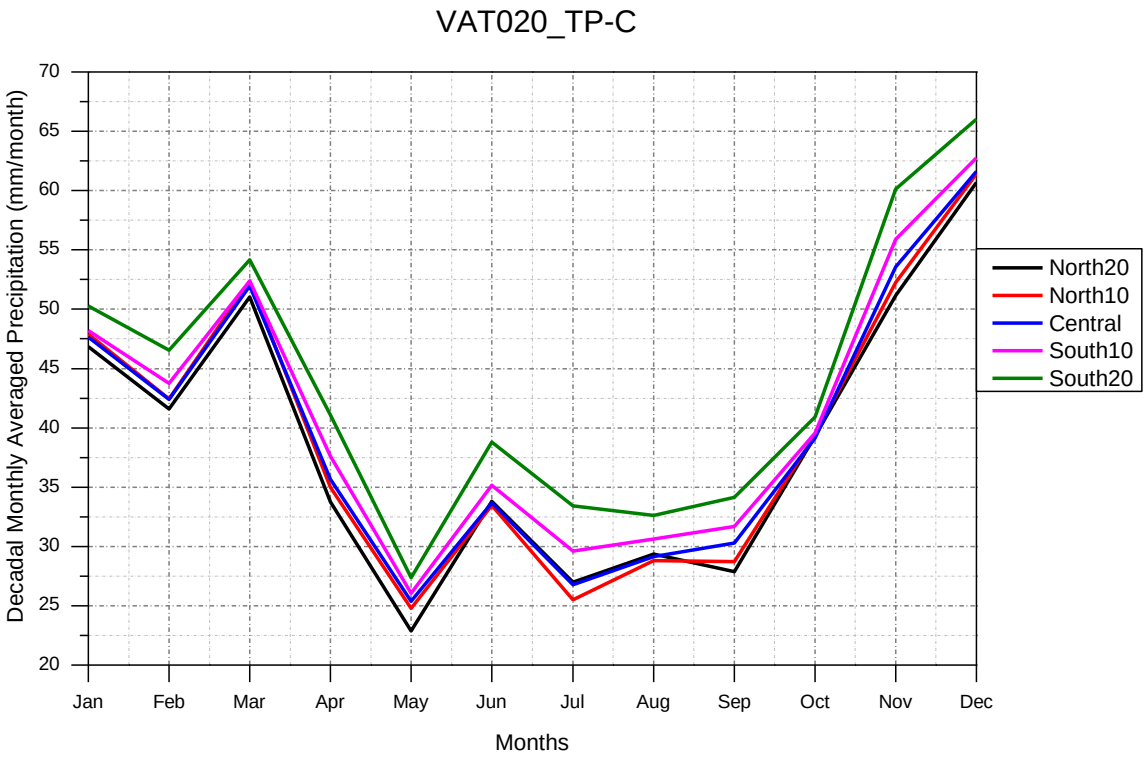

Figure 4.4: Decadal averaged large scale precipitation (mm/month) for VAT020 simulation.

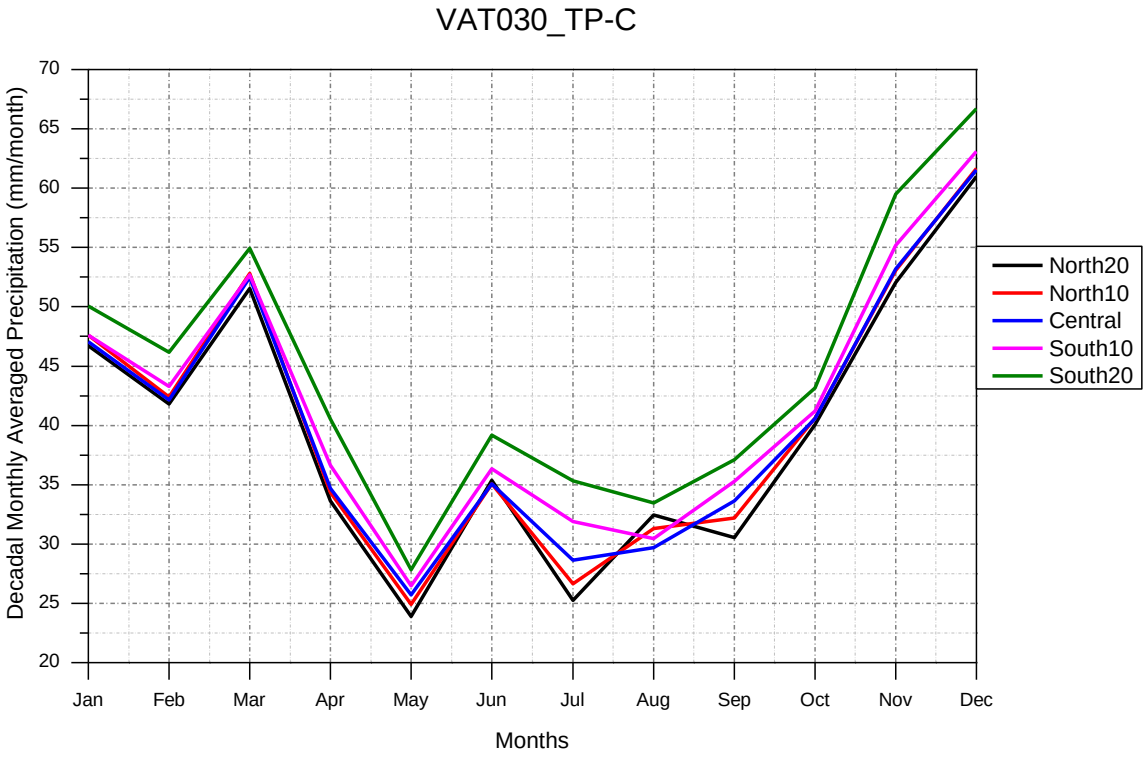

Figure 4.5: Decadal averaged large scale precipitation (mm/month) for VAT030 simulation.

Figures 4.3 to 4.5 show decadal monthly averaged sum of total precipitation (without convective precipitation and henceforth will be referred as TP-C throughout the thesis) for three simulations. In all simulations, precipitation gradient from North- to South directions can be observed. More precipitation is observed in the south than in north of the Central grid cell and this precipitation variation behavior is observed in all the three simulations. Maximum difference among grid cells appeared in July, with a difference of 8 mm/month in VAT010 simulation and of 10 mm/month in VAT020 and VAT030 simulations. For rest of the months maximum difference is within 8 mm/month.

In order to further examine the effect of LULC change among three simulations for TP-C parameter, differences between simulations are made. As it is known that, VAT010 simulation represents the potential natural vegetation (see Chapter 4.2), so it is treated as a reference for other two simulations. As, simulations VAT020 and VAT030 represents the altered version of VAT010, so it is expected that when they will be compared to the reference, they will incorporate the LULC change effect.

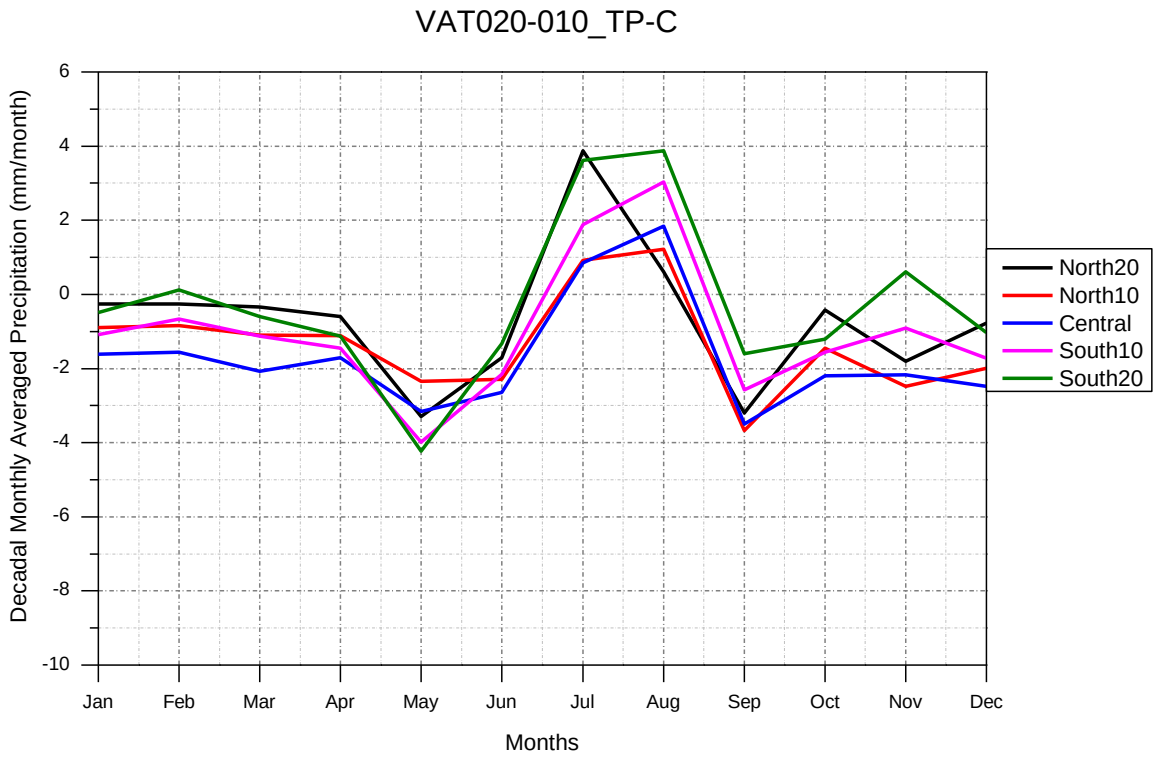

Figure 4.6: Difference of Decadal averaged large scale precipitation (mm/month) between VAT020 and VAT010 simulations.

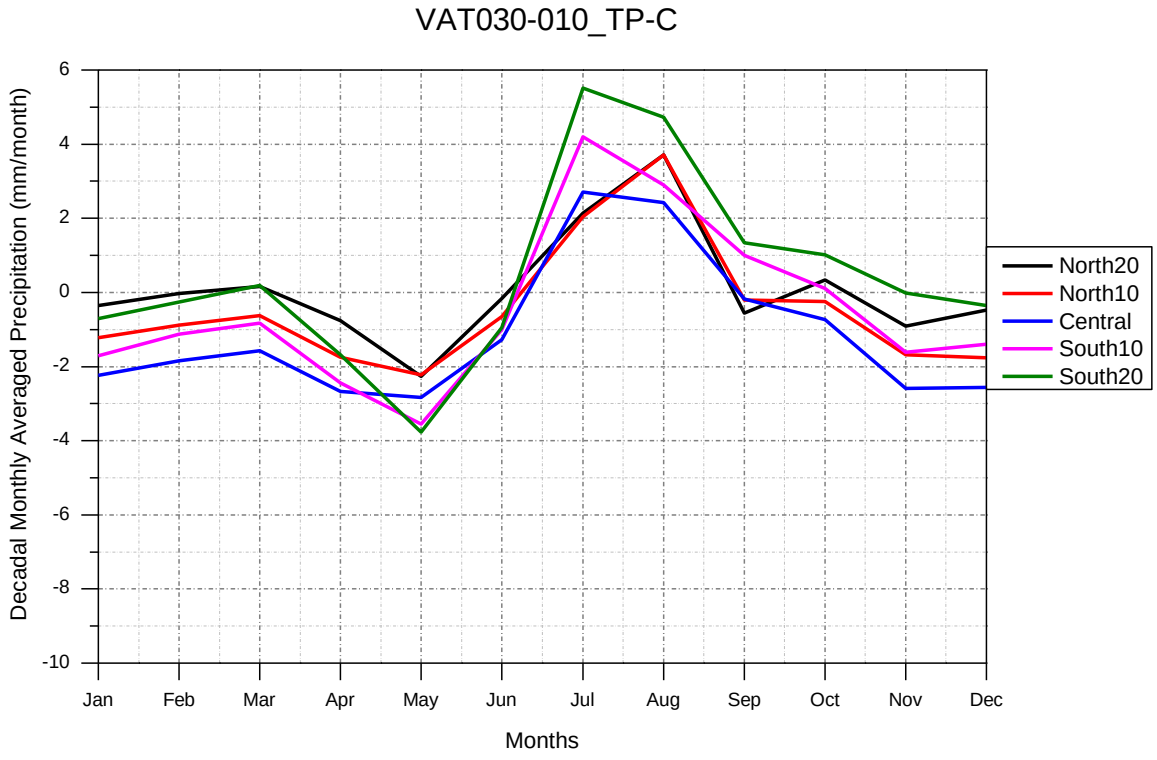

Figure 4.7: Difference of Decadal averaged large scale precipitation (mm/month) between VAT030 and VAT010 simulations.

Figures 4.6 and 4.7 show the decadal monthly averaged TP-C values differences in VAT020 and VAT030 simulations to the reference simulation (VAT010). From the figures it is clear that only during late summer; maximum difference of about 4 mm/month is observed in precipitation values moving from south to north but for rest of the year maximum differences are well within 2 mm/month. So, for TP-C parameter all three simulations have more or less same value moving from south to north. During late summer; higher TP-C values are observed in VAT020 and VAT030 simulations than in VAT010 simulation but the difference is small. Hence it can be said that TP-C parameter has more or less same values in all the three simulations. Further same process is carried out for convective precipitation and is shown below. Legends description is same as in the case of simulations for TP-C parameter discussed before.

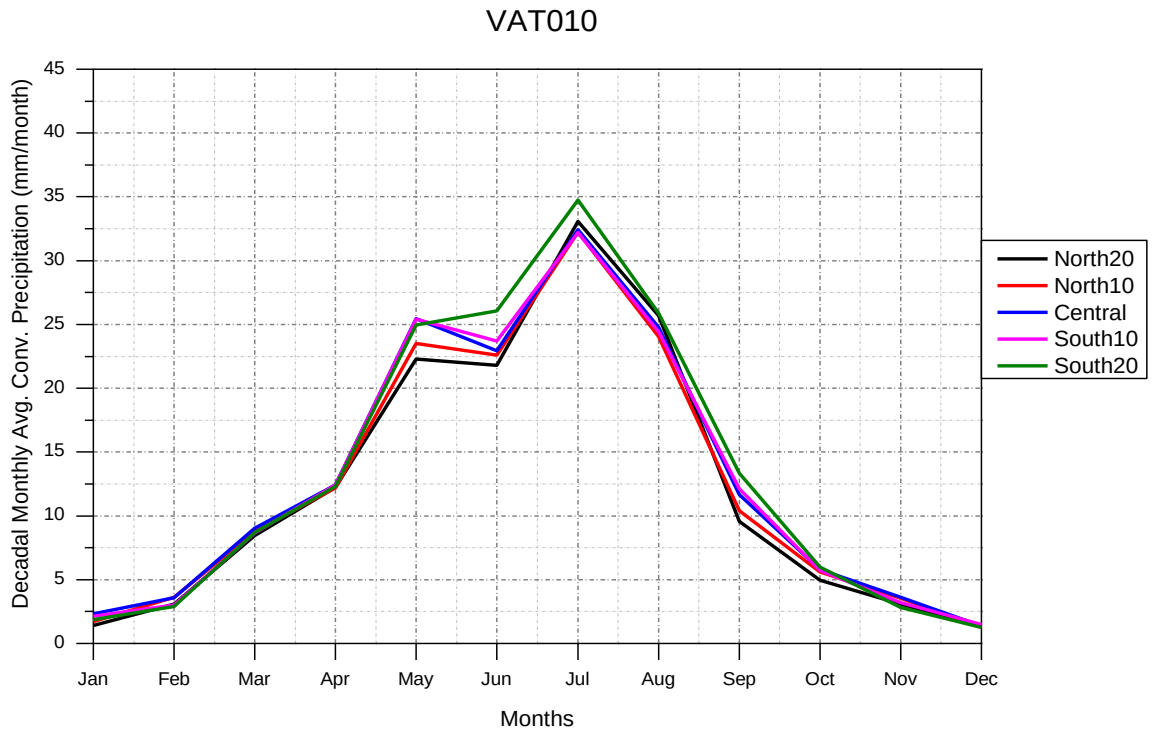

Figure 4.8: Decadal monthly average of convective precipitation (mm/month) for VAT010 simulation.

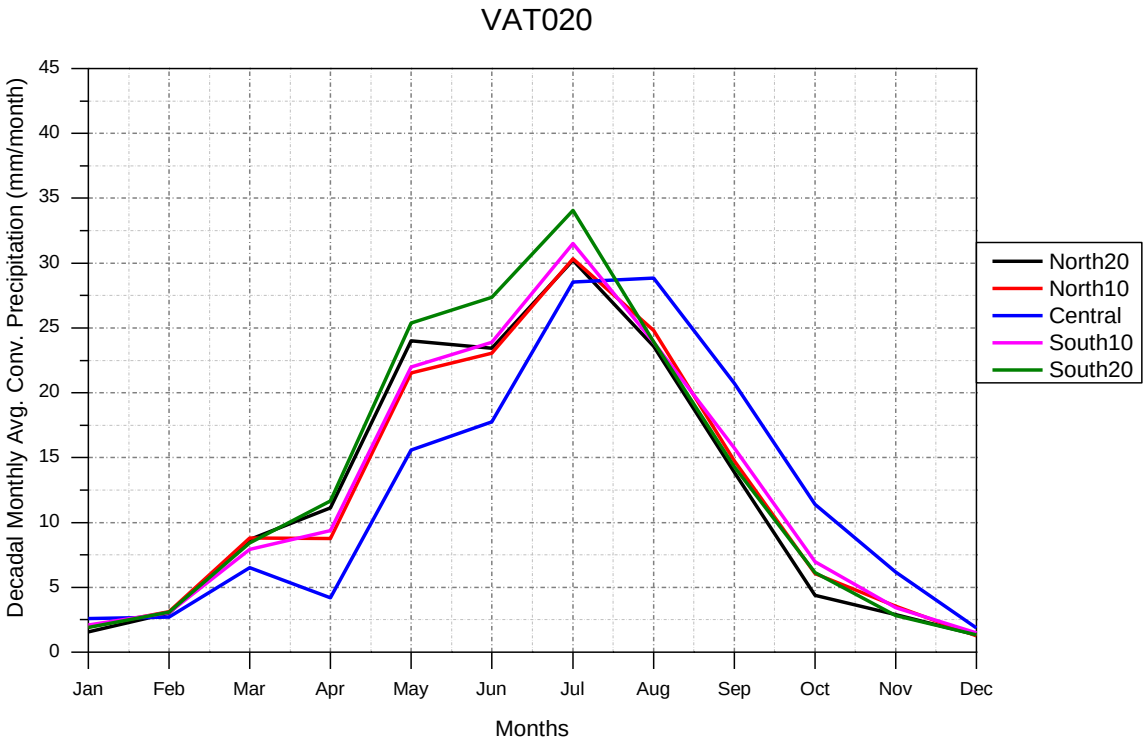

Figure 4.9: Decadal monthly average of convective precipitation (mm/month) for VAT020 simulation.

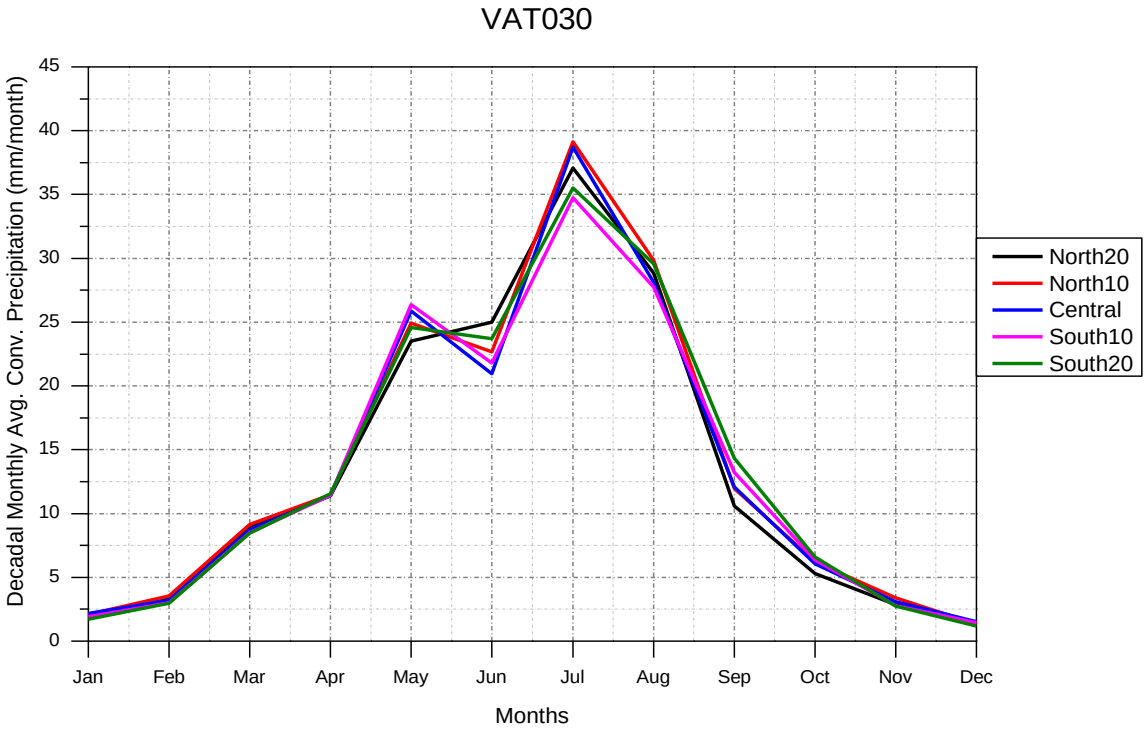

Figure 4.10: Decadal monthly average of convective precipitation (mm/month) for VAT030 simulation.

Figures 4.8 to 4.10 show decadal monthly averaged convective precipitation for different simulations. In simulations VAT010 and VAT030, either there is no precipitation gradient from south to north direction or shows little during months of June, July and September. Maximum convective precipitation difference observed among grid cells is within 5 mm/month. Hence in simulations VAT010 and VAT030 during most of the months same amount of convective precipitation is observed in North-South direction. But in case of VAT020; the Central grid cell shows maximum difference of about 10 mm/month during May and June and for most of the months there exists a difference of 5 mm/month from other grid cells. Even though south and north grid cells have maximum precipitation gradient below 5 mm/month (excluding Central) but introduction of Central has shown more variation in convective precipitation. To further examine the effect of LULC, differences among simulations are carried out as done in case of TP-C parameter. Further explanation is given in difference plots.

Table 4.3: Maximum variability and uncertainty in the model domain

Month	**VAT020-VAT010 (mm/month)**		**VAT030-VAT010 (mm/month)**	
	variability	**uncertainty**	**variability**	**uncertainty**
January	±3	±0.5	±2	±0.3
February	±3	±0.5	±2	±0.3
March	±4	±0.8	±3	±0.5
April	±5	±1	±4	±0.7
May	±6	±1.5	±5	±1
June	±9	±2	±9	±1.8
July	±13	±3	±11	±2.2
August	±13	±3	±10	±2
September	±9	±2.3	±5	±1
October	±6	±1.6	±3	±0.5
November	±4	±1	±3	±0.5
December	±3	±0.5	±2	±0.3

Uncertainty of the convective precipitation is carried out using method mentioned in Chapter 2.3. In order to introduce the expected variance of measured convective precipitation, model domains of size 500 km from the lake in all geographical directions are considered, in VAT020-VAT010 and VAT030-VAT010 simulations. This domain is considered to be area having no immediate influence from the lake. The maximum difference occurred is chosen to be the variance expected among different grid cells (Table 4.3). Lake grid cells and surrounding 30 km were excluded in determining expected maximum variability. MCS is carried out making this value the highest and lowest boundary limit for the variance in mean value with the help of random number generator. This is done for each month separately. More explanation is given in Chapter 2.3. Table 4.3 gives the information about the variability assumed for MCS and uncertainty calculated for simulations VAT020-VAT010 and VAT030-VAT010 using equations 8 and 9.

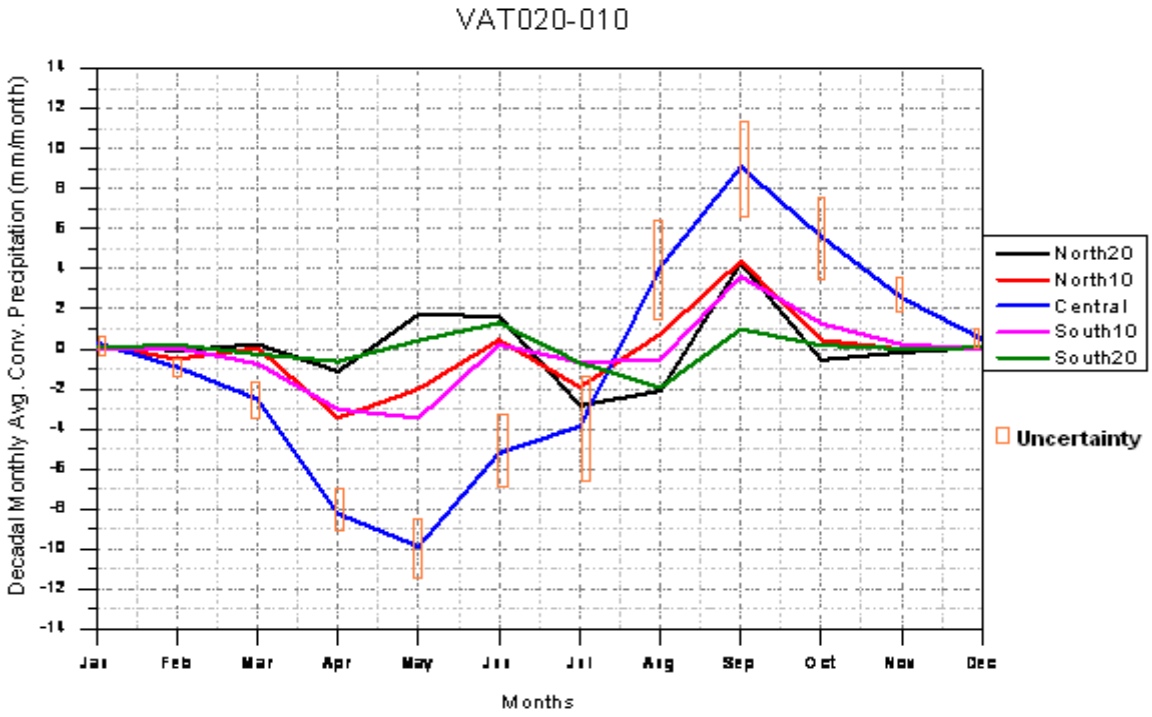

Figure 4.11: Decadal difference of monthly averaged convective precipitation (mm/month) between VAT020 and VAT010 simulations.

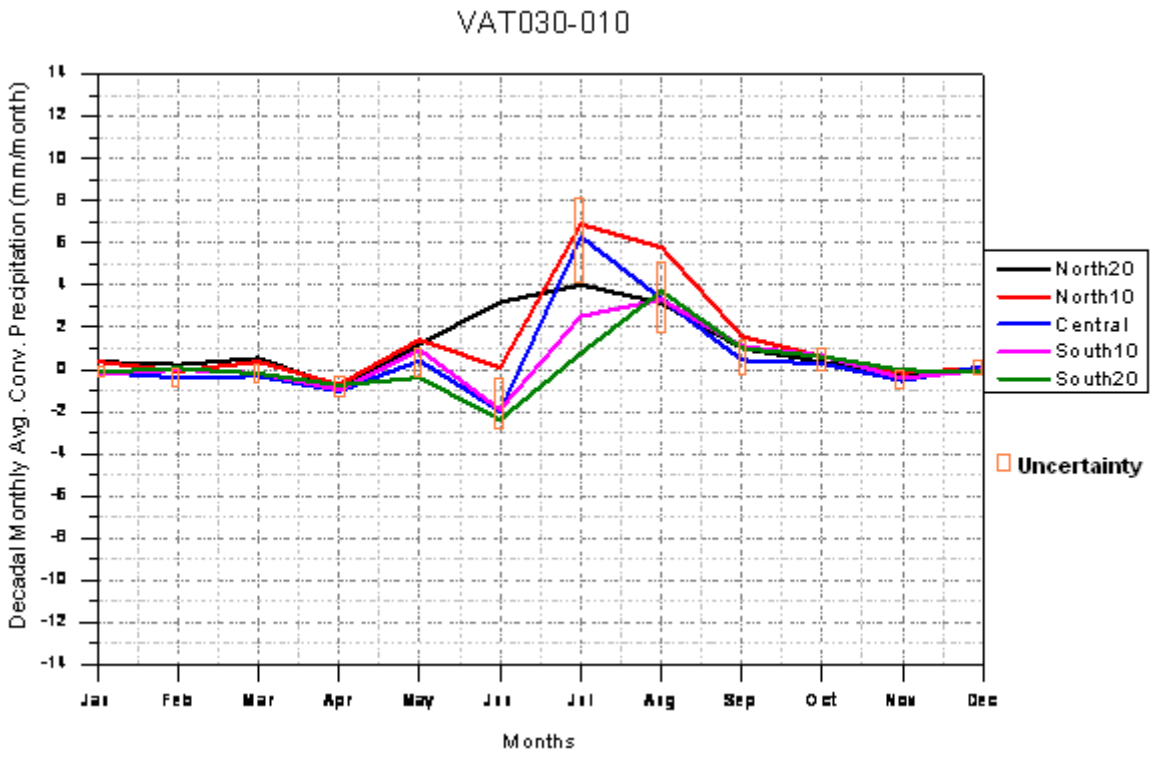

Figure 4.12: Decadal difference of monthly averaged convective precipitation (mm/month) between VAT030 and VAT010 simulations.

Figures 4.11 and 4.12 show decadal averaged convective precipitation values differences in VAT020 and VAT030 simulations to the reference simulation (VAT010). Figures 4.11 and 4.12 represent the area under study. In Figure 4.12 uncertainty is shown for the Central grid cells only for readability of the graph. Maximum uncertainty value is observed during summer of around ±2.2 mm/month and for rest of the year value is within ±1 mm/month. Maximum difference observed among grid cells is during summer of about 4 mm/month in June and 6 mm/month during August. Uncertainty range during summer has reduced the maximum difference among grid cells to be around ±2 mm/month; hence probability of these values to be same is more likely. Hence from Figure 4.12 it can be said that simulations VAT010 and VAT030 might have similar values for convective

precipitation and that mining phase (VAT030) shows no effect on convective precipitation.

But unlike Figure 4.12, in Figure 4.11 more difference in convective precipitation values among Centre grid cells can be seen, which is negative during late winters and spring and positive during summer, fall and early winter. Maximum difference, greater than 10 mm/month can be seen during May and difference of 6 mm/month can be observed for most of the months. Excluding Central grid cell, among rest of the grid cells maximum difference is well within ±4 mm/month throughout the year. In the figure maximum uncertainty range is found to be ±3 mm/month during July and August. But as Central grid cell in Figure 4.11 show higher values, hence it can be said that Central in VAT020 and VAT010 simulations do not show same convective precipitation values. This means that more precipitation is observed for Central grid cell during summer and less precipitation during late winters and fall in VAT020 simulation than in VAT010 simulation.

Explanation for the difference in Central grid cell values with other grid cells in Figure 4.11 is because of the large heat capacity of the Lake. After winter time most of the solar radiations goes into warming lake and hence little is available for evaporation or sensible heating of the atmosphere hence less moisture available for precipitation. Lake heat peaks in late summer and early fall, after which release of the stored energy commences. In late fall and early winter, when solar radiation is small, this energy is released as latent and sensible heat fluxes to the atmosphere and hence more moisture for precipitation. This can be seen clearly from Figure 4.13. Similar effects have been observed during studies of Great Slave Lake (Figure 2.4, Blanken et al. 2000, Schertzer 1997 & Schertzer et al. 2000). Figure showing surface energy for other grids can be found in Appendix A.

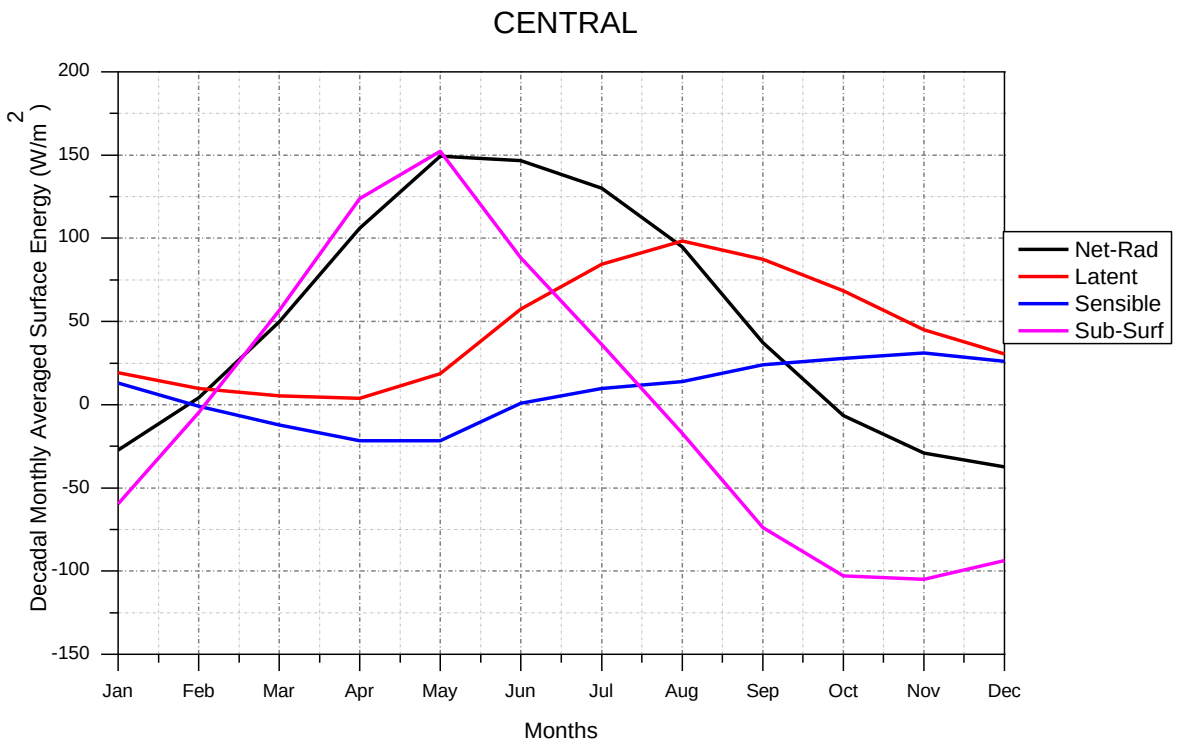

Figure 4.13: Decadal monthly averaged surface energy (W/m^2) at central of VAT020 simulation.

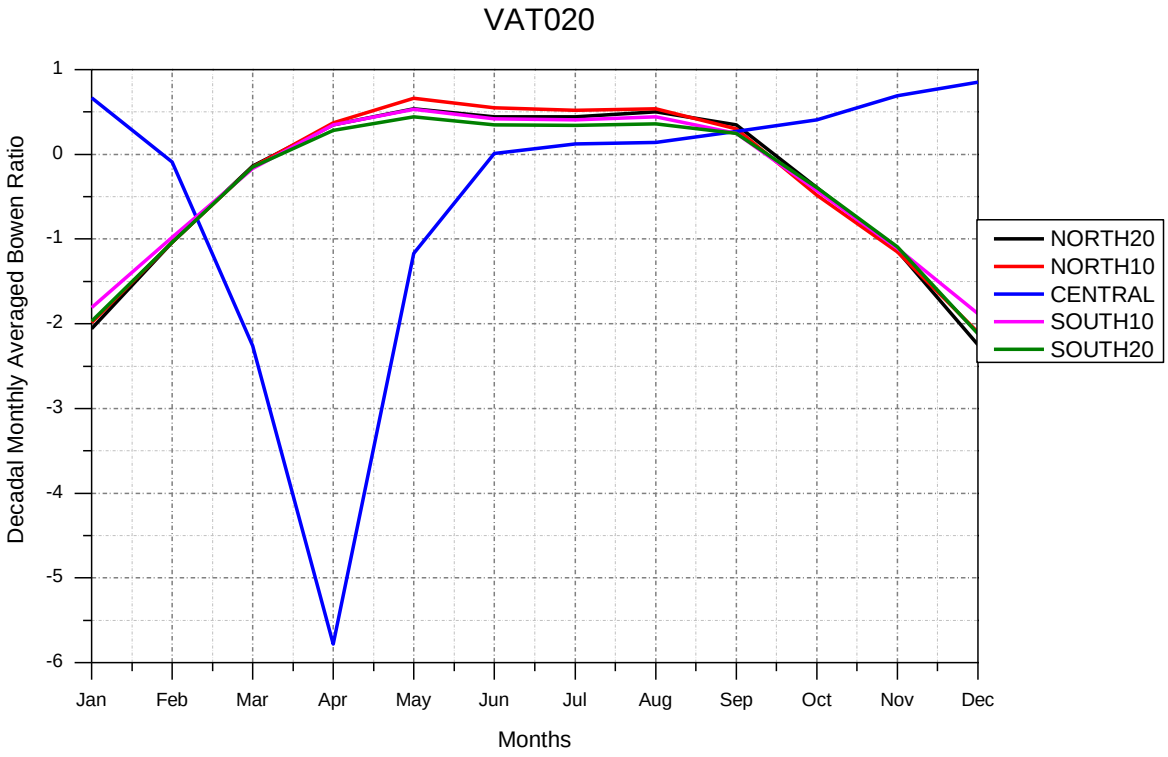

Figure 4.14: Decadal monthly averaged Bowen ratio of VAT020 simulation.

Form Chapter 2.1 we know that Segal et al. (1995) found out that with smaller Bowen ratio, the thermodynamic potential for deep cumulus convection increases. And from Figure 4.14 it can be seen that during summer and fall; Bowen ratio is small and hence might have lead to more convective precipitation over lake than other grid cells. Negative Bowen ratio occurs because of negative sensible flux which is corresponding to the findings of Rouse et al. (2002) where he showed the similar behavior during study of Great Slave Lake (Figure 2.4).

So far from the analysis and Figures 4.11 and 4.12 introduction of lake has shown maximum precipitation variation of about 10 mm/month in Central grid cell which is high in comparison to other grid cells in North- and South directions where it was about 4 mm/month. But this was only when maximum observed uncertainty among grid cells is within ±3 mm/month. So it can be said that Lake's presence has shown small change in convective precipitation but its effect is limited to lake only.

Even though wider portion of lake is oriented in the South- and North directions but it will also be interesting to see its influence in East and West directions. So, for further analysis, inclusion of other parameters wind speed and direction knowledge will help in better understanding the influence of Lake.

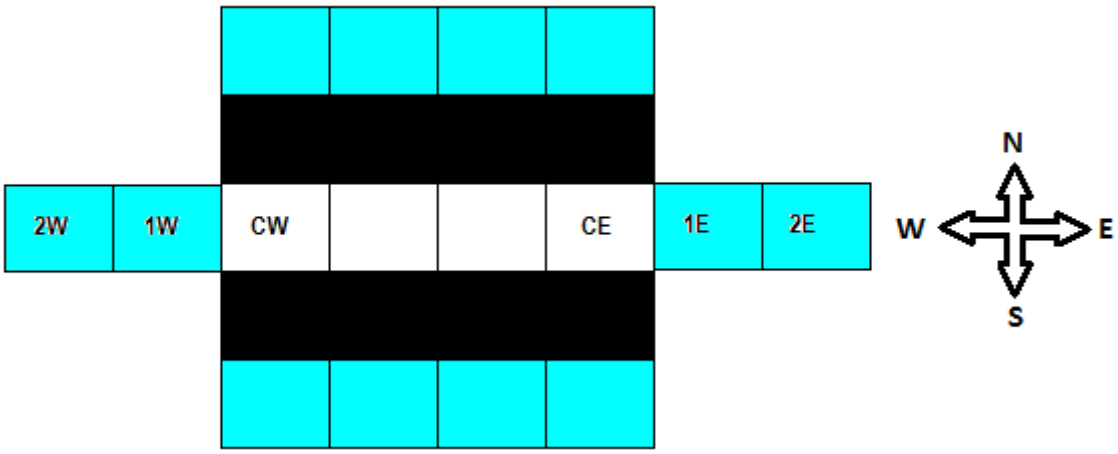

Figure 4.15: Grid cells used for wind dependent precipitation analysis.

Figure 4.15 is an extended form of Figure 4.2 in the East- and West directions. It represents the same grid cells with Central grid cell in white color as was in the case of Figure 4.2. In the figure CW (Centre West) stands for grid cell which is part of Central grid cell but is on the extreme West side and similarly CE (Centre East) stands for grid cell in the extreme East of Central grid cell. 1E and 2E stands for grid cells 10 km and 20 km away from CE grid cell in East direction and 1W and 2W stands for grid cells 10 km and 20 km away from CW grid cell in West direction. Spacing of two grid cells exists between CW and CE which mean that CW and CE grid cells are 20 km apart.

For the analysis in East and West direction, only 6 grid cells are selected as shown in Figure 4.15. Three grid cells are in West direction and other three are in East direction of the lake (VAT020). For this purpose, wind roses are plotted only for these grid cells. Precipitation along with other parameters is analyzed for these six grid cells in the simulations.

Figures 4.16 to 4.18 below show wind rose diagrams plotted for hourly values over 10 years of simulation when convective precipitation was greater and equal to 0.1 mm/day in the simulations. These are plotted only for grid cells 1W, CW, CE and 1E as shown in Figure 4.15. Plot is divided into 8 geographical directions. Legends with different color represent different wind speed ranges. The plots have series of circles within a circle separated at equal spacing. In order to understand the meaning of spacing, legend on left hand side has to be considered. Space between each circle represents 100 values. So when wind is around 200 times in the same direction when convective precipitation occurred more or equal to 0.1 mm/day then plot will cover space of two circles in that direction. Wind direction can be determined by the direction of plotted values pointing towards e.g. when wind is westerly then it will

point towards East or in other words it can be said that when wind is flowing westerly then it is plotted in West.

From wind rose diagram it can be seen that for simulation VAT010 and VAT030; plots are almost identical. But when VAT010 wind roses are compared to VAT020, then it is observed that in all grid cells, winds are more westerly in VAT020- than in VAT010 simulation. CE grid cell in the VAT020 simulation shows mostly westerly winds when convective precipitation occurred than in case of VAT010 simulation. So, it can be said that when convective precipitation greater and equal to 0.1 mm/day occurred in grid cell CE then most of the time in simulation VAT020 winds were westerly.

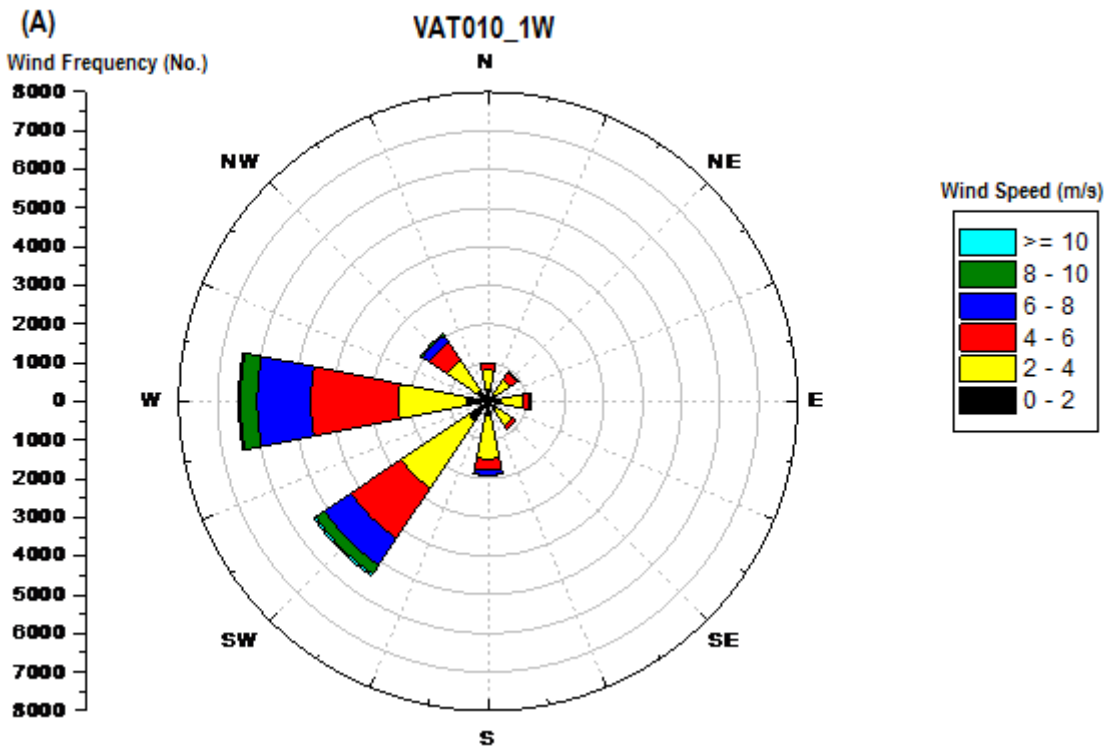
(A)
VAT010_1W
Wind Frequency (No.)
8000
7000
6000
5000
4000
3000
2000
1000
0
1000
2000
3000
4000
5000
6000
7000
8000
N
NE
E
SE
S
SW
W
NW
Wind Speed (m/s)
>= 10
8 - 10
6 - 8
4 - 6
2 - 4
0 - 2

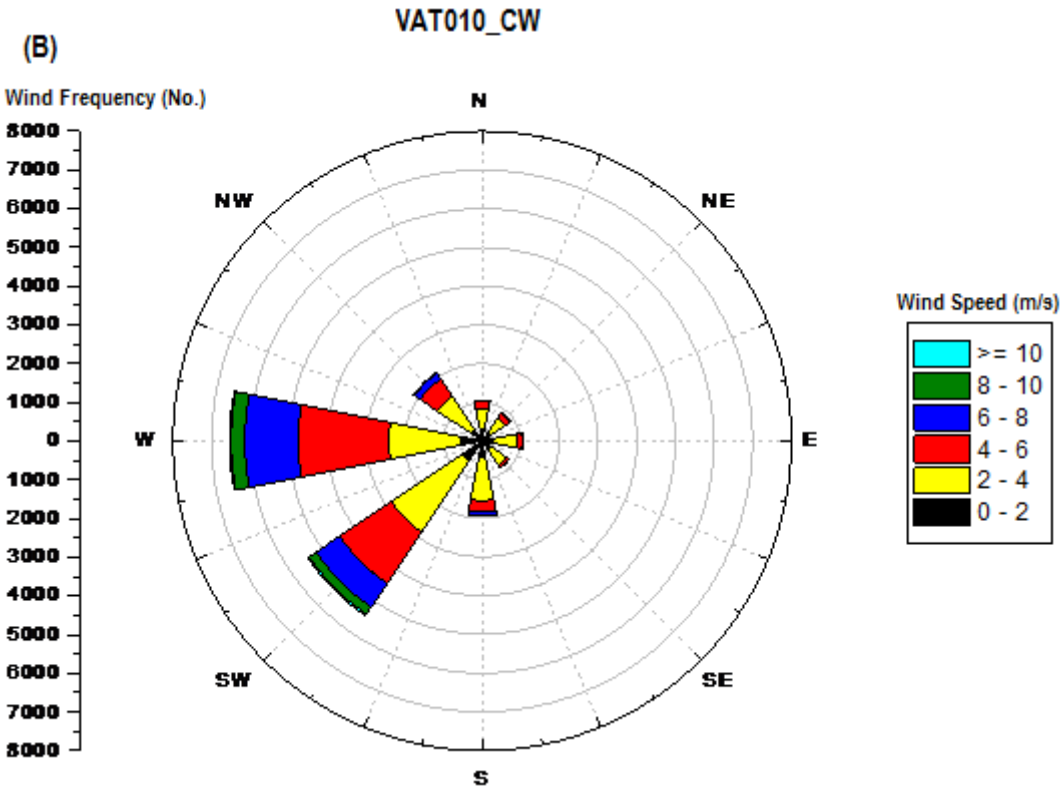
(B)
VAT010_CW
Wind Frequency (No.)
8000
7000
6000
5000
4000
3000
2000
1000
0
1000
2000
3000
4000
5000
6000
7000
8000
N
NE
E
SE
S
SW
W
NW
Wind Speed (m/s)
>= 10
8 - 10
6 - 8
4 - 6
2 - 4
0 - 2

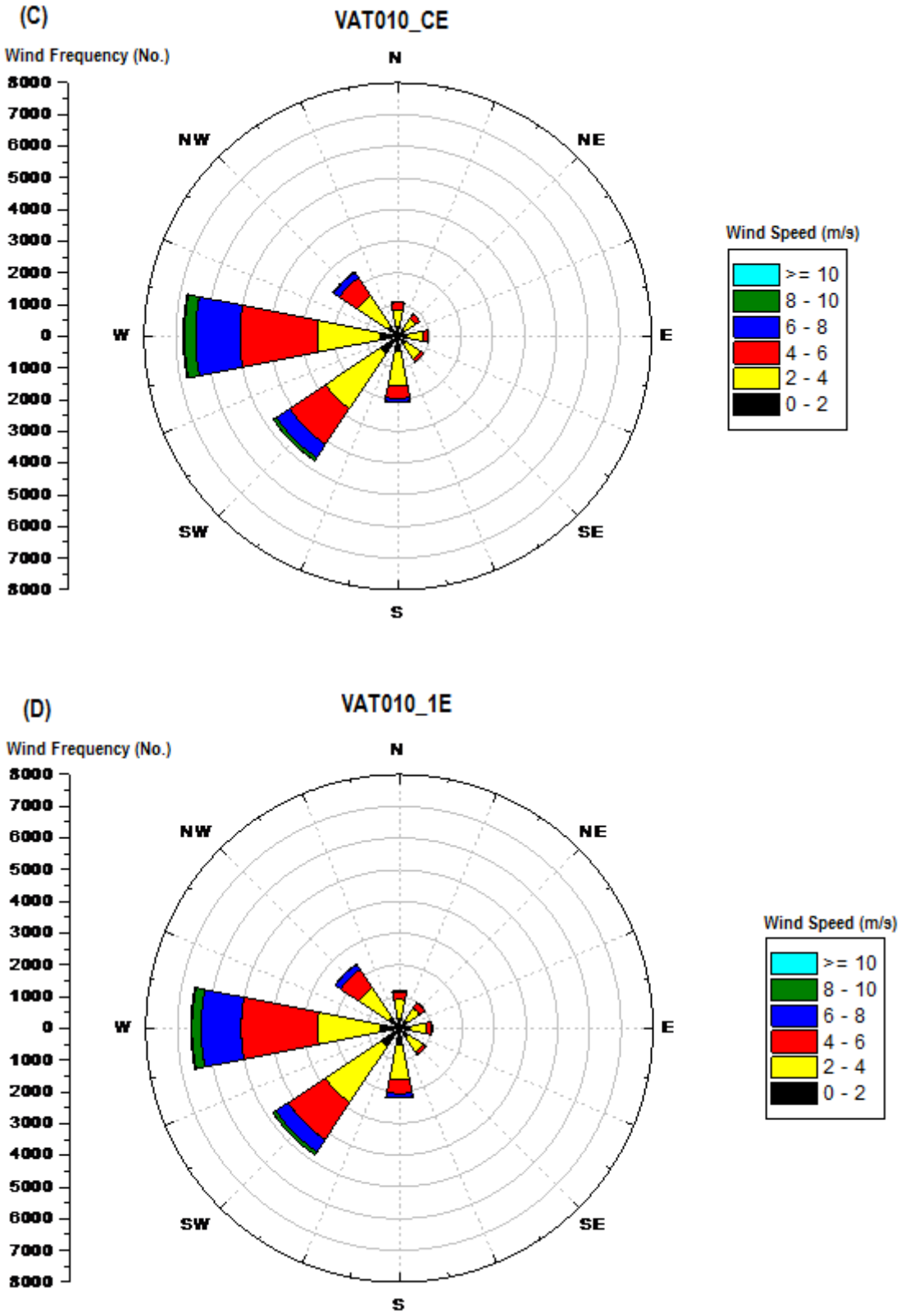

Figure 4.16: A,B,C,D represent Grid cells 1W,CW,CE,1E plotted as 10 years Wind Rose when convective precipitation >= 0.1 mm/day occurred in VAT010 simulation.

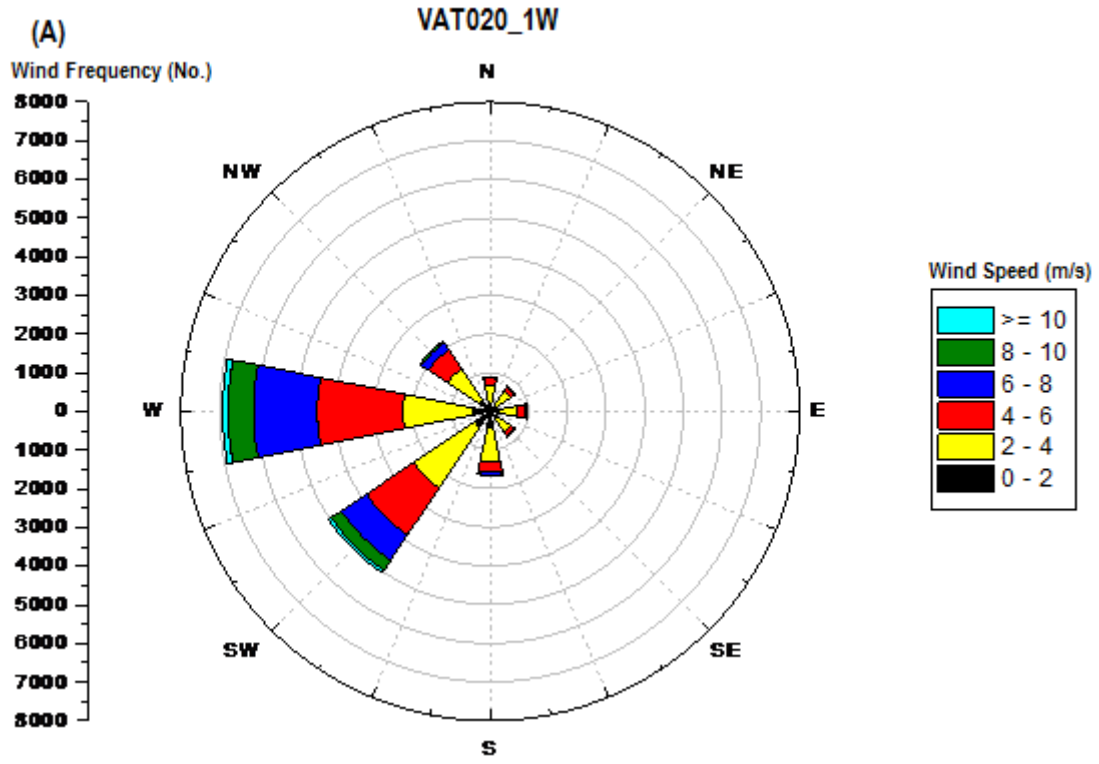
(A)
VAT020_1W
Wind Frequency (No.)
8000
7000
6000
5000
4000
3000
2000
1000
0
1000
2000
3000
4000
5000
6000
7000
8000
N
NE
E
SE
S
SW
W
NW
Wind Speed (m/s)
>= 10
8 - 10
6 - 8
4 - 6
2 - 4
0 - 2

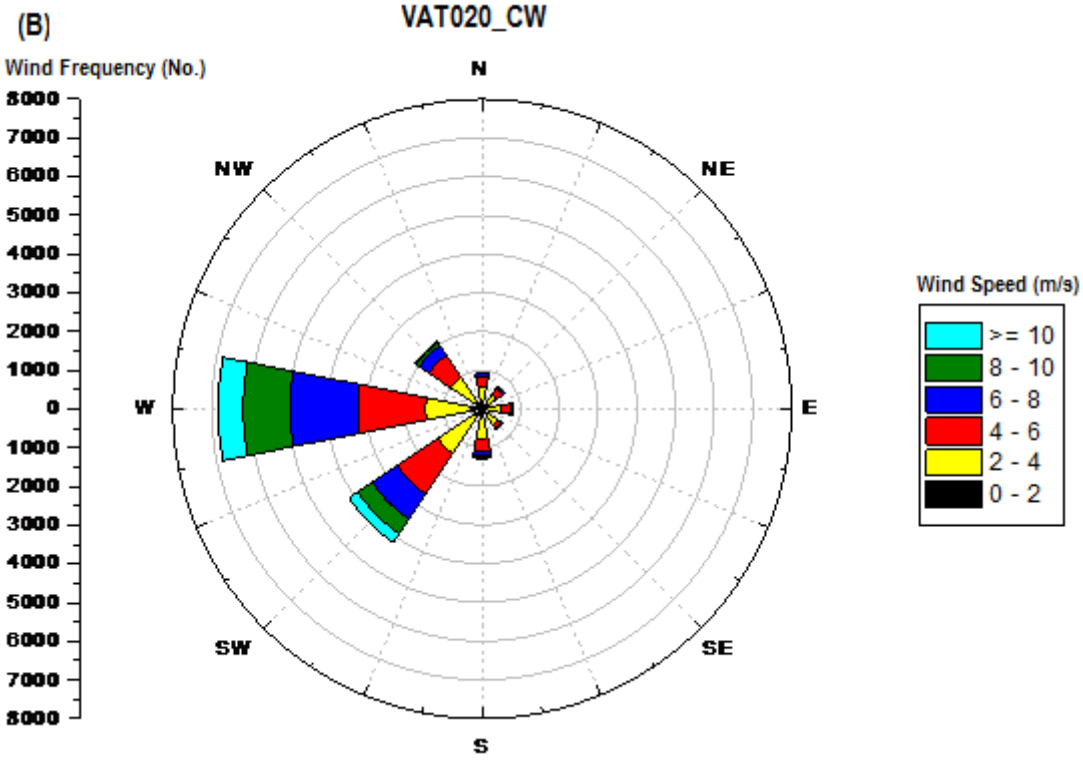
(B)
VAT020_CW
Wind Frequency (No.)
8000
7000
6000
5000
4000
3000
2000
1000
0
1000
2000
3000
4000
5000
6000
7000
8000
N
NE
E
SE
S
SW
W
NW
Wind Speed (m/s)
>= 10
8 - 10
6 - 8
4 - 6
2 - 4
0 - 2

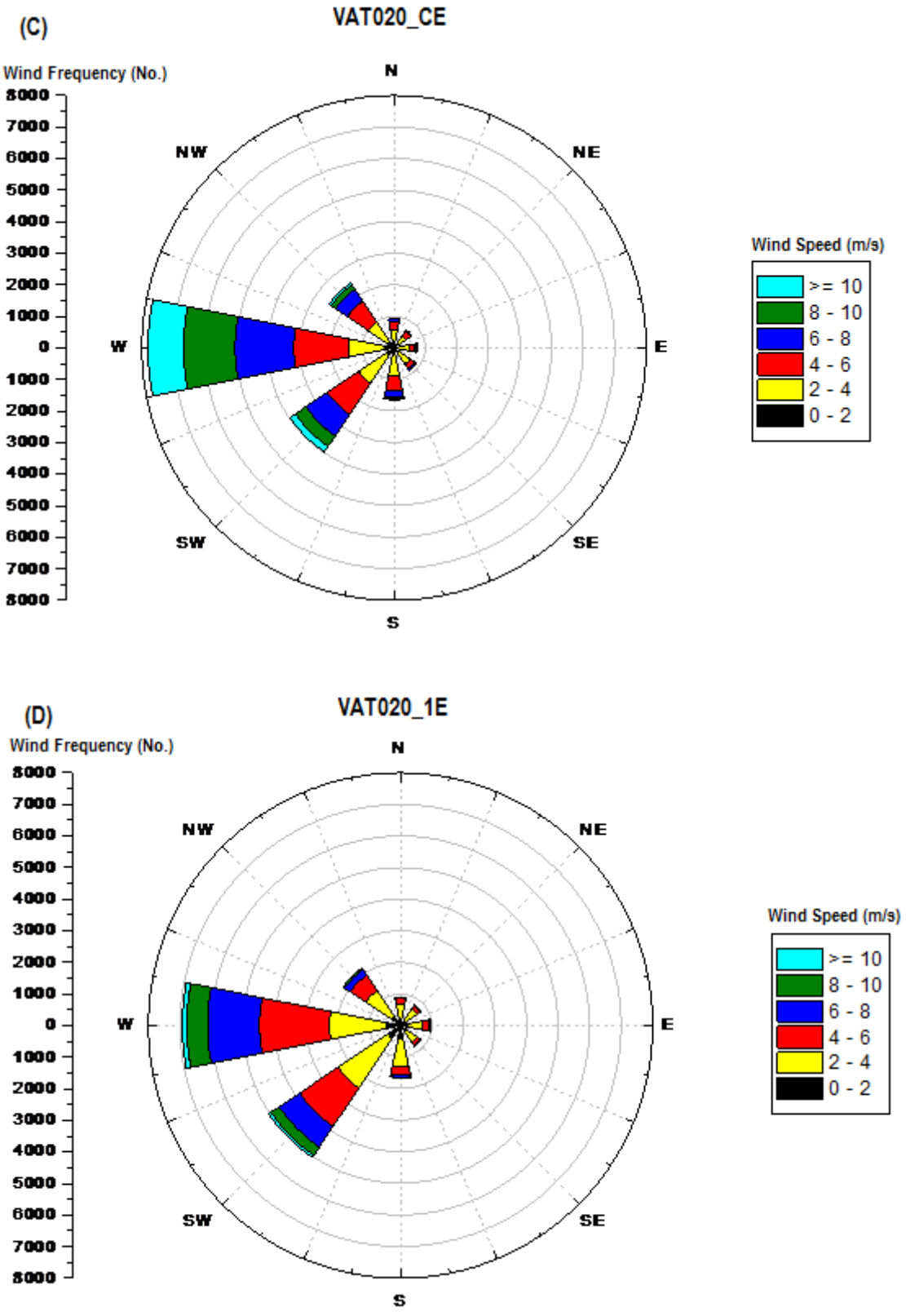

Figure 4.17: A,B,C,D represent Grid cells 1W,CW,CE,1E plotted as 10 years Wind Rose when convective precipitation >= 0.1 mm/day occurred in VAT020 simulation.

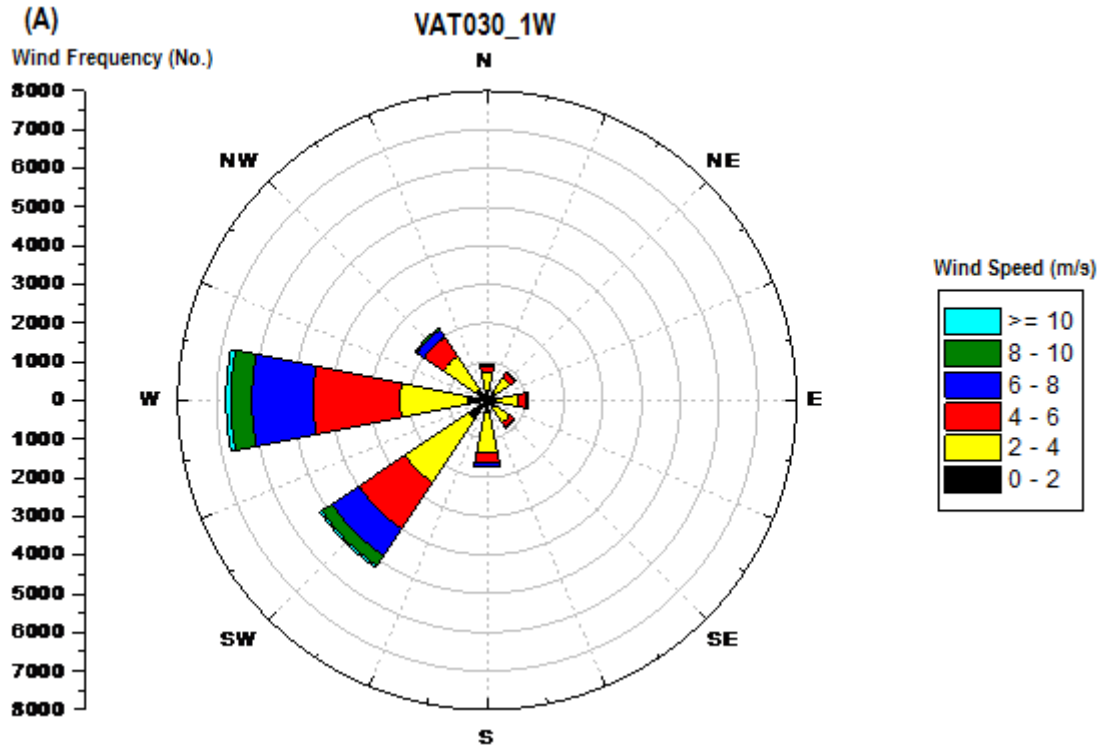
(A)
VAT030_1W
Wind Frequency (No.)
8000
7000
6000
5000
4000
3000
2000
1000
0
1000
2000
3000
4000
5000
6000
7000
8000
N
NE
E
SE
S
SW
W
NW
Wind Speed (m/s)
>= 10
8 - 10
6 - 8
4 - 6
2 - 4
0 - 2

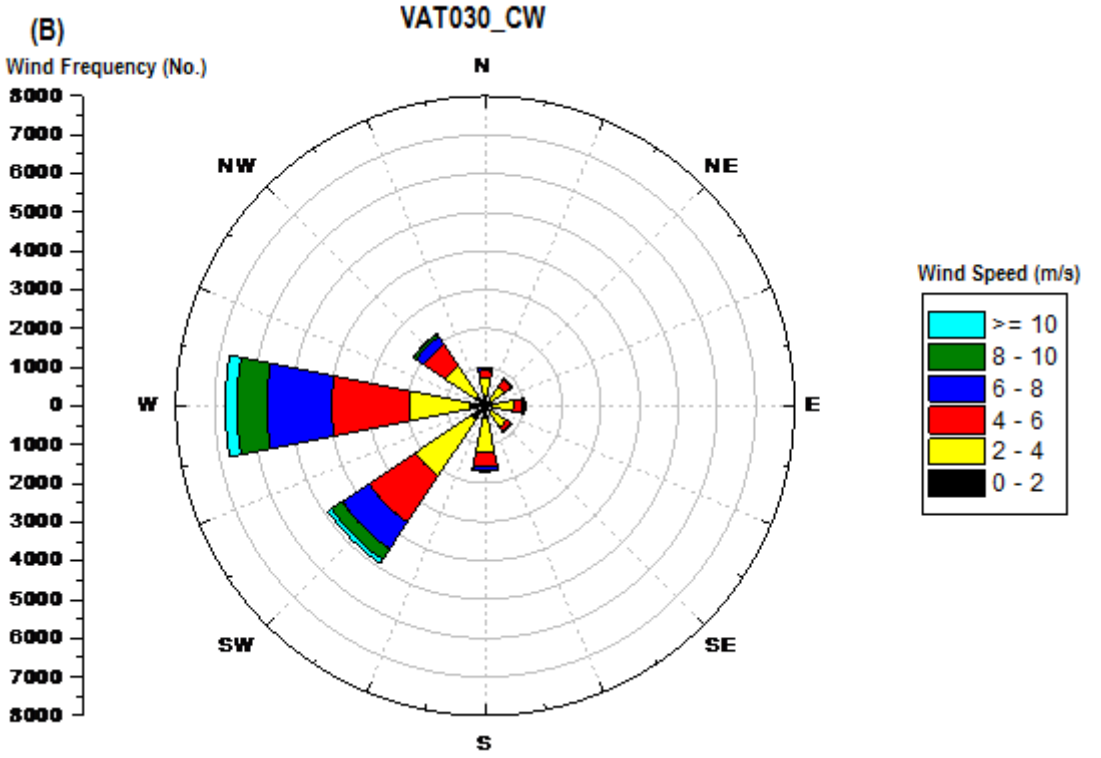
(B)
VAT030_CW
Wind Frequency (No.)
8000
7000
6000
5000
4000
3000
2000
1000
0
1000
2000
3000
4000
5000
6000
7000
8000
N
NE
E
SE
S
SW
W
NW
Wind Speed (m/s)
>= 10
8 - 10
6 - 8
4 - 6
2 - 4
0 - 2

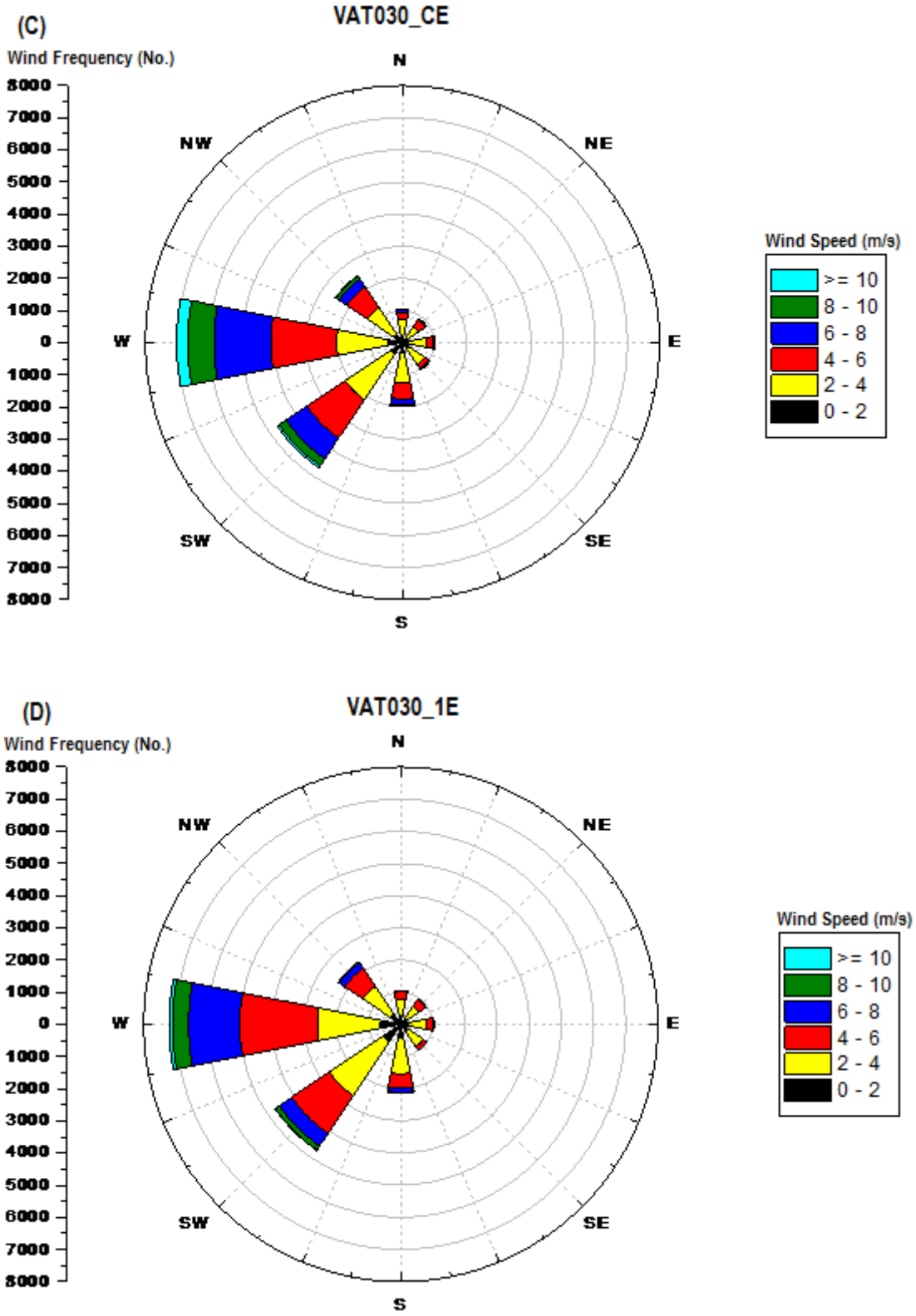

Figure 4.18; A,B,C,D represent Grid cells 1W,CW,CE,1E plotted as 10 years Wind Rose when convective precipitation >= 0.1 mm/day occurred in VAT030 simulation.

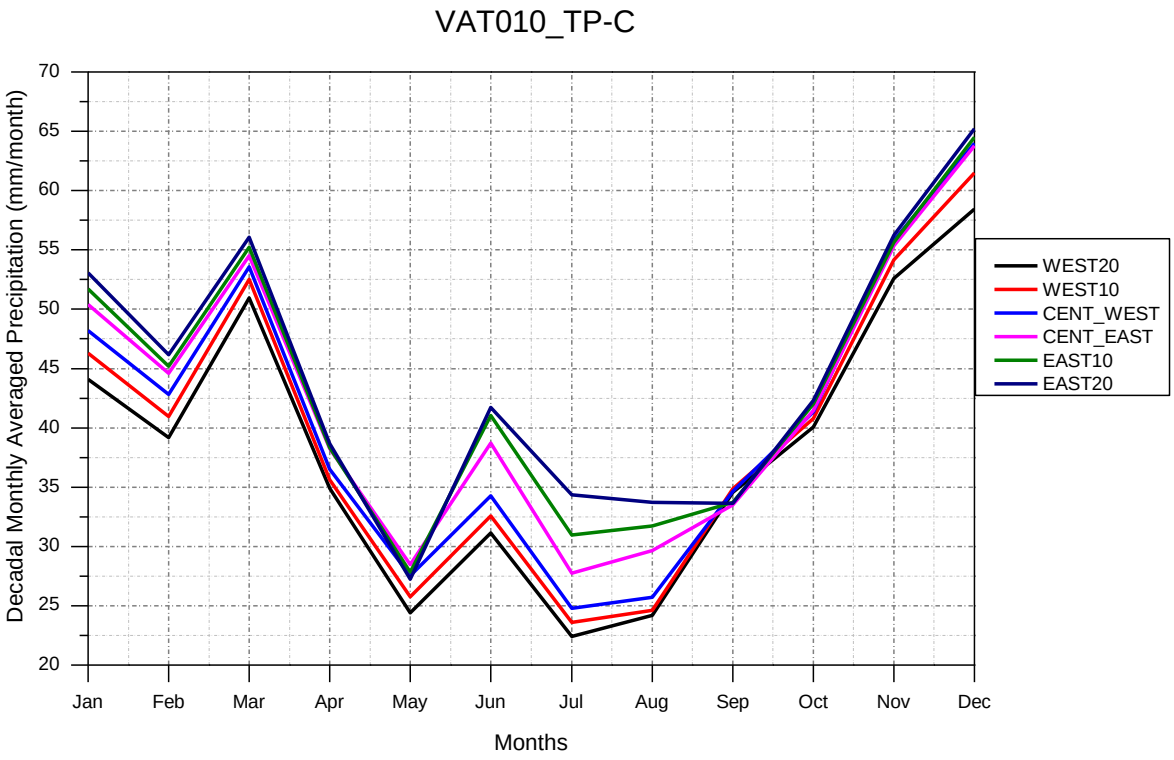

Figure 4.19: Decadal monthly averaged large scale precipitation (mm/month) for VAT010 simulation.

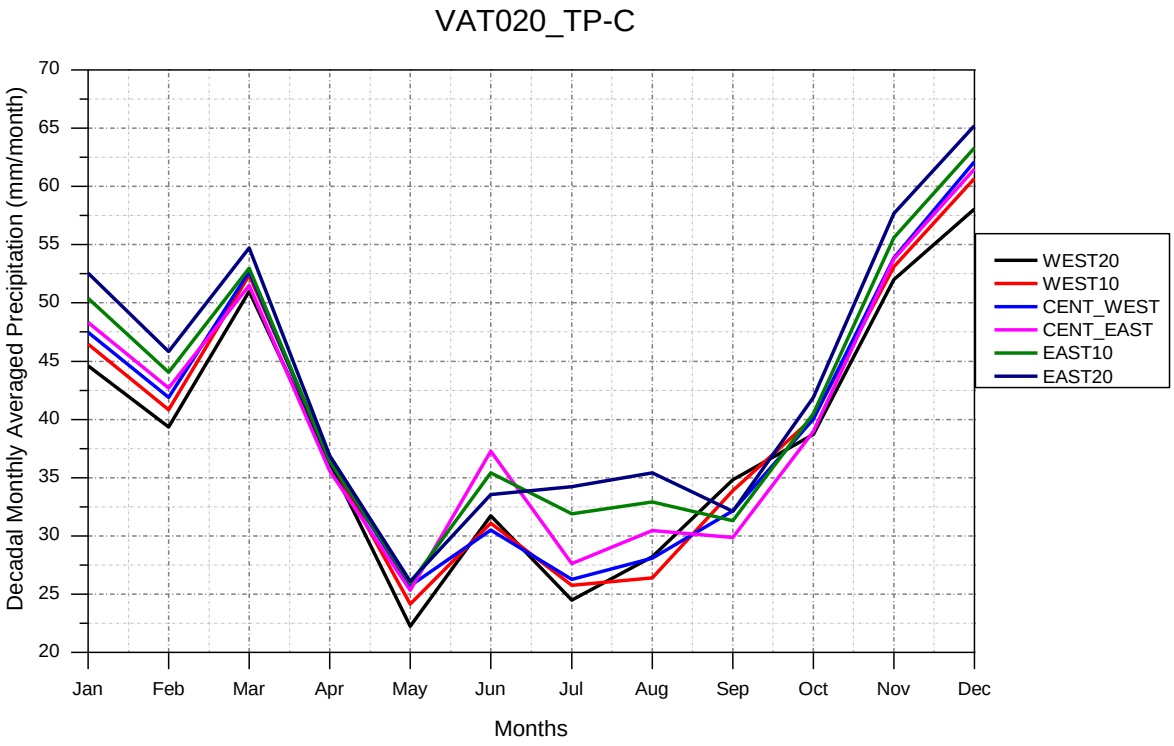

Figure 4.20: Decadal monthly averaged large scale precipitation (mm/month) for VAT020 simulation.

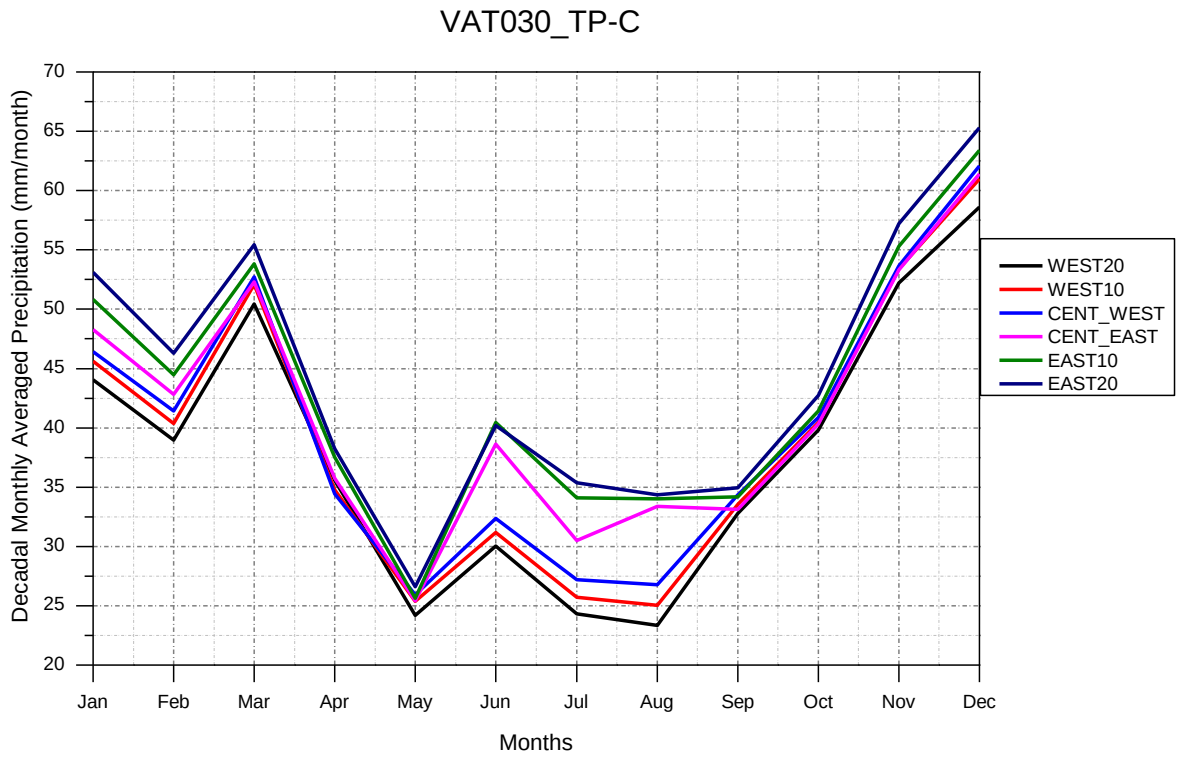

Figure 4.21: Decadal monthly averaged large scale precipitation (mm/month) for VAT030 simulation.

Figures 4.19 to 4.21 show decadal monthly averaged TP-C values for three simulations. In figures legend WEST20, WEST10, CENT_WEST, CENT_EAST, EAST10 and EAST20 represent grid cells 2W, 1W, CW, CE, 1E and 2E respectively (Figure 4.15). In all the simulations a maximum precipitation gradient of about 10 mm/month from West- to East direction can be seen during summer and winter season but for rest of the year the gradient is below 5 mm/month in all the simulations. So, there is high precipitation in that East than that in the West in all the simulations. It can also be seen that especially during summer and winter; grid cells located in the East show more TP-C corresponding to its neighboring grid in west direction in all simulations. So, all simulations have similar TP-C gradient.

Analogous to North- and South directions (Figures 4.6 and 4.7) to further examine the effect of LULC change among three simulations on TP-C, differences between simulations are made for East- and West directions.

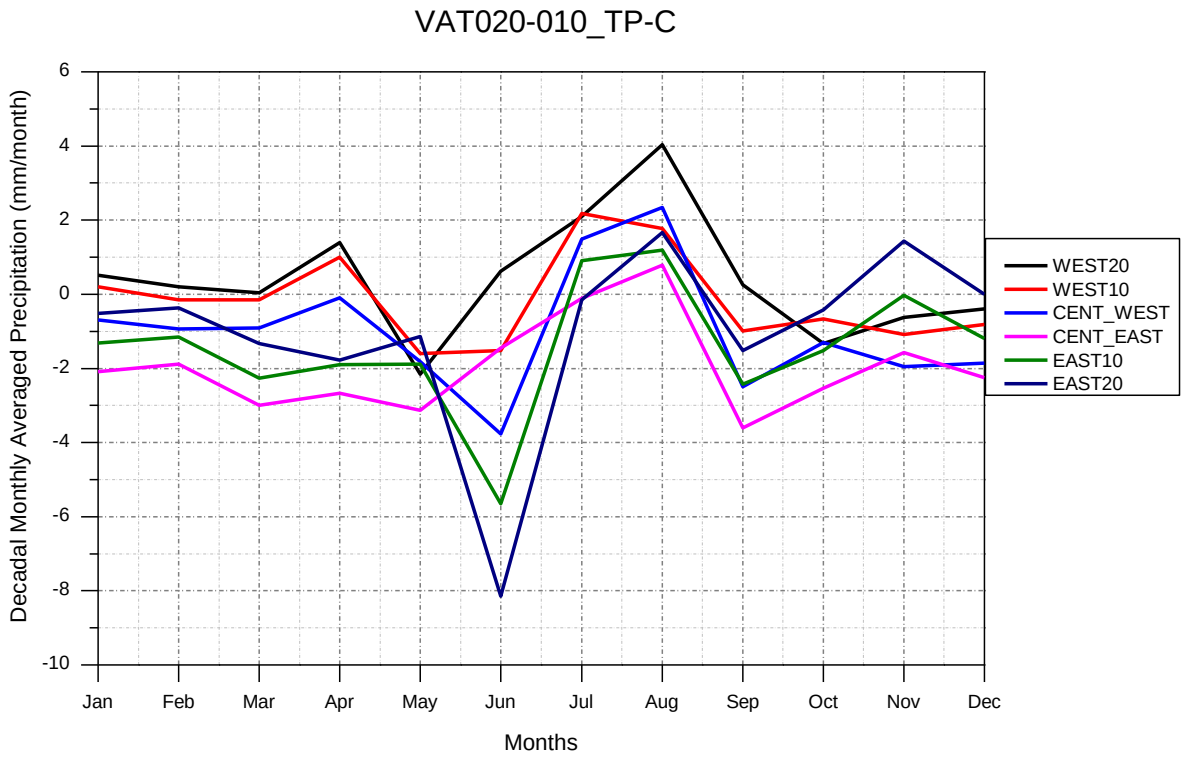

Figure 4.22: Decadal difference of monthly averaged of large scale precipitation (mm/month) between VAT020 and VAT010 simulations.

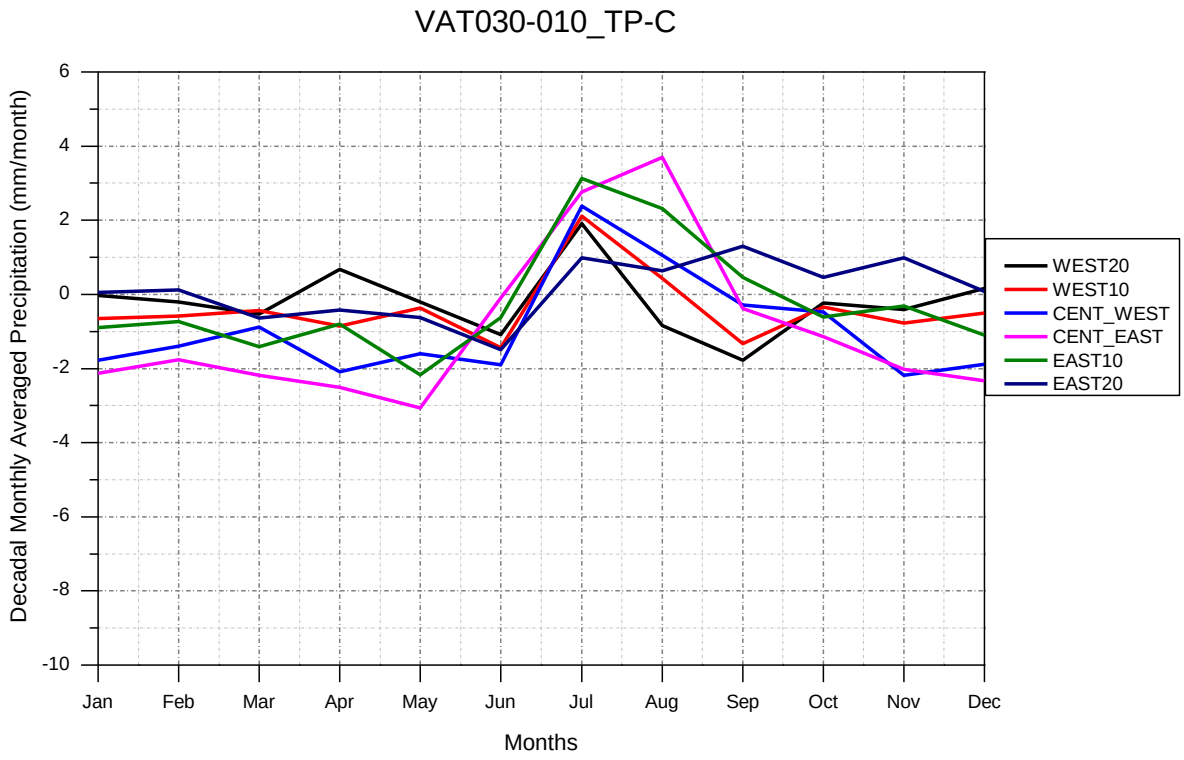

Figure 4.23: Decadal difference of monthly average of large scale precipitation (mm/month) between VAT020 and VAT010 simulations.

Analogous to South-North grid cells, differences between simulations are plotted for East-West grid cells. As simulation VAT010 represents potential vegetation (see Chapter 4.2), so it is treated as a reference for other simulations. Figures 4.22 and 4.23 show the decadal monthly averaged TP-C values differences for VAT020- and VAT030 simulations with the reference simulation (VAT010). Maximum difference of not more than 4 mm/month is observed among grid cells in both the cases except in month of June, when maximum difference of 8 mm/month was observed (Figure 4.22). So, it can be said that simulations have TP-C variation well within 4 mm/month. Further same process is carried out for convective precipitation and is shown below. Legends description is same as in the case of simulations for TP-C parameter discussed before.

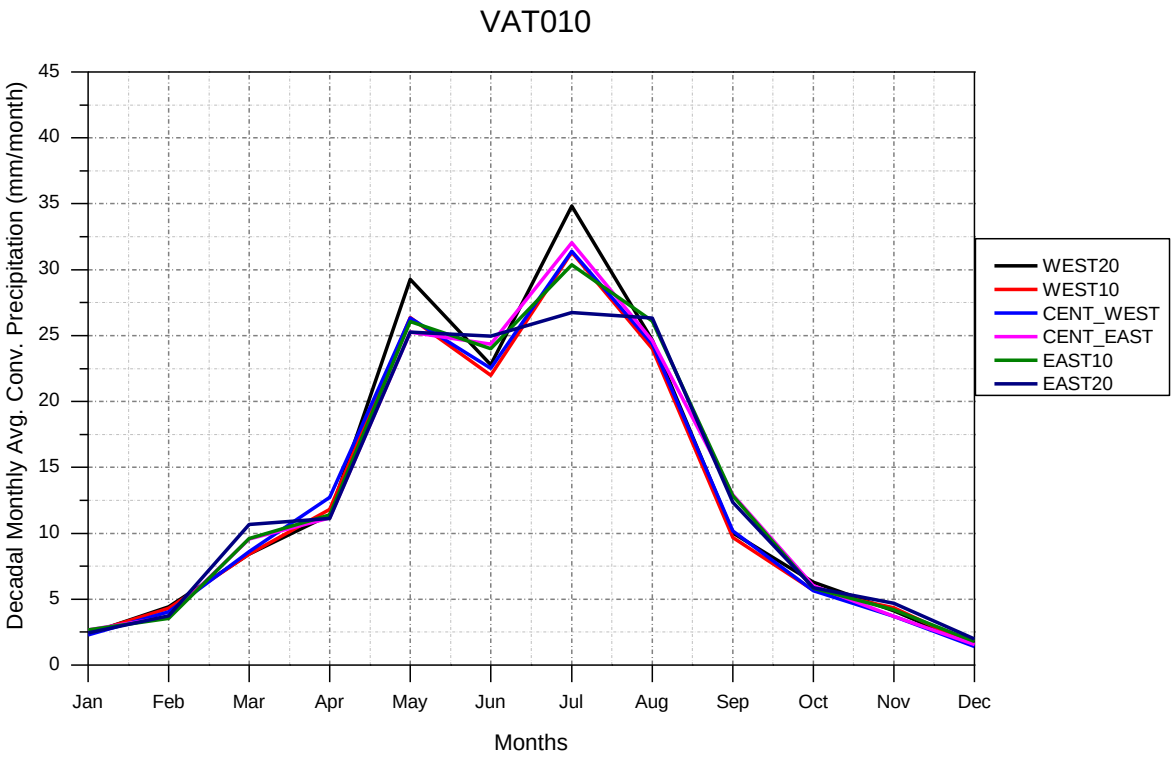

Figure 4.24: Decadal monthly averaged convective precipitation (mm/month) for VAT010 simulation.

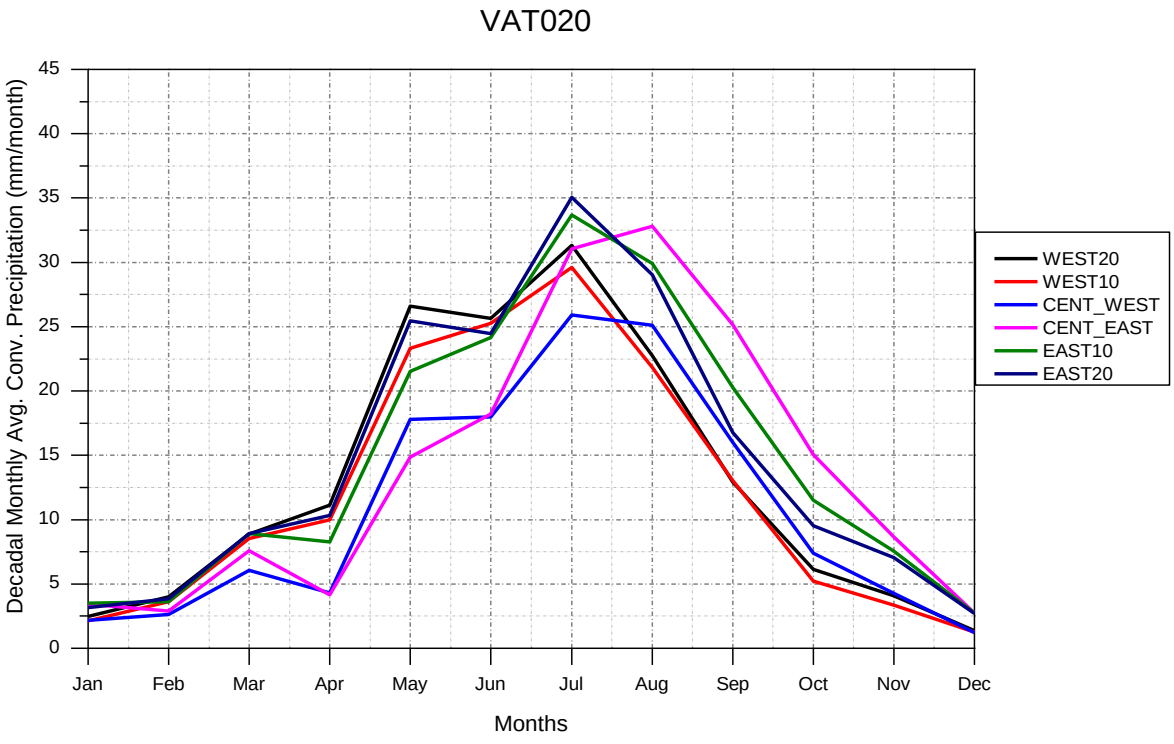

Figure 4.25: Decadal monthly averaged convective precipitation (mm/month) for VAT020 simulation.

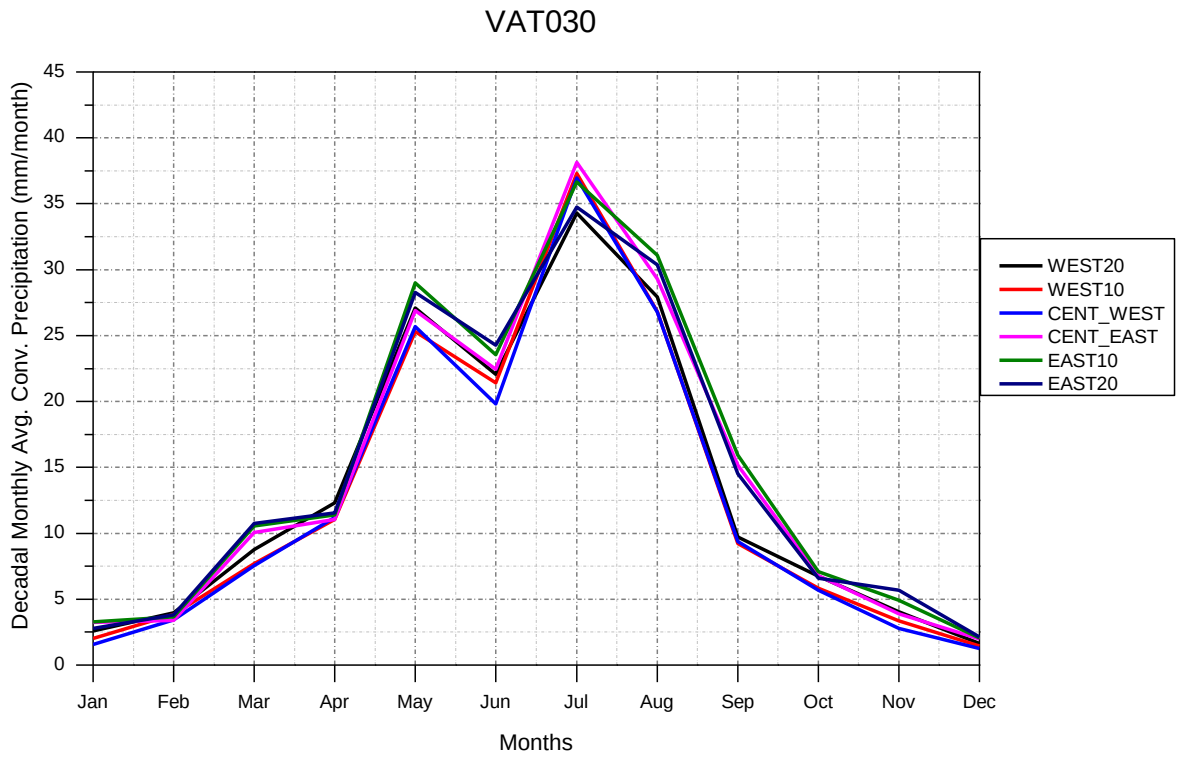

Figure 4.26: Decadal monthly averaged convective precipitation (mm/month) for VAT030 simulation.

Figures 4.24 to 4.26 show decadal monthly averaged convective precipitation for three simulations. For simulations VAT010 and VAT030; maximum precipitation difference among grid cells is less than 5 mm/month as we move from West to East. Like in case of TP-C, for convective precipitation also for most of the months; precipitation difference is less than 3 mm/month among grid cells in West to East directions. But in case of VAT020 simulation, grid cell CE and CW have maximum difference of about 8 mm/month during spring. During late summer and fall CE shows maximum convective precipitation difference of about 10 mm/month. But during spring, precipitation is low in grid cells CW and CE as compared to that in other grid cells but during summer and fall it is high in CE grid than in other grid cells. During summer and fall; 1E grid cell also shows maximum difference of about 5 mm/month from other grid cells (excluding CE) even though such a behavior was not observed

in case of VAT010 and VAT030 simulations. To further examine the effect of LULC, differences among simulations are carried out as done in case of TP-C parameter.

Analogous to simulation study in North and South directions, uncertainty analysis is carried out using the same methodology (MCS) for East and West directions.

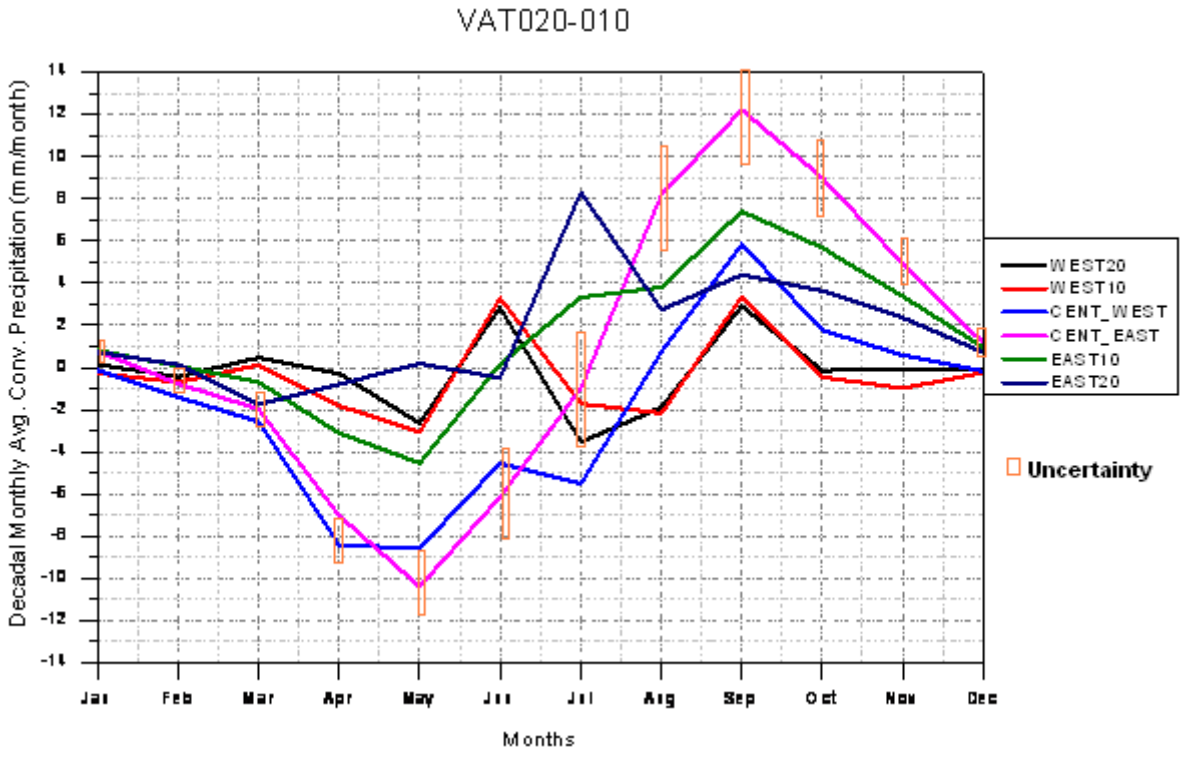

Figure 4.27: Decadal difference of monthly averaged convective precipitation (mm/month) between VAT020 and VAT010 simulations.

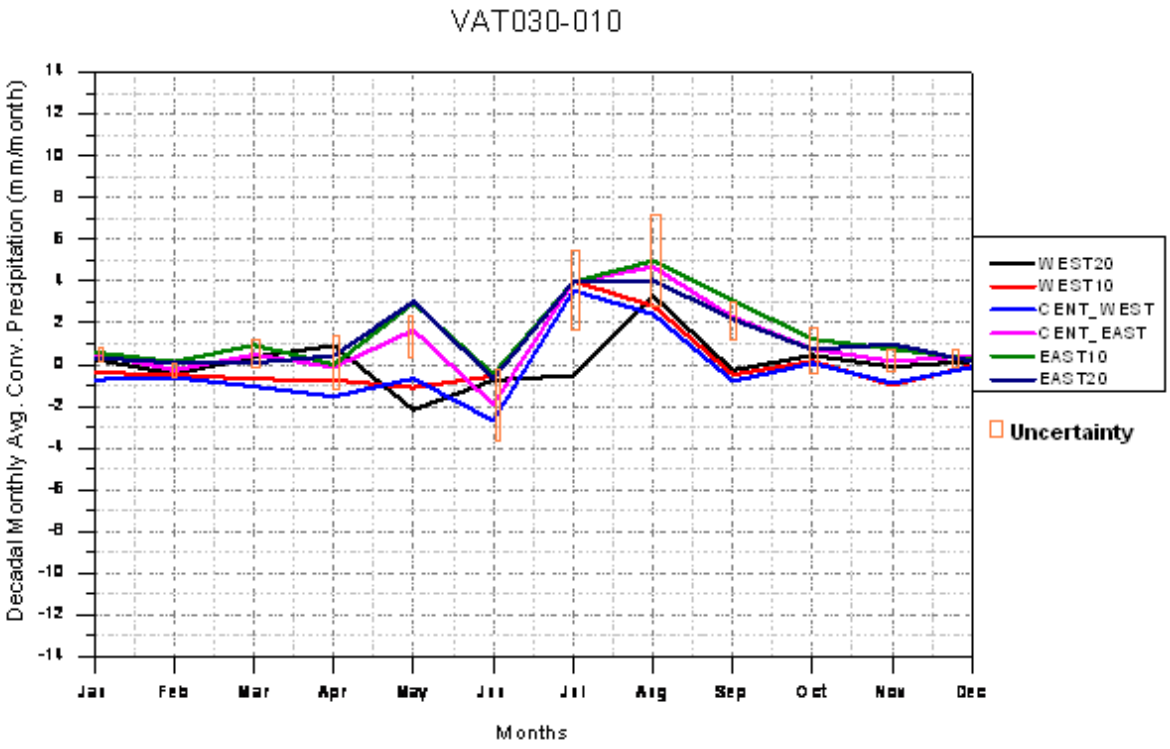

Figure 4.28: Decadal difference of monthly averaged convective precipitation (mm/month) between VAT030 and VAT010 simulations.

Figures 4.27 to 4.28 show decadal averaged convective precipitation values differences in VAT020 and VAT030 simulations with the reference simulation (VAT010). In Figure 4.28 except for July, when maximum convective difference of 5 mm/month occurred between grid cells 2W and 2E, for rest of the months the values are within 3 mm/month among various grid cells. From Figure 4.28 uncertainty of ±2.2 mm/month is observed during months of July and August. So from uncertainty analysis it can be said that the convective precipitation values are well within the variation of ±2 mm/month and hence probability of simulations VAT010 and VAT030 to have same values for convective precipitation is more likely. But unlike in simulation VAT030-VAT010, in Figure 4.27; grid cells CE and CW show maximum precipitation difference of about 10 mm/month during spring and early summer. During late summer and fall, maximum precipitation gradient of about 10 mm/month

exists between grid cell CE and other grid cells. Uncertainty analysis shows maximum convective precipitation difference of ±3 mm/month. But as CE and CW grid cells in Figure 4.29 show values more than their uncertainties, hence it can be said that CE and CW in VAT020 and VAT010 simulations do not show same convective precipitation values. This can be explained in analogy to Central grid cell in South-North simulations results (Thermal capacity of Lake and Segal et al. (1995)). Figures 4.29 and 4.30 showing surface energy flux and Bowen ratio support the explanation given by thermal capacity of lake and Segal et al. (1995). Hence more convective precipitation is observed during late summer and fall in grid cells CW and CE of VAT020 simulation than in VAT010 simulation, even though difference is very small.

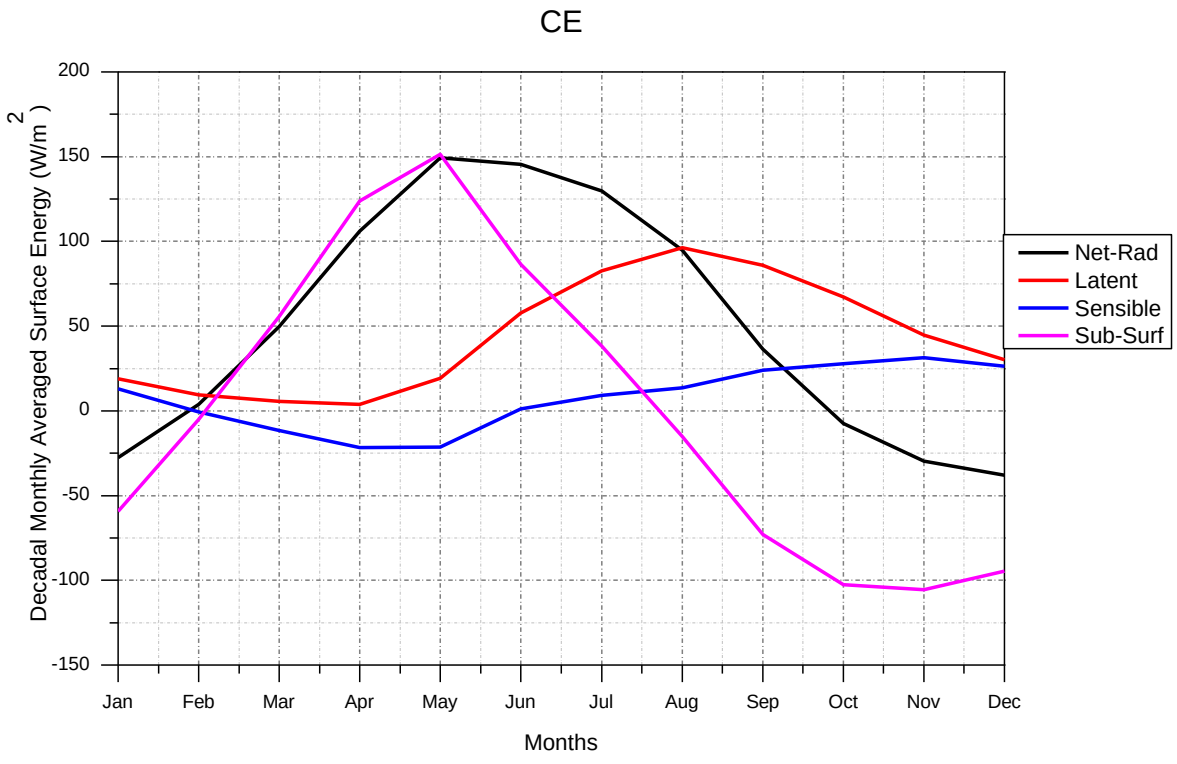

Figure 4.29: Decadal monthly averaged surface energy (W/m^2) at CE in VAT020 simulation.

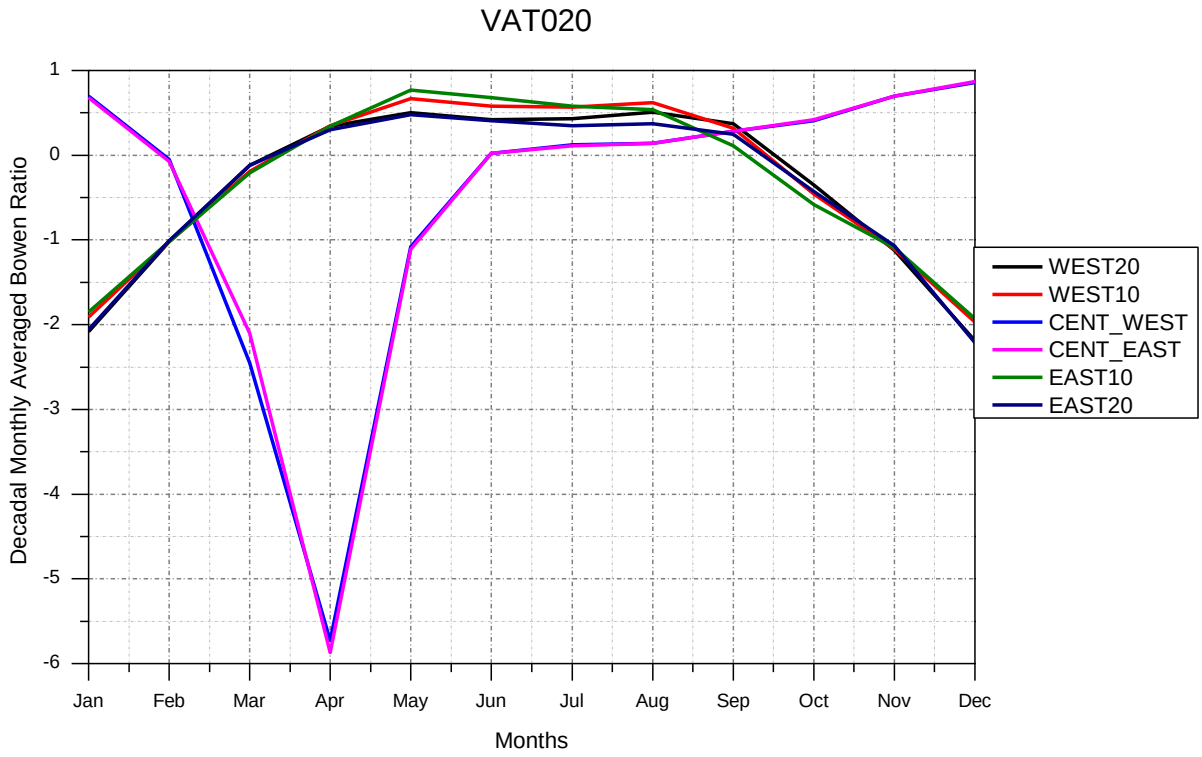

Figure 4.30: Decadal monthly averaged Bowen ratio of VAT020 simulation.

But interestingly even though grid cells CE and CW represent lake but during late summer and fall maximum difference in convective precipitation value of about 8 mm/month is observed between them. It can also be seen from Figure 4.29 that during late summer, fall and winter it is precipitating more in CE than in CW. To analyze this, a hypothesis is laid out, according to which the introduction of Lake has altered the grid cells surface roughness in VAT020 simulation (see Table 4.2). Because of this acceleration in westerly wind is produced over the lake thereby enhancing chances of more convective precipitation in East than its counterpart in West. From Figure 4.19 it is seen that for grid cells CW and CE most of the time winds are westerly when convective precipitation occurred in VAT020 simulation.

In order to quantify the increase in convective precipitation in CE compared to CW in VAT020 simulation, plots for the convective precipitation counts and amounts are plotted in Figures 4.31 to 4.34. In the figures, the number of days and amount are counted, when convective precipitation of more and equal to 0.1 mm/day occurred in simulation VAT010 and VAT020 for grid cells CW and CE when wind were westerly. In the Figures 4.31 to 4.34, red color legend counts the convective precipitation days and amount, when on a day of precipitation, more than 90% times hourly winds were westerly. Similarly green (>=75) and violet (>=50) counts the convective precipitation days and convective precipitation amount when 75% and 50% times hourly wind were westerly.

Figures 4.31 to 4.34 are plots for the same simulation but represent differences in convective precipitation count and amount for grid cells CE and CW. In case of VAT010 simulation from Figures 4.31 and 4.32, red (>=90) and green (>=75) legend values have difference within ±2 counts and corresponding difference in amount of convective precipitation less than 1 mm/month among grids CW and CE. So it can be said that in VAT010 simulations, among grid cells CW and CE, exists a small difference in convective precipitation of 1 mm/month. But in case of VAT020 simulation from Figures 4.33 and 4.34, it can be seen that for grid cell CE during late summer and fall, convective precipitation count is always more than CW by at least 2 days and reaching maximum of 9 days during July for red legend (>=90) and corresponding to convective precipitation amount difference of 3 mm/month. During Late summer and fall, average variation in green legend (>=75) of about 6 days can be seen among CE and CW which corresponds to convective precipitation amount of more than 4 mm/month. So it can be said that summer and fall convective precipitation is favored by westerly winds and hence more precipitation is observed in

CE grid cell than in CW. When this is compared to Figure 4.27 then most differences among CE and CW grid cells can be accounted from this.

Hence form this West-East direction analysis it is observed that Lake induced in VAT020 simulation have enhanced convective precipitation by 8 mm/month in grid cell CE as compared to its CW Lake counterpart during late summer and fall with a uncertainty of ±3 mm/day. Even though effect over grid cell 1E can also be noticed but value is well within 2 mm/month. So it can be said that lake has enhanced convective precipitation but the effect is limited to lake only. This also corresponds with the finding of Ahmed et al. (2011) (Chapter 2.2) which showed that in the Warm Summer Continental region in U.S introduction of Lake didn't show any increase in precipitation values around the Lake region.

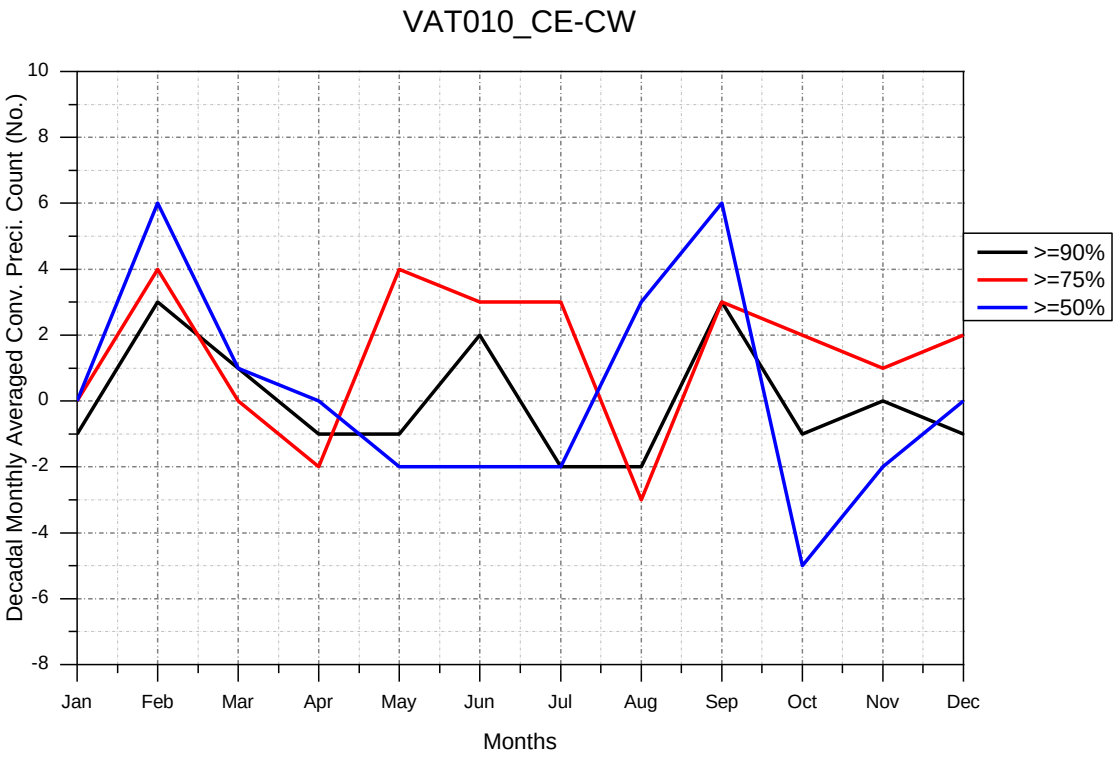

Figure 4.31: Decadal difference of monthly averaged convective precipitation count when wind was westerly at gird cells CW and CE in VAT010 simulation.

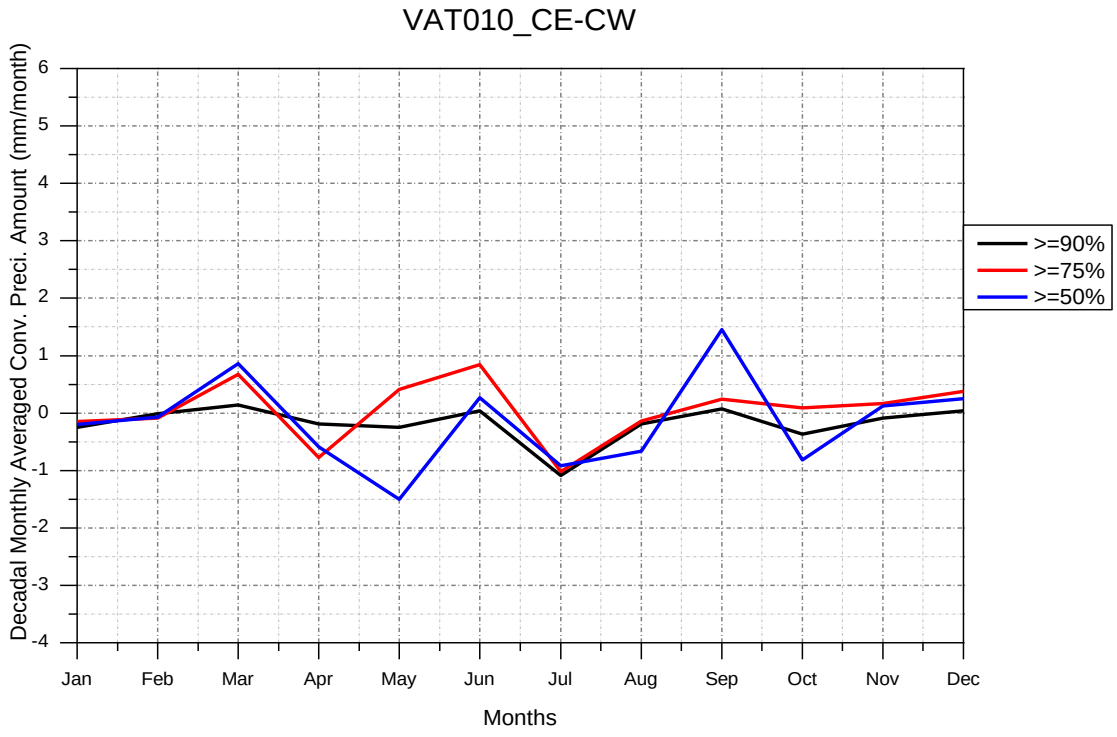

Figure 4.32: Decadal difference of monthly averaged convective precipitation amount when wind was westerly at gird cells CW and CE in VAT010 simulation.

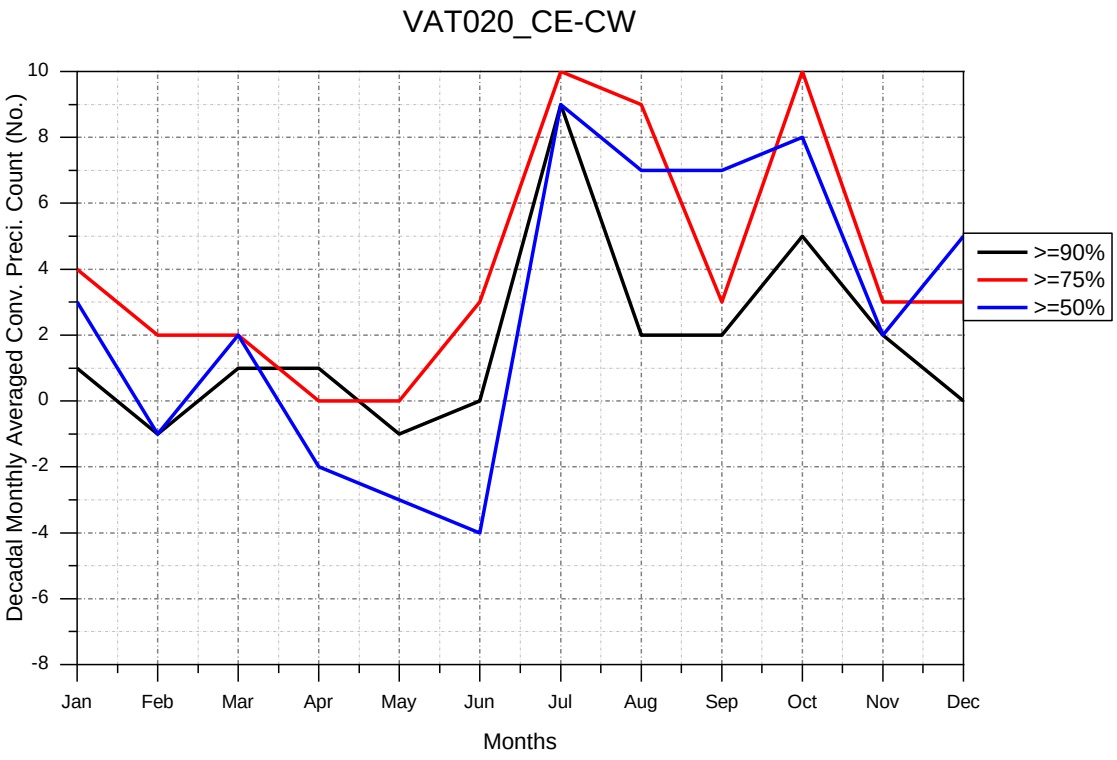

Figure 4.33: Decadal difference of monthly averaged convective precipitation count when wind was westerly at gird cells CW and CE in VAT010 simulation.

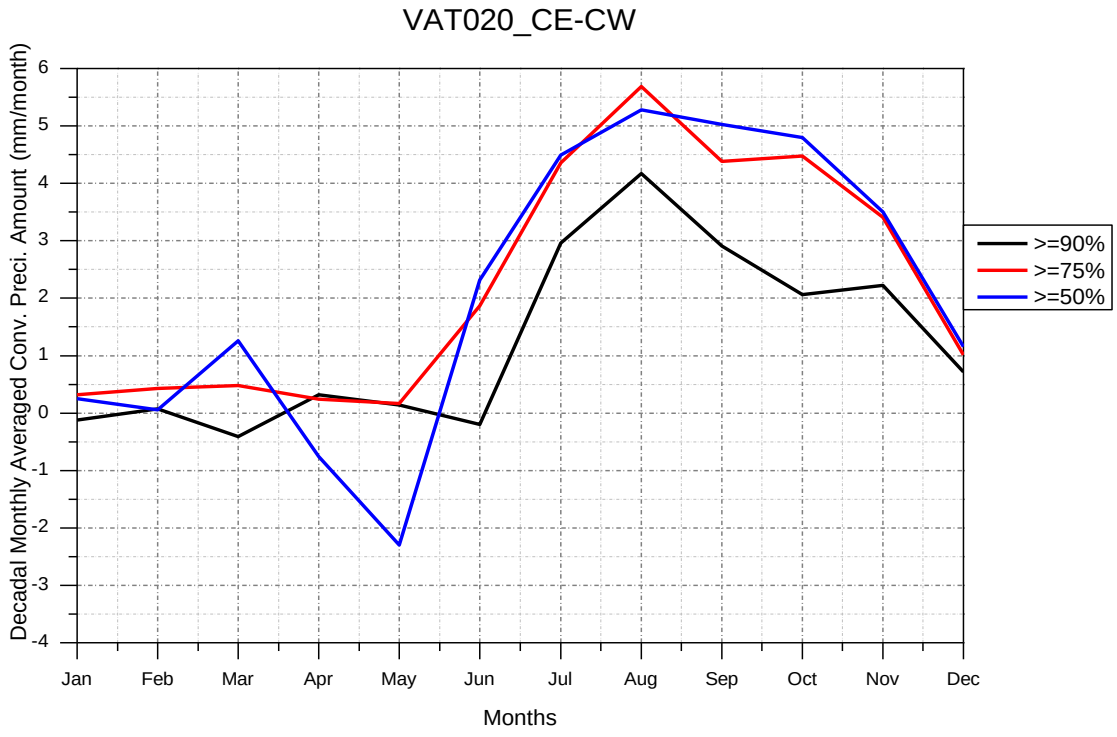

Figure 4.34: Decadal difference of monthly averaged convective precipitation amount when wind was westerly at gird cells CW and CE in VAT010 simulation.

4.4 Model and observation data comparison

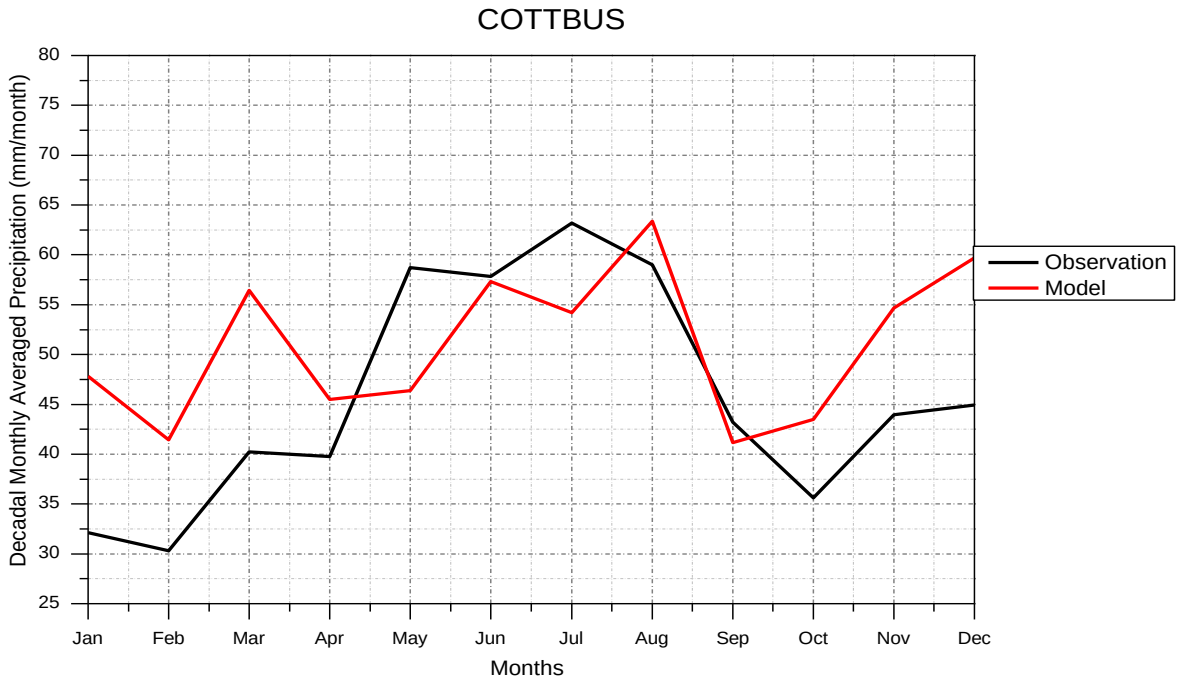

Figure 4.35: Decadal monthly averaged precipitation of Cottbus in observation and VAT010 simulation.

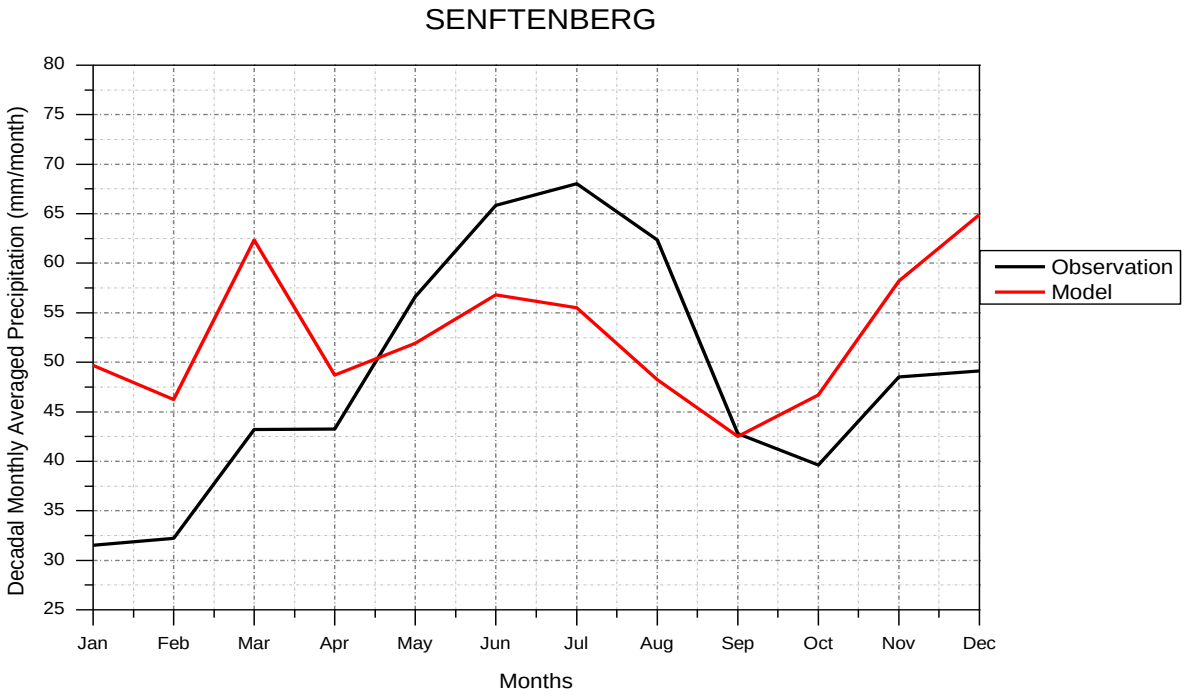

Figure 4.36: Decadal monthly averaged precipitation of Senftenberg in observation and VAT010 simulation.

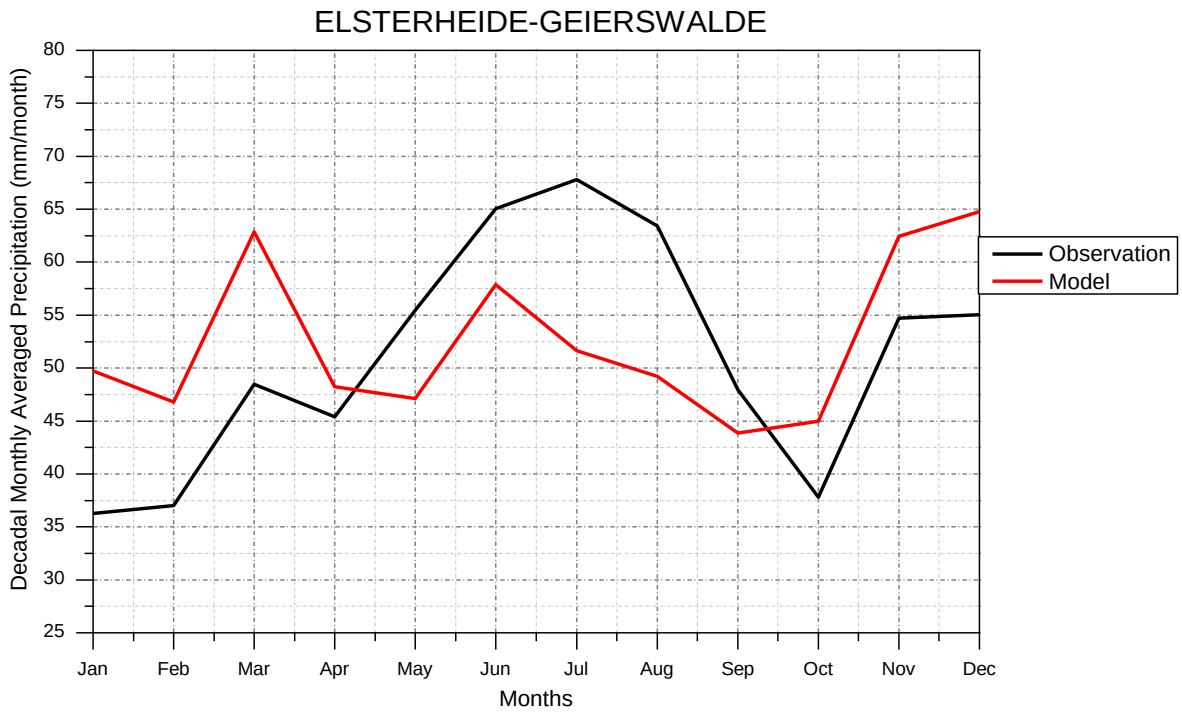

Figure 4.37: Decadal monthly averaged precipitation of Elsterheide-Geierswalde in observation and VAT010 simulation.

Observation data (DWD database, Chapter 3.1) of precipitation for stations Cottbus, Senftenberg and Elsterheide-Geierswalde are compared with VAT010 (Potential vegetation) simulation. In VAT010 simulation station grids were identified using geographical coordinates of stations (Table 3.2). Figures 4.35 to 4.37 show the comparison of the decadal monthly averaged precipitation between observation and VAT010 simulation. Decadal period is from 1st of January 1989 to 31st of December 1998. In the comparison, precipitation amount includes both large scale and convective precipitation.

Figures 4.35 to 4.37 show that during fall and winter season more precipitation in model is observed and during spring and summer more precipitation in observation values (measured field data) is seen to occur. Except for summer season same pattern is observed in all the three stations. During summer while maximum

difference of more than 15 mm/month is observed at Senftenberg and Elsterheide-Geierswalde stations but station Cottbus has maximum difference of 7 mm/month. In winter and fall, maximum difference of 15 mm/month is observed at all the stations. The resolution of VAT010 simulation is 10 km x 10 km, which is coarse. Figure 3.1 shows location of stations and it can be seen that except Cottbus other stations are surrounded by different terrain. Difference in terrain changes the ground properties like surface roughness, soil type etc. which might affect the precipitation results. Comparing observation data with VAT010 simulation will be much better with finer resolution of 1 km or less.

5. SUMMARY, CONCLUSIONS AND FUTURE RESEARCH

Intensive coal mining in the region of Lusatia has believed to have an impact on neighboring areas (by the people living in vicinity of mining area), especially as the completion of mining will be followed by the formation of lake covering large area in southern Brandenburg and Saxony. As by the end around 130 km^2 surface will emerge, people living in the vicinity of mining area had serious doubt that lake formation might increase precipitation. Having knowledge of impact of Great lakes (Wilson 1977), increasing convective precipitation in the vicinity might lead to weathering of structures. This formed the very base of aim to investigate the Lusatia region.

The study about the impact of lake was carried out using data and CCLM simulation analysis. For the data analysis stations with parameters such as temperature, precipitation, wind speed and directions are searched around various active and inactive mining areas in Brandenburg and Saxony. But out of 55 stations located near a mining area only 4 stations had data for various parameters. Stations with precipitation data were many and as precipitation being the most important parameter, further analysis was carried out for this parameter. Firstly stations close to same mining area but located in different directions were searched. This was done to study its impact on different geographical location. But unfortunately either no such mining area was found or stations had many missing values for the precipitation parameter.

At last approach was changed and station Elsterheide-Geierswalde was selected which had precipitation values during mining and the time the area was being converted to Lake. This station happened to be within the mining area and hence

was closed down after year 2006 when lake was formed. To study the impact of Lake Formation, two stations having entirely different neighboring areas were selected i.e. Cottbus and Senftenberg. Cottbus station is located 10 km away from the nearest mining area while Senftenberg is 1.1 km away from Senftenberg See in South and 1.7 km away from mining area Meuro. In absence of other parameters, analysis was based on precipitation during summer season only because of expected influence on convective precipitation.

For the analysis six 10 years time series CPDF were analyzed for all the three stations. Last three time series included the period of lake formation. Even though stations Senftenberg and Cottbus had different neighboring landscapes but still six 10 years time series were almost identical. But in case of Elsterheide-Geierswalde when years during lake formation were introduced, time series showed little deviation from other time series with no lake. But in absence of other parameters and as data were not available after 2006 nothing could be concluded from the data analysis.

For the CCLM analysis three simulations viz. VAT010, VAT020 and VAT030 were carried out. VAT010 representing potential natural vegetation, VAT020 had four grid cells as Lake and VAT030 had similar four grid cells in VAT020 as pit resembling mining phase. Each grid cell had a size of 10 km x 10 km, so lake and pit in VAT020 and VAT030 simulations had total area of 400 km^2 and is oriented with maximum surface in North-South direction. The only difference in all the three simulations was the surface characteristics of these four grid cells. All the three simulations were carried out for 10 years starting from year 1989 to 1998.

As large portion of lake is oriented in the South-North direction so firstly analysis was carried out in this direction. For this purpose average of four grid cells as Lake in VAT020 and corresponding grid cells in the North and South direction and 10 km and

20 km from lake was calculated. Simulation VAT010 representing potential vegetation was treated as reference for other two simulations. Uncertainty analysis was carried out using MCS technique. Plots of difference for VAT020-VAT010 showed difference in convective precipitation for the averaged four grid cells as Lake. It showed negative value during late winter and spring and positive during summer and fall. So it was precipitating more in VAT020 simulation (over the lake) during summer and fall and less in late winter and spring than in VAT010 simulations but uncertainty analysis showed that difference was small. The effect of this is explained by the thermal capacity of water and due to small Bowen ratio (Segal et al. 1995).

For further analysis wind direction distribution was analyzed using wind rose plots for the grids in the East-West direction when convective precipitation of ≥ 0.1 mm/day occurred. Wind rose showed that at extreme East end of the lake most of the times winds were westerly when convective precipitation occurred. Here only six grid cells were analyzed. Three grid cells were located each on West- and East sides of Lake, among which one grid cell was located at extreme ends of lakes on both sides. Similarly difference between simulations VAT020-VAT010 and VAT030-VAT010 for convective precipitation were plotted. Uncertainty analysis showed that convective precipitation values were within the variability of values in various grid cells and hence no difference in convective precipitation values in simulations VAT010 and VAT030 were observed. But on analyzing uncertainty on VAT020-VAT010 plot high precipitation was observed in grid cells representing lake than in corresponding grid cells in VAT010 simulation. Rest of the grid cells had convective precipitation within the variability range and hence considered same. Similar explanation was given for the lake grid cells as in case of North-South analysis. But interestingly convective precipitation gradient existed among extreme West and East ends of lake grid cells

for VAT020 simulations. This was explained by the surface roughness property of the grids in VAT020 simulations. Thus over the lake, acceleration of westerly wind caused more precipitation in the East end of lake than in the West. It will be interesting to carry out the same study with much finer resolution of 1 km x 1 km or less. Because at finer resolution surface, characteristics like soil moisture, surface roughness etc. change and surface characteristics come close to the real situation. Earlier studies have shown that soil moisture influences quantity- and spatial distribution of precipitation at the local and regional scales (Seuffert et al. 2003 & Schär et al. 1999).

Conclusion by the CCLM analysis is that the conversion of area into Lake has lead to slight increase in convective precipitation but this effect is limited to lake only. As the aim of this study was to investigate the effect of lake on convective precipitation parameter over the neighboring region, hence it can be concluded that no effect over the vicinity of lake area was observed. This observation was similar to the observation made by Ahmed et al. (2012) about Warm Summer Continental region.

Bibliography

Ahmed, M. D., Hossain, F., Niyogi, D., Pielke Sr., R., Shepherd, J. M., Voisin, N. & Chronis, T., 2011: The influence of large dams on surrounding climate & precipitation patterns. Geophys. Res. Letters, Vol. 38, L04405.

Asokan, S. M., Jarsjö, J. & Destouni, G., 2010: Vapor flux by evapotranspiration: Effects of changes in climate, land use, and water use. J. Geophys. Res., 115, D24102, doi:10.1029/2010JD014417.

Avissar, R., 1995: Recent advances in the representation of land-atmosphere interactions in general circulation models. Rev. Geophys. 33,1005-1010.

Avissar, R. & Liu, Y., 1996: Three-dimensional numerical study of shallow convective clouds and precipitation induced by land surface forcing. J. Geophys. Res., 101, 7499-7518.

Avissar, R. & Schmidt, T., 1998: an evaluation of the scale at which ground-surface heat flux patchiness affects the convective boundary layer using large-eddy simulations. J. Atmos. Sci., 55, 2666-2689.

Bachner, S., Kapala, A. & Simmer, C., 2008: Evaluation of daily precipitation characteristics in the CLM and their sensitivity to parameterizations. Meteo. Zeit., Val. 17, No. 4, 407-419.

Baede, A. P. M., 2007: Climate Change 2007: The Physical Science Basis. Contribution of working group I to the fourth assessment report of the Intergovernmental Panel on Climate Change. Ed. By S. Solomon et al., Cambridge and New York: Cambridge University Press. Chap. Annex I: pp. 941-954 (cit. on p.2).

Basil, M., Papadopoulos, C., Sutherland, D. & Yeung, H., 2001: APPLICATION OF PROBABILISTIC UNCERTAINTY METHODS (MONTE CARLO SIMULATION) IN FLOW MEASUREMENT UNCERTAINTY ESTIMATION. International conference- Flow measurement.

Berkner, A., 1989: Braunkohlenbergbau, Landschaftsdynamik und territoriale Folgewirkungen in der DDR. Petermanns Geographische Mitteilungen 3, 173-190.

Blanken, P. D., Rouse, W. R., Culf, A. D., Spence, C., Boudreau, L. D., Jasper, J. N., Kochtubajda, B., Schertzer, W. M., Marsh, P. & Verseghy, D., 2000: Eddy covariance measurements of evaporation from Great Slave Lake, Northwest Territories, Canada. Water Resour. Res., 36, 1069-1077.

Böhm, U., Kücken, M., Ahrens, W., Block, A., Hauffe, D., Keuler, K., Rockel, B. & Will, A., 2006: CLM- The Climate Version of LM: Brief Description and Longterm Applications, COSMO Newsletter No. 6, German Weather Service (DWD), P.O: Box 100465, 63004 Offenbach, Germany, 225-235.

Boucher, O., Myhre, G. & Myhre A., 2004: Direct human influence of irrigation on atmospheric water vapor and climate. Clim. Dyn., 22, 597-603, doi:10.1007/s00382-004-0402-4.

Bundesanstalt für Geowissenschaften und Rohstoffe, ed. 2009: Energy resources 2009: Reserves, Recourses, Availability. Federal Institute for Geosciences and Natural Resources, Hannover, Germany, 275 pp.

Chen, F. & Avissar, R., 1994a: The impact of land-surface wetness heterogeneity on mesoscale heat fluxes. J. Appl. Meteorol., 33, 1323-1340.

Chen, F. & Avissar, R., 1994b: Impact of land-surface moisture variability on local shallow convective cumulus and precipitation in large scale models. J. Appl. Meteorol., 33, 1382-1401.

Clark, D.B., Taylor, C.M. & Thorpe, A.J., 2004: Feedback between the land surface and rainfall at convective length scales. J. Hydromet. 5(4), 625-639.

Cooley, H. S., 2005: Impact of agricultural practice on regional climate in a coupled land surface mesoscale model. J. Geophys. Res. 110, D03113.

Cotton, W. R. & Pielke Sr., R. A., 2007: Human impacts on weather and climate . Cambridge Univ. Press, Cambridge U.K., 330 pp.

Cuo, L., Lettenmaier, D. P., Alberti, M. & Richey, J. E., 2009: Effects of a century of climate and land cover change on the hydrology of the Puget Sound basin. Hydrol. Processes, 23(6), 907-933, doi:10.1002/hyp.7228.

Dalu, G. A. & Pielke, R. A., 1993: Vertical heat fluxes generated by mesoscale atmospheric flow induced by thermal inhomogeneities in the PBL. J. Atmos. Sci., 50, 919-926.

Dalu, G. A., Pielke, R. A., Baldi, M. & Zheng, X., 1996: Heat and momentum fluxes induced by thermal inhomogeneities. J. Atmos. Sci., 53, 3286-3302.

Dirmeyer, A. P. & Shukla, J., 1993: Observational and modeling studies of the influence of soil moisture anomalies on the atmospheric circulation, in Prediction of Interannual Climate variations. NATO ASI Ser., Ser. I, vol. 6, pp. 1-23, Springer-Verlag, New York.

Dirmeyer, A. P. & Shukla, J., 1994: Albedo as a modulator of climate response to tropical deforestation. J. Geo. Res., Vol. 99, No. D10, Pages 20, 863-20,877.

Doms, G., Förstner, J., Heise, E., Herzog, H. J., Raschendorfer, M., Schrodin, R., Reinhardt, T. & Vogel, G., 2005: A description of the nonhydrostatic regional model LM, Part II: Physical parametrization. Technical report, DWD 133 pp.

Finger, R, Heideger, W. & Schmid, S., 2011: Irrigation as adaption strategy to climate change-a biophysical and economical appraisal for Swiss maize production. Climate Change 105, pp. 509-528.

Fitzjarrald, D. R., Acevedo, O. C. & Moore, K. E., 2001: Climatic consequences of leaf presence in the eastern United States. J. Clim., 14, 598-614.

Frei, C., Schöll, R., Fukutome, S., Schmidli, J. & Vidale, P. L., 2006: Future change of precipitation extremes in Europe: Intercomparison of scenarios from regional climate models, J. Geophys. Res. 111, D06105, DOI:10.1029/2005JD005965.

Gordon, L. J., Steffen, W., Jönsson, B. F., Folke, C., Falkenmark, M. & Johanessen A., 2005: Human modification of global water vapor flows from the land surface. Proc. Natl. Acad. Sci. U.S.A., 102(21), 7612-7617.

Großer, K. H., 1998: Der Naturraum und seine Umgestaltung. Pages 461-474 in W. Pflug, ed. Braunkohletagebau und Rekultivierung. Landschaftsökologie – Folgenutzung – Naturschutz. Springer Verlag, Berlin, Germany.

Jacob, D., Bärring, L., Christensen, O. B., Christensen, J. H., Castro, M. DE, Déqué, M., Giorgi, F., Hagemann, S., Hirschi, M., Jones, R., Kjellström, E., Lenderink, G., Rockel, B., Sánchez, E., Schär, C., Seneviratne, S. I., Somot, S., Ulden, A. Van & Hurk, Van Den, 2007: An inter-comparision of regional climate models for Europe: model performance in present-day climate, Climate Change 81, 31-52, DOI:10.1007/s10584-006-9213-4.

Kitoh, A., Yamakazi, K. & Tokioka, T., 1988: Influence of soil moisture and surface albedo changes over the African tropical rain forest on summer climate investigated with the MRI-GCM-I. J. Meteorol. Soc. Jpn., 66, 65-86.

Kondratyev, K. Ya., Korzov VI, Mukhenberg VV, Dyachenko, L. N., 1982: The shortwave albedo and the surface emmisivity. In 'Land surface Processess in General Circulation Models'. PS Eagleson ed. Pp 463-514. Cambridge university press, Cambridge.

Kotlarski, S., Block, A., Böhm, U., Jacob, D., Keuler, K., Knoche, R., Rechid, D. & Walter, A., 2005: Regional climate model simulations as input for hydrological applications: evaluation of uncertainties, Adv. Geosci. 5, 119-125.

Krümmelbein, J., Horn, R., Raab, T., Bens, O. & Hüttl, R., 2010: Soil physical parameters of a recently established agricultural recultivation site after brown coal mining in Eastern Germany. Soil Tillage Res. 111: 19-25.

Krümmelbein, J., Bens, O., Raab, T. & Naeth, A., 2012: A history of lignite coal mining and reclamation practices in Lusatia, eastern Germany. Can. J. Soil Sci. (2012) 92: 53-66.

Kueppers, L. M., Snyder, M. A. & Sloan, L. C., 2007: Irrigation cooling effect: Regional climate focing by land-use change. Geophys. Res. Lett., 34, L03703, doi:10.1029/2006GL028679.

Laprise, R., 2006: Regional climate modeling. Journal of Computational Physics 227, pp. 3641-3666.

Laval, K. & Picon, L., 1986: Effects of a change of the surface albedo of the Sahel on climate. J. Atmos. Sci., 43, 2418-2429.

Lawton, R. O., Nair, U. S., Pielke Sr, R. A. & Welch, R. M., 2001: CLimate impact of lowland deforestation on nearby montane cloud forests. Science 294, 584-587.

Li, B. & Avissar, R., 1994: The impact of spatial variability of land surface heat fluxes. J. Clim., 7, 527-537.

Lobell, D. B., Bala, G., Bonfils, C. & Duffy, P. B., 2006: Potential bias of model projected greenhouse warming in irrigated regions. Geophys. Res. Lett., 33, L13709, doi:10.1029/2006GL026770.

Lynn, B., Rind, D. & Avissar, R., 1995: The importance of mesoscale circulations generated by subgrid-scale landscape heterogeneities in general circulation models. J. Clim., 8, 191-205.

Lyons, T. J., Smith, R. C. G. & Xinmei, H., 1996: The impact of clearing for agriculture on the surface energy budget. Int. J. Climatol., 16,551-558.

Marshall, C. H., Pielke Sr., R. A., Steyaert, L. T. & Willard, D. A., 2004: The impact of anthropogenic land-cover change on the Florida Peninsula sea breezes and warm season sensible weather. Monthly Weather Review 132(1), 28-52.

Mironov, D. V., 2008: Parameterization of lakes in numerical weather prediction. Description of a lake model. COSMO Technical Report, No. 11, Deutscher Wetterdienst, Offenbach am Main, Germany, 41 pp.

Mylne, M. F. & Rowntree, P. R., 1992: Modelling the effects of albedo change associated with tropical deforestation. Clim. Change, 21, 317-344.

Nicolis, G., 1995: Introduction to non-linear science. Cambridge University Press, ISBN 0521 46228 2.

Niyogi, D., Kishtawal, C. M., Tripathi, S. & Govindaraju, R. S., 2010: Observational evidence that agricultural intensification and land use change may be reducing the Indian summer monsoon rainfall. Water Resour. Res., 46, W03533, doi:10.1029/2008WR007082.

Oguntoyinbo, J. S., 1970: Reflection coefficient of natural vegetation, crops and urban surfaces in Nigeria. J. R. Meteo. Soc. 96:430-441.

Pielke, R. A., 1984: Mesoscale Meteorological Modeling, 612 pp., Academic, San Diego, Calif..

Pielke, R. A., Dalu, G., Snook, J. S., Lee, T. J. & Kittel, T. G. F., 1991: Nonlinear influence of mesoscale land use on weather and climate. J. Clim., 4, 1053-1069.

Pielke , R. A., 2001: Influence of the spatial distribution of vegetation and soils on the prediction of cumulus convective rainfall. Rev. Geophys. 39(2), 151-177.

Pielke Sr., R. A., Marland, G., Betts, R. A., Chase, T. N., Eastman, J. L., Niles, J. O., Niyogi, D. D. S. & Running, S. W., 2002: The influence of land-use change and landscape on the climate system: relevance to climate-change policy beyond the radiative effect of greenhouse gases. Phil. Trans. R. Sco. Lond. 360, 1705-1719.

Pielke Sr., et al., 2009: Climate change: The need to consider human forcings besides greenhouse gases, Eos Trans. AGU, 90(45),doi:10.1029/2009EO450008.

Pitman, A. J., Narisma, G. T., Pielke Sr., R. A. & Holbrook, N. J., 2004: Impact of land cover change on the climate of southwest Western Australia. J. Geophys. Res. D Atmospheres 109(18), D18109.

Pitman, A. J. & Narisma, G. T., 2005: The role of land surface processes in regional climate change: a case study of future land cover change over south western Australia. Met. Atmos. Phys. 89(1/4), 235-249.

Rockwood, A. A. & Cox, S. K., 1978: Satellite-inferred surface albedo over northwestern Africa. J. Atoms. Sci. 35:513-522.

Roesch, A., Jaeger, E. B., Lüthi, D. & Seneviratne, S. I., 2008: Analysis of CCLM model biases in relation to intr-ensemble model variability. Meteo. Zeit., Vol. 17, No. 4, 369-382.

Rouse, R. W., Oswald, M. C. & Binyamin J., 2003: Interannual and Seasonal Variability of the Surface Energy Balance and Temperature of Central Great Slave Lake. J. of Hydrometeo., Vol. 4.

Roy, Baidya S. & Avissar, R., 2002: Impact of land use / land cover change of regional hydrometeorology in Amazonia. J. Geophys. Res. 107(D20, 8037), LBA 4-1-LBA 4-12.

Schär, C., Lüthi, U. B. & Heise, E., 1999: The soil-Precipitation feedback: A process study with a regional climate model. J. Climate, 12, 722-741.

Schertzer, W. M., 1997: Freshwater lakes. The Surface Climates of Canada. W. G. Bailey, T. Oke and W. R. Rouse, Eds., Mcgill-Queens University Press, 124-148.

Schertzer, W. M., Rouse, W. R. & Blanken, P. D., 2000: Cross-lake variation of physical limnological and climatological processes of Great Slave Lake. Phys. Geogr., 21, 385-406.

Schulz, F., 2000: Drei Jahrhunderte Lausitzer Braunkohlebergbau. Lusatia Verlag, Bautzen. Germany. 192 pp.

Schwartz, M. D., 1994: Monitoring global change with phenology: The case of the spring green wave. Int. J. Biometeorol., 38, 18-22.

Scott, R. W. & Huff, F. A., 1996: Impacts of the Great Lakes on regional climate conditions. J. Great Lakes Res. 22(4), 845-863.

Segal, M. & Arritt, R. W., 1992: Non-classical mesoscale circulations caused by surface sensible heat-flux gradients. Bull. Am. Meteorol. Soc., 73, 1593-1604.

Segal, M., Avissar, R., McCumber, M. C. & Pielke, R. A., 1988: Evaluation of vegetation effects on the generation and modification of mesoscale circulations. J. Atmos. Sci., 45, 2268-2292.

Segal, M., Garratt, J. R., Kallos, G. & Pielke, R. A., 1989: The impact of wet soil and canopy temperatures on daytime boundary-layer growth. J. Atmos. Sci., 46, 3673-3684.

Segal, M., Arritt, R. W., Clark, C., Rabin, R. & Brown, J., 1995: Scaling evaluation of the effect of surface characteristics on potential for deep convection over uniform terrain. Mon. Weather Rev., 123, 383-400.

Sen, O. L., Wang, B. & Wang, Y., 2004: Impacts of re-greening the desertified lands in northwestren China: implications from a regional climate model experiments. J. Met. Soc. Japan 82(6), 1679-1693.

Seuffert, G., Wilker, H., Viterbo, P., Mahfouf, J., Drusch, M., & Calvet, J. C., 2003: Soil moisture analysis combining screen level parameters and microwave brightness temperatures. *Geophys. Res. Let.*, **30**, 1498, doi:10.1029/2003GL017128.

Shibuo, Y., Jarsjo, J. & Destouni, G., 2007: Hydrological responses to climate change and irrigation in the Aral Sea drainage basin. Geophys. Res. Lett., 34, L21406.

Smiatek, G., Rockel, B. & Schaettler, U., 2008: Time invariant data preprocessor for the climate vesion of the COSMO model (COSMO-CLM). Meteo. Zeitschrift, Vol. 17, No. 4, 395-405.

Statistik der Kohlenwirtschaft e.V. ed. 2009. Der Kohlenbergbau in der Energiewirtschaft der Bundesrepublik Deutschland im Jahre 2008. CW Haarfeld, Essen, Germany, 83 pp.

Steppeler, J., Doms, G., Schättler, U., Bitzer, H. W., Gassmann, A., Damrath, U. & Gregoric, G., 2003: Meso-gamma scale forecasts using non-hydrostatic model LM. Meteo. Atmos. Phys. 82, 75-96.

Stewart, J. B., 1971: The albedo of a pine forest. Quart. J. R. Meteo. Soc. 97:561-564.

Sud, Y. C. & Fennessy, M. J., 1982: An observational-data based evapotranspiration function for general circulation models. Atmos. Ocean, 20, 301-316, 1982.

Sud, Y. C. & Molod, A., 1988: A GCM simulation study of the influence of Saharan evapotranspiration and surface-albedo anomalies on july circulation and rainfall. Mon. Weather Rev., 116, 2388-2400.

Takata, K. S. & Yasunari, T., 2009: Changes in the Asian monsoon climate during 1700-1850 induced by preindustrial cultivation. Proc. Natl. Acad. Sci. U.S.A., 106, 9586-9589, doi:10.1073/pnas.0807346106.

Vattenfall Europe AG ed. 2009. The year 2009 in facts and figures. Vattenfall, Berlin, Germany. 124 pp.

Walker, J., Rowntree, P. R., 1977: The effects of soil moisture on circulation and rainfall in a tropical model. Quart. J. R. Meteorol. 41:57-64.

Wang, J., Bras, R. & Eltahir, E. A. B., 1996: A stochastic linear theory of mesoscale circulation induced by the thermal heterogeneity of the land surface. J. Atmos. Sci., 53, 3349-3366.

Wang, J., Bras, R. & Eltahir, E. A. B., 1998: Numerical simulation of nonlinear mesoscale circulations induced by the thermal heterogeneity of the land surface. J. Atmos. Sci., 55, 447-464.

Wang, J., Bras, R. & Eltahir, E. A. B., 2000: The impact of observed deforestation on the mesoscale distribution of rainfall and clouds in Amazonia. J. Hydrometeorol., 1, 267-286.

Wang, Y., Leung, L.R., Mcgregor, J. L., Lee, D. K., Wang, W. C., Ding, Y. & Kimura, F., 2004: Regional Climate Modeling: Progress, Challenges, and Prospects. Journal of t he Meteorological Society of Japan, 82, 1599-1628.

Wetzel, P. J., Argentini, S. & Boone, A., 1996: Role of land surface in controlling daytime cloud amount: Two case studies in the GCIP-SW area. J. Geophys. Res., 101, 7359-7370.

Wilson, J. W., 1977: Effect of Lake Ontario on precipitation. Monthly Weather Review 105(2), 207-214.

Zweckverband Elstertal 2006. Regionales Entwicklungskonzept Lausitzer Seenland Teilkonzept Landmarken. Endbericht Landmarken – Prioritäre Handlungsschwerpunkte – ausgewählte Landmarken – Maßnahmenübersicht. Kamenz, 58 pp.

APPENDIX A

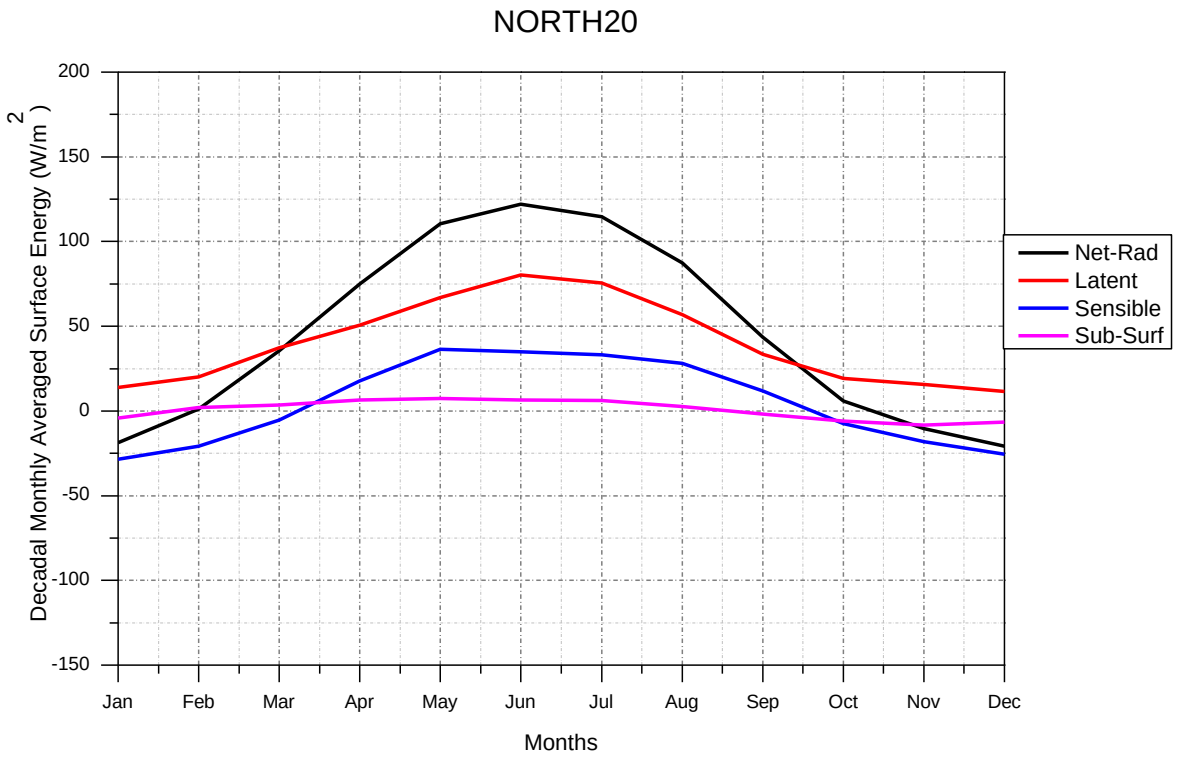

Figure A.1: Decadal monthly averaged surface energy (W/m^2) at NORTH20 of VAT020 simulation.

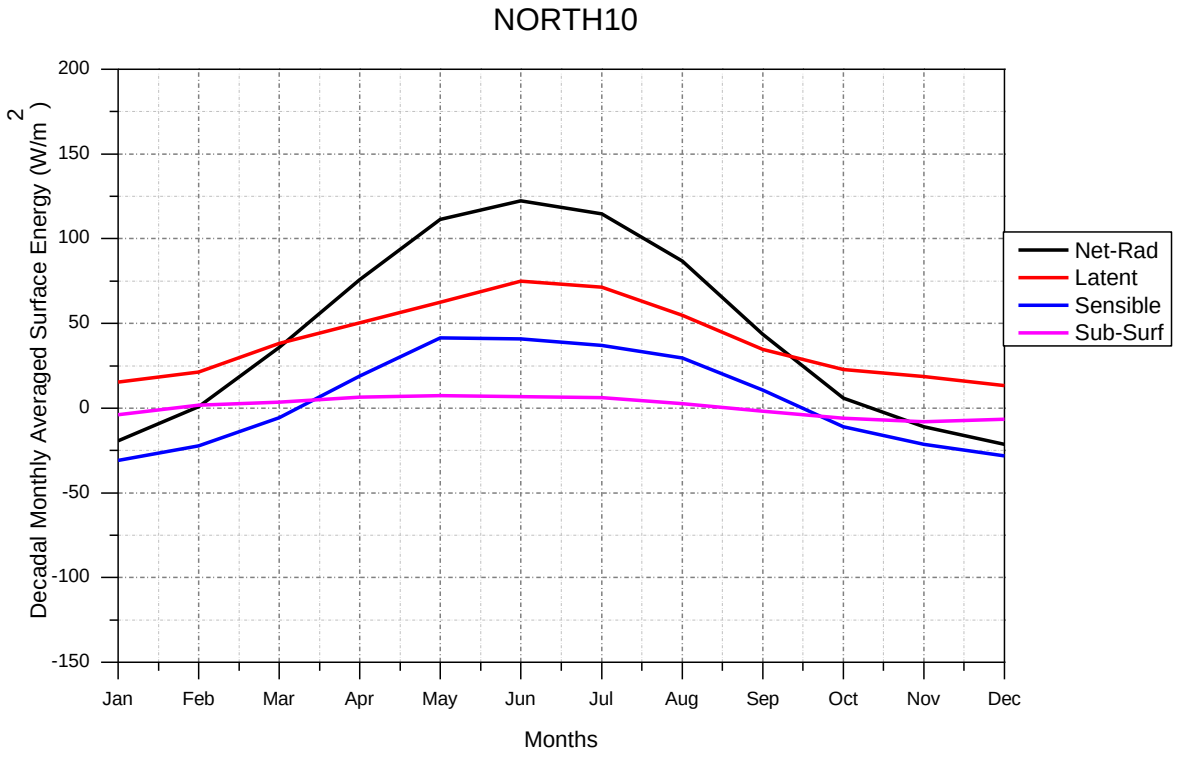

Figure A.2: Decadal monthly averaged surface energy (W/m^2) at NORTH10 of VAT020 simulation.

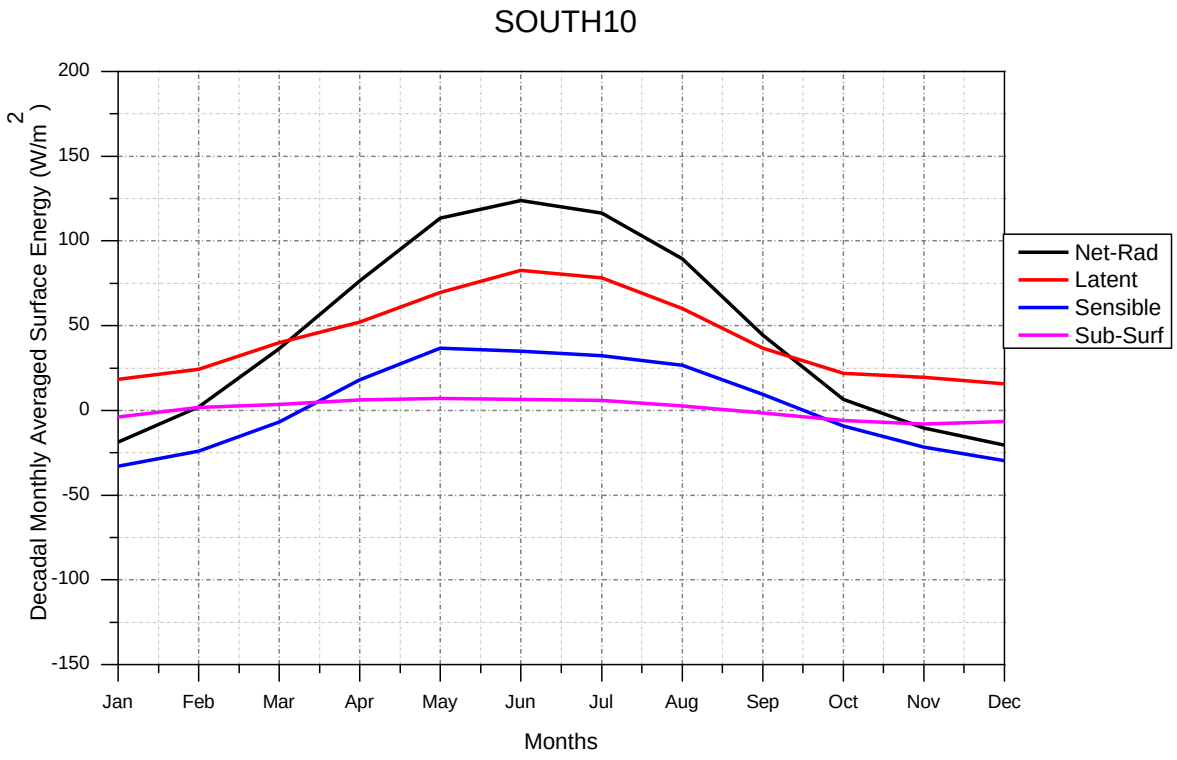

Figure A.3: Decadal monthly averaged surface energy (W/m^2) at SOUTH10 of VAT020 simulation.

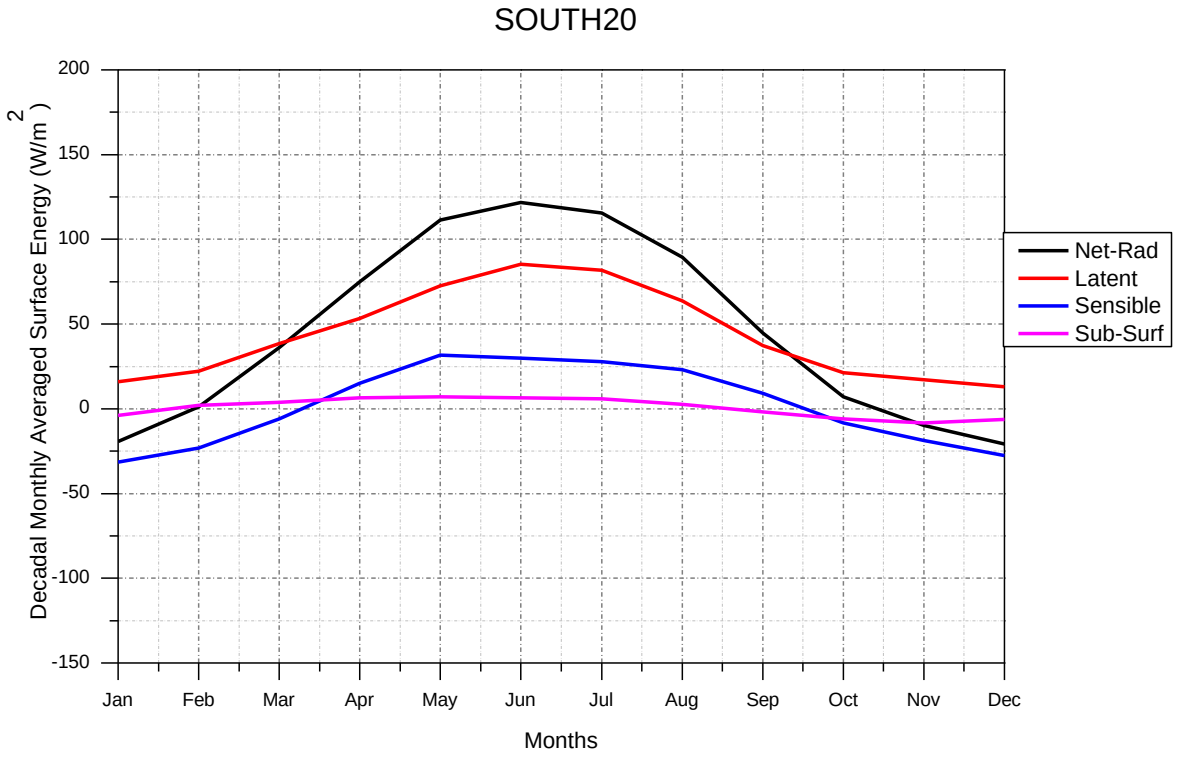

Figure A.4: Decadal monthly averaged surface energy (W/m^2) at SOUTH20 of VAT020 simulation.

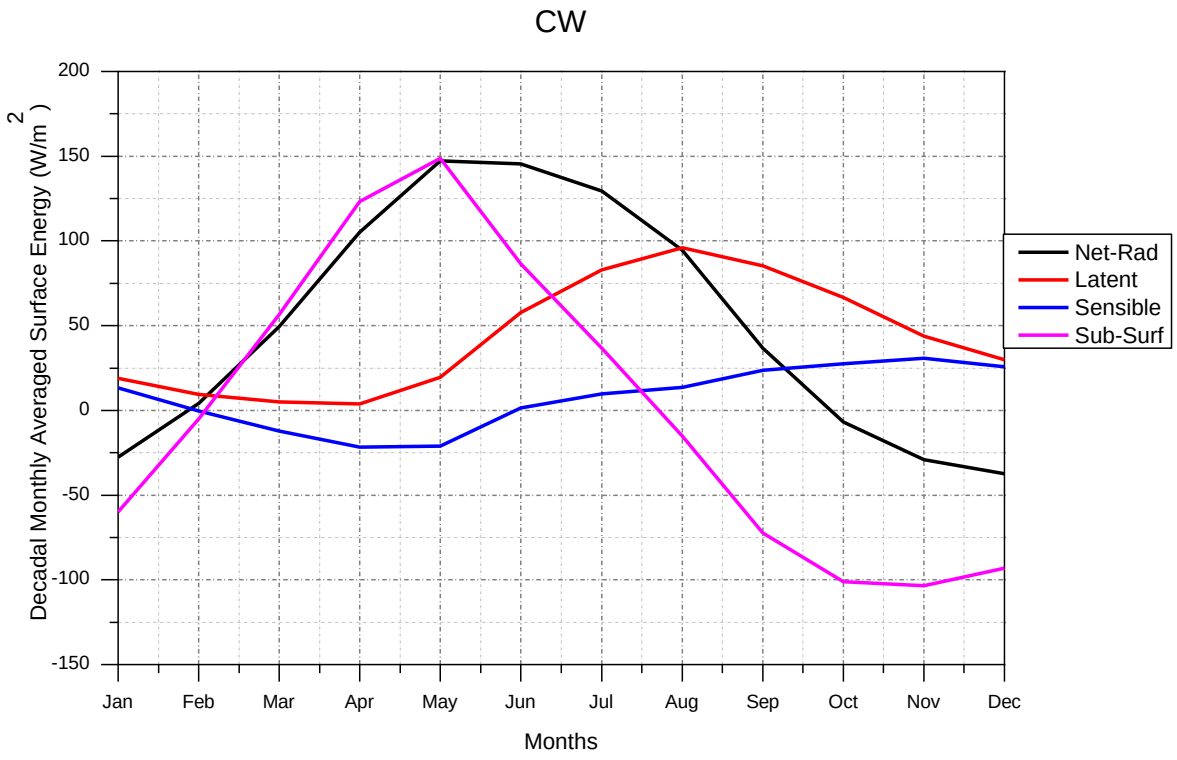

Figure A.5: Decadal monthly averaged surface energy (W/m^2) at CW of VAT020 simulation.

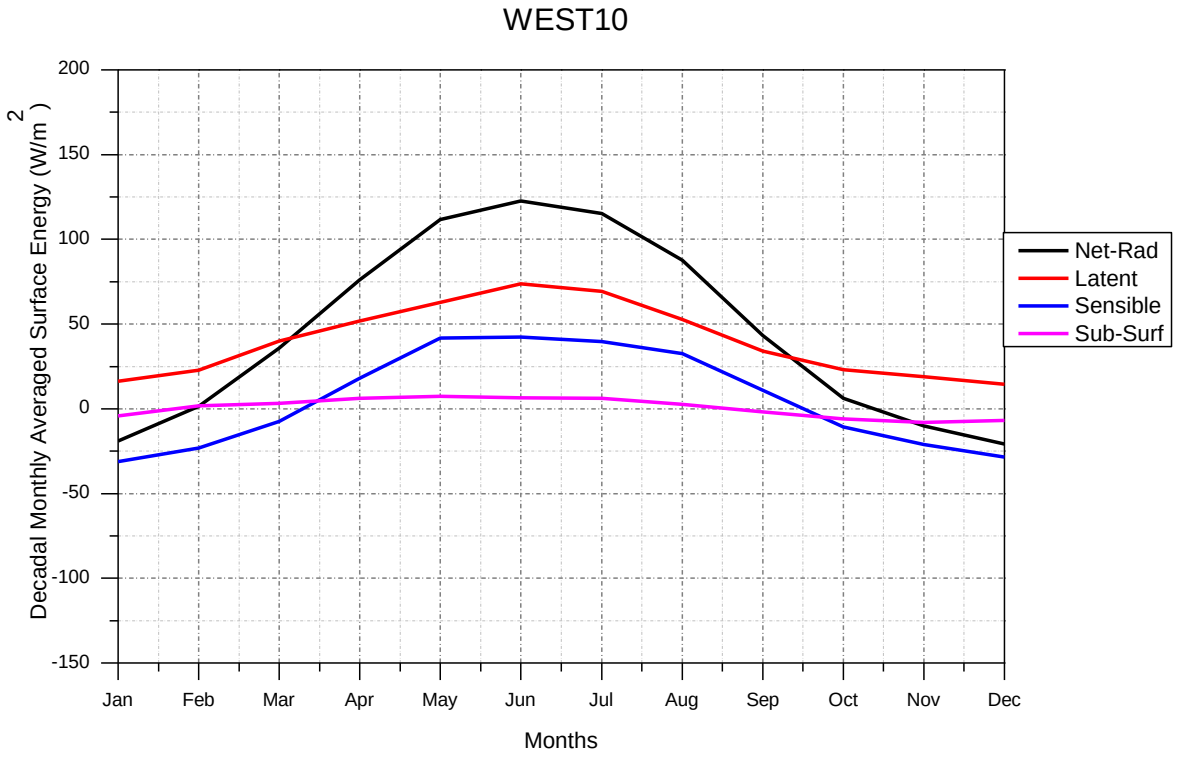

Figure A.6: Decadal monthly averaged surface energy (W/m^2) at WEST10 of VAT020 simulation.

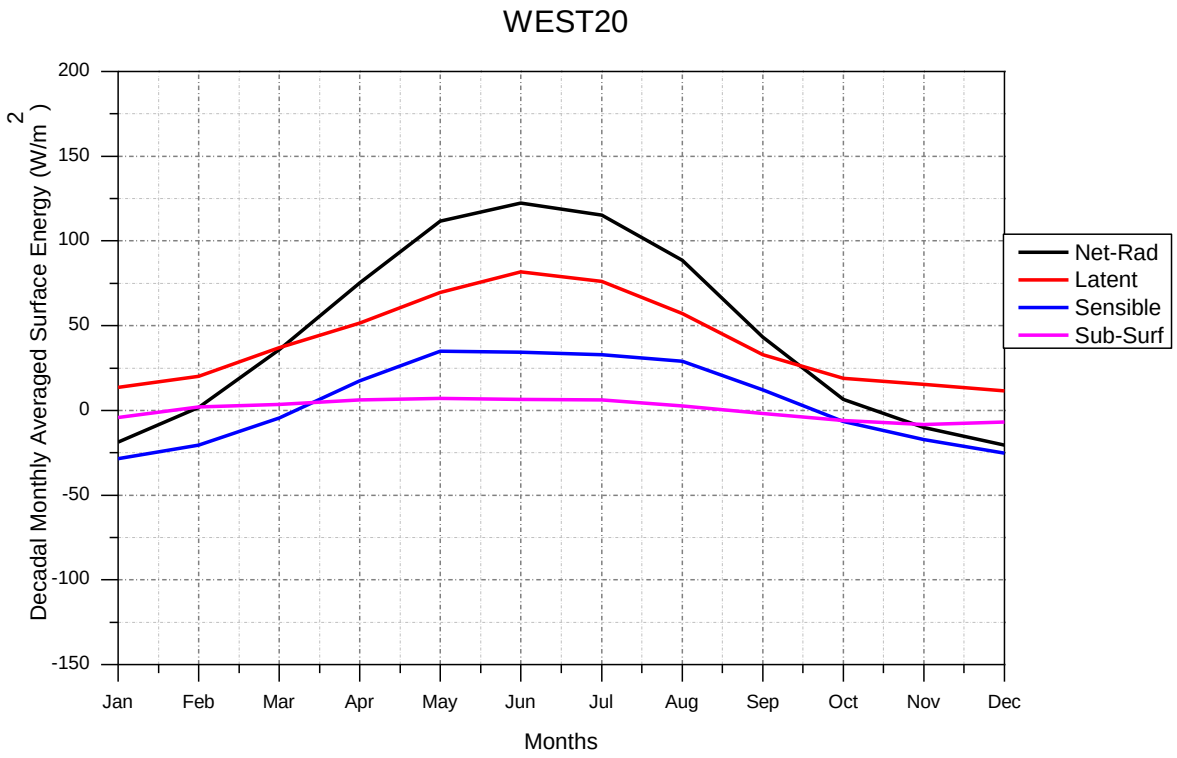

Figure A.7: Decadal monthly averaged surface energy (W/m^2) at WEST20 of VAT020 simulation.

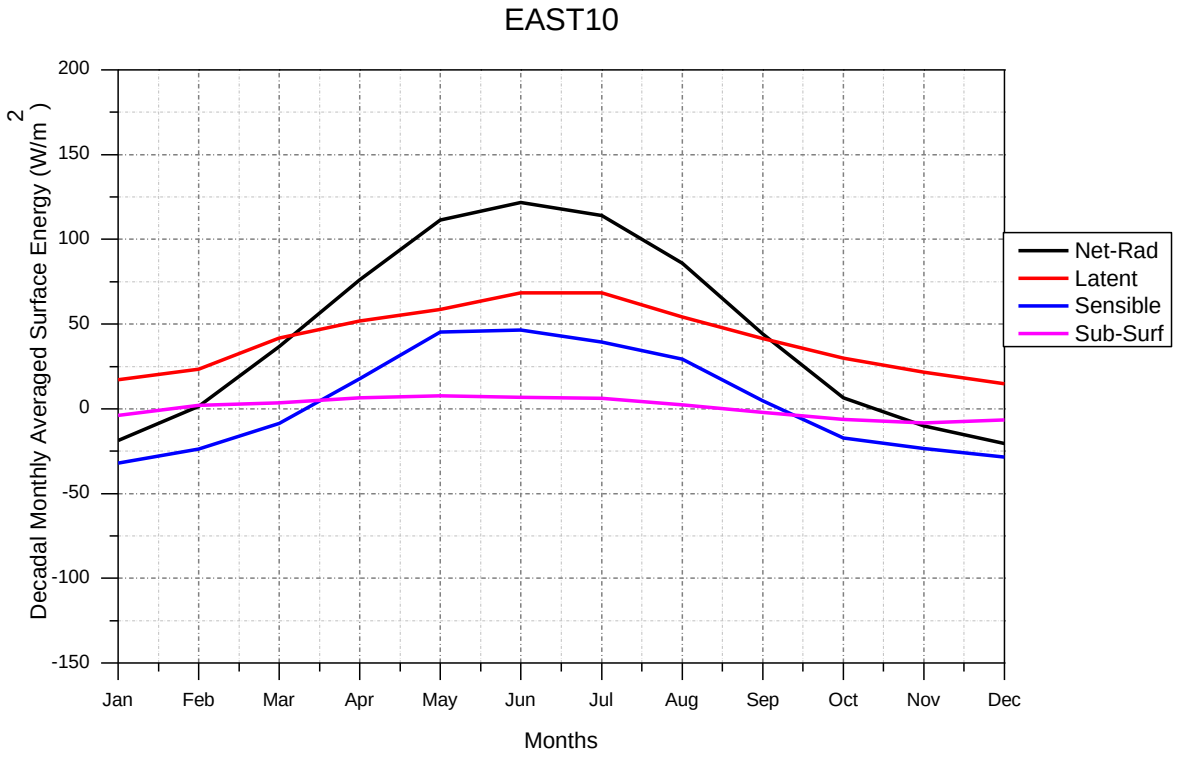

Figure A.8: Decadal monthly averaged surface energy (W/m^2) at EAST10 of VAT020 simulation.

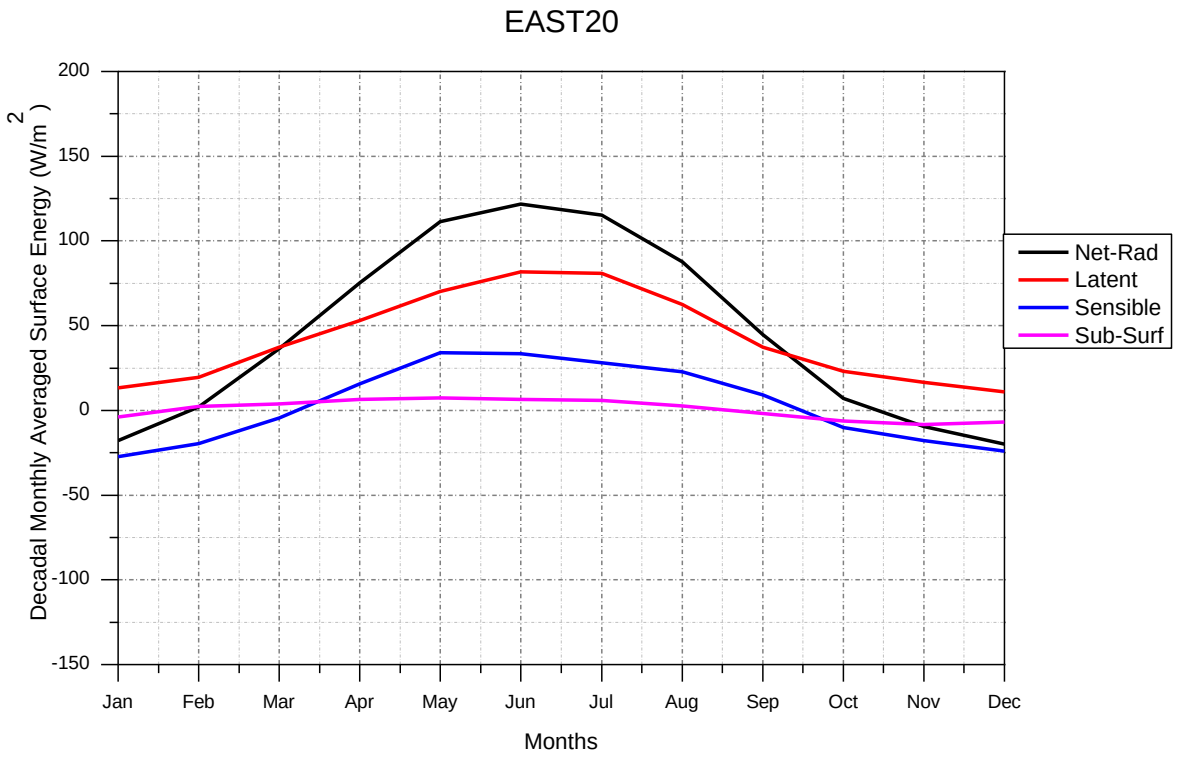

Figure A.9: Decadal monthly averaged surface energy (W/m^2) at EAST20 of VAT020 simulation.

GLOSSARY (SYMBOLS)

Symbol	Explanation
A	Albedo
B	Bowen Ratio
E	Evaporation
G	Sub surface heat flux
H	Sensible heat flux
I	Amount of precipitation got infiltrated
L	Latent heat of vaporization
P	Precipitation
R_N	Net radiative flux density
RO	Precipitation surface runoff
T_{ran}	Transpiration

GLOSSARY (ABBREVIATIONS)

Abbreviation	Explanation
CAPE	Convective Available Potential Energy
CCLM	COSMO Climate Limited-area Modelling
CLM	Climate Limited-area Modelling
CPDF	Cummulative probability density function
DMT	Daily mean temperature
DMaxT	Daily minimum temperature
DMinT	Daily maximum temperature
DMWS	Daily mean of wind speed
DSP	Daily sum of precipitation
DWD	Deutscher Wetterdienst
GCM	Global Climate Model
GHCN	Global Historical Climate Network
LULC	Land Use and Land Cover
MCS	Monte Carlo Simulation
NARR	North American Regional Reanalysis
NCEP	National Centre for Environmental Prediction
PEP	PrEProcessor
RCM	Regional Climate Model
SVAT	Soil Vegetation Atmosphere Transfer
TP-C	Difference of total and convective precipitation

ACKNOWLEDGEMENTS

First and foremost, I would like to express my heartfelt gratitude to my thesis supervisor Prof. Dr. rer. nat. Eberhard Schaller for giving me the opportunity to do this thesis under his valuable guidance. His esteemed suggestions and constant encouragement led to the successful completion of this thesis work. I would like to thank Apl. Prof. Dr. rer, nat. habil. Uwe Harlander for reviewing my thesis and giving his valuable suggestions. I would also like to thank Dr. Klaus Keuler for helping me to understand the CLM model. I would like to thank Michael Woldt to configure the CCLM model. I would like to thank Dr. Detlef Biemelt to provide me information about mining sites in Lusatia. I would also like to thank Dr. Andreas Will for giving different perspective to solve a problem. I would also like to thank my colleagues Marten, Abouzar, Jack and Stefan for being real stress buster. I am grateful to the chair Secretary Mrs. Sabine Printschitsch for her friendly assistance during my work and stay in Cottbus. Finally I would like to thank my parents for their constant support and understanding through the many years of my Ph.D. education. I would like to thank my wife Amruta Nawdiyal for her patience, love and support for these years. I could never have finished this research without her support and encouragement. Finally I dedicate my thesis to my beloved son Atharv Nawdiyal who was born during this time.